

UCSF

UC San Francisco Electronic Theses and Dissertations

Title

Physiological requirements for lysis by a peptidoglycan-degrading interbacterial toxin

Permalink

<https://escholarship.org/uc/item/0q21g54f>

Author

Trotta, Kristine

Publication Date

2023

Supplemental Material

<https://escholarship.org/uc/item/0q21g54f#supplemental>

Peer reviewed|Thesis/dissertation

Physiological requirements for lysis by a peptidoglycan-degrading interbacterial toxin

by
Kristine Trotta

DISSERTATION
Submitted in partial satisfaction of the requirements for degree of
DOCTOR OF PHILOSOPHY

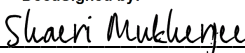
in


Biochemistry and Molecular Biology

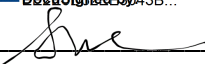
in the

GRADUATE DIVISION
of the
UNIVERSITY OF CALIFORNIA, SAN FRANCISCO

Approved:

DocuSigned by:

7AA908684B40471... Shaeri Mukherjee
Chair

DocuSigned by:

DocuSigned by:
43B... Geeta Narlikar

DocuSigned by:

8BD0E7DC6FB141A... Seemay Chou

Committee Members

ACKNOWLEDGEMENTS

I'd like to thank the following people for their support throughout my graduate education:

Seemay Chou: for your charisma, creativity, and intrepid curiosity. Our work together has offered a wellspring of life lessons. Thank you for seeing me through. Beth Hayes: for your compassion, friendship, and drive to solve hard problems. Thank you for carrying me to safe harbor when I needed it most. Atanas Radkov: the very highest example of a passionate scientist who is unconditionally kind. I am so grateful to have learned and laughed with you. FMoM LBoC next week? Krisna Van Dyke: I love being your friend and it is a privilege to witness you grow into yourself. I am so proud of you. Thank you for all the laughter, unconditional support, and deep-fried memes. My labmates (Fauna Yarza, Calla Martyn, Elizabeth Martinez-Bond, Ziyi Zhao, Anne Sapiro, Domi Laukos, Sebastian Flores, Patrick Grimes, Rachel Kim, Steven Massa, Victoria Bowcut, Chase Mateusiak, Eleanor Wang, Shivani Phadke): I am most fulfilled when working alongside folks whose creative thinking and passion for scientific discovery can cross disciplines. I am grateful for the years we spent building our community up.

My collaborators (Melanie Silvis, Horia Todor, Byoung Mo Koo, John Hawkins, Marco Jost, Carol Gross, Johannes Schneider, Jing Wang, Marek Basler, and Will Hatleberg): it has always been my express wish to do collaborative science. Working with you has pushed my thinking in ways I could never accomplish on my own. I am grateful for your knowledge, perspectives, and hard work. My thesis committee (Shaeri Mukherjee,

Geeta Narlikar, and Oren Rosenberg): Thank you for bearing witness to all the challenges in my graduate work and motivating me to work through them. The UCSF Tetrad graduate program (Toni Hurley, Danny Dam, Miles Bacchus, and Billy Luh): Thank you for creating order out of chaos. Your work has been vital to my ability to do the best science possible. Ethel Enoex-Godonoo: Thank you for always offering a helping hand.

L. Stirling Churchman: I have always looked up to you as a leader who is truly fair, thoughtful, and rigorous. Thank you for believing in my capacity to do great science and for exposing me to the very best that scientific teamwork has to offer. Steven Williams and Kevin Shea: for showing me the far-reaching impact of collaborative science. I am inspired by your infectious drive to pursue new ways to solve challenging and meaningful problems. Channing and Johanna: for seeing me as I am and helping to illuminate more compassionate approaches to living. Your work has changed my life. Thank you.

My family (Cynthia Trotta, Frederick Trotta, Lauren Trotta, Freddy Trotta, Zach Siders): for instilling in me the idea that education is one of the most valuable investments that I could make for myself, and then supporting my decision move 3,000 miles away to do it. Thank you for rooting for me. Maggie Sullivan: my best friend, my number one, my forever emergency contact. I love you. Thank you for sticking by me. Ann and Ed Sullivan, Bidy Sullivan, Erica Brancato, and Scott Allen: Your support, laughter, and gobbling has been a lifeline for me. Thank you for keeping me grounded. Greyson

Lewis and Frances Brittingham: for getting me through this pandemic in (mostly) one piece, one bowl of noodles at a time. Sarah Gaffney and Jessica Hopson: for every cup of tea, bucket of goldfish, and video call since 2010. And look at us now! To all the friends (too many to name!) whose paths have crossed with mine: each of you has touched my life in an important way. Thank you for showing up.

Finally, I'd like to extend gratitude to myself for finishing this project. There were times in this process where I struggled to know whether it was worth sticking around to see it through. Ultimately, I am proud of this body of work, but not only because of the knowledge gained. I am also proud to be here to tell you about it.

I believe there are only two ideas that have universal value: kindness to others, and kindness to self. There are no intellectual advancements or ideological stances that matter more than being kind. If you are reading this: thank you. I'm glad we're here together.

CONTRIBUTIONS

Chapters 2 and 3 contain sections reprinted as a manuscript in preparation:

Trotta KL, Hayes BM, Schneider JP, Wang J, Todor H, Rockefeller Grimes P, Zhao Z, Hatleberg WL, Silvis MR, Kim R, Koo BM, Basler M, Chou S. Lipopolysaccharide integrity primes bacterial sensitivity to a cell wall-degrading intermicrobial toxin

KLT and SC conceived and designed the study; KLT, BMH, JPS, JW, PRG, ZZ, and BMK performed experiments; KLT, MRS, and HT analyzed data; KLT, BMH, JPS, HT, WLH, BM, and SC wrote and/or edited the manuscript.

“It is winter, my friends, and it has been winter for a long time. It may be winter for a while longer. But spring is coming.”

-John Green

Physiological requirements for lysis by a peptidoglycan-degrading interbacterial toxin

Kristine Trotta

Abstract

Gram-negative bacteria can antagonize neighboring microbes using a type VI secretion system (T6SS) to deliver toxins that target different essential cellular features. Despite the conserved nature of these targets, T6SS potency can vary across recipient species. To understand the molecular basis of intrinsic T6SS susceptibility, we screened for essential *Escherichia coli* genes that affect its survival when antagonized by a cell wall-degrading T6SS toxin from *Pseudomonas aeruginosa*, Tae1. We revealed genes associated with both the cell wall and a separate layer of the cell envelope, surface lipopolysaccharide, that modulate Tae1 toxicity *in vivo*. Disruption of lipopolysaccharide synthesis provided *Escherichia coli* (*Eco*) with novel resistance to Tae1, despite significant cell wall degradation. These data suggest that Tae1 toxicity is determined not only by direct substrate damage, but also by indirect cell envelope homeostasis activities. We also found that Tae1-resistant *Eco* exhibited reduced cell wall synthesis and overall slowed growth, suggesting that reactive cell envelope maintenance pathways could promote, not prevent, self-lysis. Together, this study highlights the consequences of co-regulating essential pathways on recipient fitness during interbacterial competition, and how antibacterial toxins leverage cellular vulnerabilities that are both direct and indirect to their specific targets *in vivo*.

TABLE OF CONTENTS

Chapter 1: Introduction	1
<i>Type VI secretion systems facilitate selective interbacterial competition</i>	<i>1</i>
<i>Pseudomonas aeruginosa deploys Tae1 from its H1-T6SS to kill Escherichia coli.....</i>	<i>3</i>
<i>Biochemical specificity for Eco PG is key to Tae1 toxicity.....</i>	<i>5</i>
<i>Eco susceptibility to T6SS is also dependent on non-immunity protein defenses.....</i>	<i>6</i>
<i>Intrinsic determinants of Eco susceptibility to Tae1 in vivo.....</i>	<i>7</i>
Chapter 2: Essential lipopolysaccharide genes drive intrinsic susceptibility to Tae1 in Eco.....	9
INTRODUCTION.....	9
RESULTS.....	10
<i>Adaptation of native T6SS competitions to study Eco susceptibility to Tae1</i>	<i>10</i>
<i>CRISPRi reveals toxin-specific and non-specific determinants of Eco fitness against H1-T6SS.....</i>	<i>13</i>
<i>msbA-KD disrupts LPS biosynthesis and affords resistance to Tae1.....</i>	<i>15</i>
<i>Tae1 resistance is independent of LPS biosynthesis master-regulator LpxC</i>	<i>17</i>
<i>Wildtype Eco downregulate Lipid-A biosynthesis genes during Tae1 attack.....</i>	<i>18</i>
DISCUSSION.....	19
METHODS	24
Chapter 3. Disruption of lipopolysaccharide biosynthesis provides novel immunity to PG hydrolysis by Tae1	34
INTRODUCTION.....	34
RESULTS.....	35
<i>Resistance to Tae1 in msbA-KD is independent of cell wall hydrolysis.....</i>	<i>35</i>
<i>PG synthesis is suppressed in msbA-KD but sensitive to Tae1 activity.....</i>	<i>37</i>

<i>Blocks to growth and protein synthesis accompany Tae1 resistance in msbA-KD</i>	<i>38</i>
DISCUSSION.....	39
METHODS	43
FIGURES.....	49
TABLES	72
REFERENCES	74

LIST OF FIGURES

Figure 2.1: Adaptation of native T6SS competitions to study <i>Eco</i> susceptibility to Tae1	49
Figure 2.2 : CRISPRi conditionally knocks down transcription across hundreds of <i>Eco</i> gene targets	51
Figure 2.3: Non-targeting CRISPRi induction has little effect on <i>Eco</i> fitness in T6SS competition	52
Figure 2.4: CRISPRi library fitness in T6SS screen is reproducible across biological replicates	53
Figure 2.5: CRISPRi reveals toxin-specific and non-specific determinants of <i>Eco</i> fitness against H1-T6SS	54
Figure 2.6: Pooled T6SS competitions with basal CRISPRi attenuate significant fitness phenotypes	55
Figure 2.7: <i>Pae^{inactive}</i> is a neutral co-culture partner for <i>Eco</i>	56
Figure 2.8: <i>msbA-KD</i> disrupts LPS biosynthesis and imparts Tae1 resistance	57
Figure 2.9: <i>lpxK-KD</i> and <i>msbA-KD</i> modulate target gene expression and show polar effects	59
Figure 2.10: Tae1 resistance is independent of LPS biosynthesis master-regulator LpxC	60
Figure 2.11: Wildtype <i>Eco</i> downregulate Lipid-A biosynthesis genes during Tae1 attack	61
Figure 3.1: Resistance to Tae1 in <i>msbA-KD</i> is independent of cell wall hydrolysis	62

Figure 3.2: Tae1 protein expression is unaffected in <i>msbA-KD</i>	64
Figure 3.3: Plasmid-borne overexpression of <i>msbA</i> partially rescues Tae1 sensitivity in <i>msbA-KD</i>	65
Figure 3.4: Tae1 ^{C30A} hydrolyzes D44 mucopeptides in <i>rfp-KD</i> and <i>msbA-KD</i>	67
Figure 3.5: PG synthesis is suppressed in <i>msbA-KD</i> but sensitive to Tae1 activity	68
Figure 3.6: PG synthesis activity in <i>msbA-KD</i> is suppressed across all conditions	69
Figure 3.7: Blocks to growth and protein synthesis accompany Tae1 resistance in <i>msbA-KD</i>	70
Figure 3.8: <i>msbA-KD</i> growth defects are independent of <i>Pae</i> T6SS activity	71

LIST OF TABLES

Table 2.1: Cell envelope gene KDs develop strong fitness changes against Tae1 in competition	72
Table 2.2: Bacterial strains and plasmids used in this study. Supplemental File.	
Table 2.3: Primer sequences. Supplemental file.	
Table 2.4: Corrected L2FC values from screen. Supplemental file.	
Table 2.5: Final Diff values from screen. Supplemental file.	
Table 3.1: PG synthesis activity is sensitive to CRISPRi and Tae1 overexpression	73

LIST OF ABBREVIATIONS

COG – Clusters of Orthologous Genes

CRISPR – Clustered, randomly interspaced, short palindromic repeats

CRISPRi – CRISPR interference

D44 – 4,4-dimer muropeptide

dCas9 – catalytically dead CRISPR associated protein 9

D-Glu – D-glutamate

Eco – *Escherichia coli*

GlcNAc – N-acetyl glucosamine

H1-T6SS – Hcp1 secretion island I-encoded type VI secretion system

HADA – 3-[[[(7-Hydroxy-2-oxo-2*H*-1-benzopyran-3-yl)carbonyl]amino]- D-alanine
hydrochloride

IM – inner membrane

IPTG – isopropyl β -D-1-thiogalactopyranoside

KD – knockdown

Kdo₂ – 3-deoxy-D-manno-octulononic acid (dimer)

L2FC – log₂ fold change

LB – lysogeny broth

LBNS – lysogeny broth (no salt)

LPS – lipopolysaccharide

M4 – tetrapeptide monomer muropeptide

*m*DAP – meso-diaminopimelic acid

MurNAc – N-acetyl muramic acid

OM – outer membrane

Pae – *Pseudomonas aeruginosa*

PBP – peptidoglycan binding protein

PC – principal component

PG – peptidoglycan

sgRNA – single guide ribonucleic acid

T6S – type VI secretion

T6SS – type VI secretion system

Tae1 – T6S amidase effector 1

Tai1 – T6S amidase immunity protein 1

Chapter 1: Introduction

Interbacterial competition shapes polymicrobial communities

The composition of polymicrobial communities is partly driven by interbacterial competition to occupy a shared niche¹. Bacteria display a vast range of competitive phenotypes designed to control space and nutrients by either (passively) exploiting resources away from or (actively) interfering with others' lifestyles². Diffusion strategies such as the secretion of siderophores, hydrolytic enzymes, or antibiotics can affect other cells' fitness in close range or at a distance^{1,2}. On the other hand, contact-mediated mechanisms such as contact-dependent inhibition and membrane exchange prioritize hyper-local competition against neighboring microbes. The emergence of competitive phenotypes affecting multiple scales of bacterial communities indicates that competition is an essential feature of polymicrobial life². Thus, defining how competition mechanisms are used and regulated is key to understanding bacterial fitness and evolution in native contexts.

Type VI secretion systems facilitate selective interbacterial competition

The transfer of proteins, nucleic acids, and other molecules between microbial cells aids competition by affecting other cells' behavior³. Many bacteria employ secretion systems to transport molecules from their cytoplasm to locations such as other cell compartments, the extracellular milieu, or inside neighboring cells^{3,4}. At least ten secretion systems have been described for Gram-negative bacteria, which leverage their tripartite cell envelopes to transfer molecules with varying specificity⁵. Two-step secretion apparatuses use separate transporters in the inner and outer membranes (IM

and OM, respectively) to progressively move molecules through the cell envelope. For example, IM transporters like the Sec and Tat pathways transfer proteins from the cytoplasm into the periplasm using specific signal peptides which limit the types of proteins that can be secreted. Then, OM-embedded secretion systems like the Type II or Type V secretion systems move these periplasmic proteins outside the cell³⁻⁵. By contrast, one-step secretion systems like Type I directly transfer molecules from the cytoplasm to outside the cell using a single apparatus that crosses both the IM and OM^{3,4}.

Some single-step secretion systems facilitate transport across three lipid membranes, thus allowing bacteria to directly deliver molecules into neighboring cells. For example, nearly 25% of Gram-negative bacteria encode Type VI secretion systems (T6SS)⁶ which can be used to compete with other microbes and eukaryotic cells for focused niche selection⁷, virulence⁸, or DNA acquisition⁹. T6SSs are contractile nanomachines that inject protein toxins (“effectors”) directly into other cells at close range. Bearing structural and genetic similarity to contractile phage tails, a T6SS is composed of a spike-tipped proteinaceous tube which is filled with effectors, and surrounded by a contractile sheath^{10,11}. Some effectors also bind to the outward-facing spike-tip. Anchored to a baseplate in the IM and a membrane complex which spans the periplasm, the T6SS is assembled internally and can extend nearly the entire length of the donor cell¹². Upon activation, conformational changes in the membrane complex and baseplate prime the T6SS for access to the surface of the donor cell¹³. Then, the sheath contracts to push the spiked tube through to the recipient cell, where effectors

are released¹¹. The lifecycle of the T6SS is resolved through regulated disassembly and recycling of sheath and membrane-bound components in the donor cell which may be used for subsequent T6SS assemblies^{13,14}.

The principles for selectivity and target range among the wide variety of bacteria that use T6SS remain an open question. A major regulatory factor for T6SS selectivity is the stimulation of its activity. Some bacteria, such as *Vibrio cholerae* (V52), maintain a constitutively active T6SS which is insensitive to the behaviors of its neighbors¹⁵. By contrast, *Pseudomonas aeruginosa* (PAO1) harbors three T6SSs with activities that are controlled by transcriptional, post-transcriptional, and post-translational regulation tied to unique stimuli¹⁶. T6SS effector activities also play a critical role in selective T6SS toxicity. At least nine functional categories of effectors have been characterized which target cytoplasmic or periplasmic recipient cell features¹⁷. Cytoplasmic effectors disrupt/degrade DNA, proteins, protein synthesis, amino acid metabolism, and cell division. Periplasmic effectors interrupt the cell wall to destabilize the structural integrity of the cell envelope. Given the apparent diversity of effector types, T6SS-encoding bacteria may leverage multiple effectors to increase the system's overall toxicity, offer conditional toxicity, provide synergistic toxicity, or overcome recipient resistance mechanisms¹⁸.

Pseudomonas aeruginosa* deploys Tae1 from its H1-T6SS to kill *Escherichia coli

The opportunistic human pathogen *Pseudomonas aeruginosa* (*Pae*) harbors an interbacterial T6SS, called the Hcp1 secretion island I-encoded T6SS (H1-T6SS),

which is adept at killing *Escherichia coli* (*Eco*)¹⁹⁻²². The competition between these two genetically tractable species is an important model system for our molecular understanding of T6SS regulation and utility. Key to the toxicity of *Pae*'s H1-T6SS is its cocktail of seven effectors, which target the cell wall, phospholipids, nucleotide signaling, and protein translation^{11,12}. By delivering a diverse cocktail of effectors, the H1-T6SS achieves both lytic and bacteriostatic effects in recipients which could be difficult to overcome via multi-effector resistance. Despite this diverse targeting strategy, one cell wall-degrading effector called T6S amidase effector 1 (Tae1) plays a dominant role in the ability of *Pae*'s H1-T6SS to kill *Eco* by explosive lysis. Tae1 promotes *Eco* lysis by degrading peptidoglycan (PG), a structural component of the cell wall that is essential for most bacterial lifestyles²¹.

PG targeting is a powerful strategy for targeting recipient bacteria among T6SS-encoding organisms. Tae1 is a member of a superfamily of four phylogenetically distinct, PG-targeting T6SS effector types (Tae1-4) that each target different chemical bonds in the PG structure^{23,24}. T6SS-containing organisms can encode multiple *tae* genes, suggesting that the diversity and distribution of these effectors may be optimized for target selection and toxic efficacy. As H1-T6SS encodes both Tae1 and another cell-wall degrading effector, T6S glycoside hydrolase effector 1 (Tge1)²⁵, the presence of multiple PG targeting strategies in *Pae* underscores the importance of cell wall identity to bacterial viability.

Biochemical specificity for *Eco* PG is key to Tae1 toxicity

PG is a major defining feature in Gram-negative cell envelopes²⁶. Sandwiched between the IM and OM, PG is a mesh-like polymeric macromolecule that enforces cellular shape and provides mechanical support against internal turgor pressure. The minimal unit of *Eco* PG is a disaccharide of N-acetylmuramic acid (MurNAc) and N-acetylglucosamine (GlcNAc) connected by a beta-1,4 glycosidic bond²⁷, plus a MurNAc-bound peptide stem which in *Eco* is composed of L-alanine (L-Ala), D-glutamic acid (D-Glu), meso-diaminopimelic acid (*mDAP*), and two D-alanines (D-Ala). This pentapeptide monomer is polymerized into polysaccharide chains (glycans) which are variable in length and wrap circumferentially around the cell²⁷. Once incorporated, pentapeptide monomers are matured into dimers, trimers, and tetramers via interpeptide crosslinks between position 4 D-Ala of a donor peptide and position 3 *mDAP* of an acceptor peptide (4,3-crosslinks). This connects the glycan strands into a contiguous network (sacculus)²⁸. When PG is damaged or degraded, bacteria become extremely vulnerable to changes in environmental osmolarity that disrupt intracellular homeostasis and can cause lytic death by membrane disruption²⁹.

Early efforts to understand the basis of Tae1 toxicity focused on its biochemical specificity for PG *in vitro*. Tae1 is defined by its selective digestion of D-Glu-*mDAP* peptide bonds found in PG from Gram-negative bacteria such as *Eco* and *Pae*^{24,21}. Modulating Tae1's ability to interact with PG is thus a powerful regulator of its efficacy. For example, *Pae* encodes a species-specific cognate immunity protein against Tae1 called Tai1 (T6S amidase immunity protein 1) which protects against the toxin by

binding and occluding the Tae1 active site from accessing its substrate³⁰⁻³². Similarly, chemical modifications to PG can slow or arrest Tae1 hydrolysis kinetics on isolated muropeptides³³, indicating that target specificity is a driver of the enzyme's catalytic efficiency. PG remodeling that masks Tae1-targetable peptides can also immunize *Acinetobacter baumannii* against lysis by Tae1 *in vivo*³⁴. These observations support the hypothesis that Tae1 toxicity is borne out of its recognition of chemical features inherent to PG found in bacteria that *Pae* naturally antagonizes with T6SS. Thus, a parsimonious explanation for Tae1-mediated lysis is that bacteria with more Tae1-targetable PG moieties are more susceptible to mechanical disruption by Tae1 hydrolysis, and thus more likely to lyse.

Eco susceptibility to T6SS is also dependent on non-immunity protein defenses

Biochemical specificity is necessary, but not sufficient, to understanding the efficacy of T6SS competition against a specific recipient bacterium. For example, the Gram-positive bacterium *Bacillus subtilis* has an identical PG composition to *Escherichia coli* and can be digested by Tae1 *in vitro*, but *B.subtilis* cells cannot be efficiently overcome by T6SS or Tae1 *in vivo*²¹. This demonstrates that the presence or absence of an effector's substrate may not clearly indicate recipient susceptibility in T6SS competition. Another requirement for Tae1 toxicity is its compartmentalization to the periplasmic space in Gram-negative cell envelopes; neither cytoplasmic nor extracellular localized Tae1 allows for the direct PG access required to render sufficient damage for lysis²¹. Thus, the utility of Tae1 as a toxin *in vivo* depends not only on PG composition, but also on the cellular and physiological contexts surrounding the Tae1:PG interaction.

Recent works on other T6SS systems have also found that recipient cells may actively regulate effector toxicity using dynamic, nonspecific stress responses. *Eco* detects and responds to damage from the *V. cholerae* (V52) T6SS effectors TseH (a muramidase)³⁵ and TseL (a lipase)³⁶ by upregulating the envelope stress responses Rcs and BaeSR, suggesting that *Eco* could counter effector-mediated damage to the cell envelope by fortifying its surface. Similarly, *Bacillus subtilis* triggers protective sporulation in response to a *Pseudomonas chlororaphis* (PCL1606) T6SS effector, Tse1 (a muramidase)³⁷. Additional recipient-cell coordinators of T6SS effector toxicity include reactive oxygen species³⁸ and glucose-dependent gene expression³⁹. These studies demonstrate that T6SS effector toxicity *in vivo* may be dependent on multiple factors, including direct substrate interactions alongside dynamic and responsive features of recipient cells.

Intrinsic determinants of *Eco* susceptibility to Tae1 *in vivo*

Currently, we understand little about how Tae1 specifically interfaces with the living *Eco* cell to induce lysis. The cell wall is a complex and dynamic substrate that is actively regulated to protect the cell^{40–45}, yet *Eco* is highly susceptible to lysis by Tae1 *in vivo*. We therefore hypothesized that Tae1 activity promotes H1-T6SS-mediated lysis in *Eco* through a unique strategy to overcome neutralization by the recipient cell. In this project, I investigated the *Eco* cellular features that drive its intrinsic sensitivity to H1-T6SS and Tae1 during interbacterial competition with *Pae*. In Chapter 2, I describe how I used conditional gene knockdowns to screen the entire complement of essential *Eco* genes

for the most physiologically-relevant Tae1 susceptibility determinants. While cell wall-related genes indeed impact *Eco* susceptibility to Tae1, I also discovered a strong relationship between survival and another component of the cell envelope, lipopolysaccharide (LPS). Perturbation of LPS synthesis genes *msbA* and *lpxK* rendered *Eco* conditionally resistant to lysis by Tae1 from *Pae*. In Chapter 3, I describe the work done to show that LPS-related resistance was mediated through cell-biological processes that were independent of the biochemical Tae1–PG interaction. These findings suggest that beyond biochemical specificity and adaptive stress responses lies a role for essential homeostatic processes in defining T6SS effector toxicity *in vivo*.

Chapter 2: Essential lipopolysaccharide genes drive intrinsic susceptibility to Tae1 in *Eco*

INTRODUCTION

Pae outcompetes *Eco* using its H1-T6SS, and its toxicity is largely dependent on the activity of the PG-degrading effector Tae1²¹. The biochemical specificity of Tae1 for D-Glu-*m*DAP peptide bonds drives its ability to both hydrolyze *Eco* PG and lyse cells^{22,34}. However, studies concerning other T6SS toxins have demonstrated that effector toxicity *in vivo* is driven not only by its enzymology, but also by active surveillance, repair, defense, and compartmentalization by recipient cells that can influence its activity *in vivo*^{30,35,36,46,47}.

In this study, we designed a genetic screen to search for genetic determinants of *Eco* susceptibility to Tae1 to better understand the contextual features that could enable, defend against, or synergize with the toxin's cell-wall degrading activity to trigger lysis in *Eco*. Most genetic screening approaches are designed to test nonessential genes, which are more easily interrupted without significant fitness effects to the cell. However, previous efforts to screen for T6SS effector fitness determinants in recipients have yielded nonessential candidate genes with indirect or unclear physiological links to the function of the toxin studied^{46,48}. We reasoned that because most types of T6SS effectors directly interfere with *essential* cellular structures and processes, screening essential genes would yield meaningful genetic interactions with Tae1. Thus, we designed our screen to test essential genes and maximize the probability of identifying physiologically-relevant candidate genes for fitness against Tae1 in *Eco*.

At UCSF, researchers in the lab of Carol Gross pioneered a novel genetic screening approach in *Eco* which leverages an engineered version of a clustered randomly interspaced palindromic repeat (CRISPR) system from *Streptococcus pyogenes*. This CRISPR interference (CRISPRi) system introduces an inducible gene depletion module into the *Eco* chromosome to facilitate stable, tunable knockdowns of native genes^{49–51}. As it does not constitutively interrupt gene expression, CRISPRi can be used to modulate both non-essential and essential gene expression. Here, we adapted the Gross lab's CRISPRi collection in *Eco* to interbacterial competitions against *Pae* to determine if selective depletion of essential *Eco* genes impacted fitness against Tae1 as delivered by H1-T6SS.

RESULTS

Adaptation of native T6SS competitions to study *Eco* susceptibility to Tae1

We developed an *in vivo* screen for genetic interactions between the cell wall-degrading H1-T6SS effector Tae1 from *Pae* and the model target bacterium *Eco*. Our screen had two fundamental design requirements: (1) the ability to distinguish between general (T6SS-dependent) and specific (Tae1-dependent) genetic interactions, and (2) the capacity to test a broad array of target cell features. We adapted an established interbacterial competition co-culture assay between H1-T6SS-active *Pae* and *Eco*, the outcome of which is sensitive to the specific contribution of Tae1²¹. In this assay *Eco* exhibits a greater fitness advantage when competed against *Pae* missing *tae1* (*Pae*^{Δ*tae1*}) relative to an equivalent control strain (*Pae*^{WT}) (**Figure 2.1a**). We hypothesized that the *Pae*:*Eco* co-culture assay could be leveraged to quantitatively

compare recipient cell fitness against both Tae1 (toxin-specific fitness) and the H1-T6SS (Tae1-independent fitness) in interbacterial competition.

To screen broadly for *Eco* determinants, we adopted an established *Eco* CRISPR interference (CRISPRi) platform that generates hypomorphic mutants through intermediate gene expression knockdowns (KDs)⁵⁰. In contrast to knock-out or transposon mutagenesis approaches, CRISPRi is amenable to essential genes and thus provided an opportunity to make unique insights about genes that are typically challenging to screen for. This includes many essential (or conditionally essential) genes related to peptidoglycan (PG) metabolism, whose KDs we predicted would impact Tae1 toxicity. In this CRISPRi system, inducible sgRNA expression is coupled with constitutive dCas9 expression to conditionally repress transcription at specific loci with and without induction (“induced” and “basal” CRISPRi, respectively) (**Fig. 2.2a**). In total, our CRISPRi collection was composed of 596 *Eco* strains with KDs representing most cellular functions as defined by the NCBI clusters of orthologous genes (COG) system (**Fig. 2.2b**). Our collection also included 50 negative control strains with non-targeting sgRNAs, including *rfp-KD*, to ensure CRISPRi alone did not impact inherent *Eco* susceptibility to *Pae* (**Fig. 2.3a**).

For the interbacterial competition screen, we co-cultured *Pae* with the pooled *Eco* CRISPRi collection to test competitive fitness across all KD strains in parallel (**Fig. 2.1b**). To compare Tae1-dependent and -independent fitness determinants, we conducted screens against H1-T6SS-active *Pae* strains that either secrete Tae1

(*Pae*^{WT}; Δ *retS* Δ *pppA*) or are Tae1-deficient (*Pae* ^{Δ *tae1*}; Δ *retS* Δ *pppA* Δ *tae1*). As negative controls, we also competed the *Eco* collection against a genetically H1-T6SS-inactivated *Pae* strain (*Pae*^{*inactive*}; Δ *retS* Δ *pppA* Δ *icmF*) and included a condition in which the collection was grown without *Pae* present (*Eco*^{*ctrl*}). Experiments were performed under both induced and basal CRISPRi conditions to distinguish between general *Eco* fitness changes and those due to transcriptional knockdown. We used high-throughput sequencing to quantify KD strain abundance at the beginning and end of each six-hour competition. To understand the contribution of each KD to *Eco* survival against *Pae* in the presence or absence of H1-T6SS or Tae1, we calculated log₂ fold-change (L2FC) values for each KD strain after competition and normalized against abundance after growth without competition (*Eco*^{*ctrl*})^{52,53}. Across four biological replicates per condition, L2FC values were reproducible (**Fig. 2.4a**; median Pearson's *r* between all replicates = 0.91). L2FC was used as a proxy for competitive fitness of KD strains across different competition conditions.

To determine if our screen was sensitive to the effects of Tae1, H1-T6SS, and CRISPRi, we conducted a principal component analysis of L2FC values for each strain under every competition condition (**Fig. 2.1c**). We observed clear separation of datasets by CRISPRi induction (induced versus basal) across the first principal component (PC1; 85.41%), indicating that KD induction was a major contributor to the performance of the KD library in the pooled screen. We also observed clustering of datasets according to *Pae* competitor (PC2; 2.66%). These results indicate that each *Pae* competitor yielded a distinct effect on the fitness of the CRISPRi library and demonstrates that our screen

was sensitive to the presence (Pae^{WT}) or absence ($Pae^{\Delta tae1}$) of Tae1 delivery from H1-T6SS. From these data we conclude that our screen successfully captured the unique impacts of CRISPRi, Tae1, and H1-T6SS on pooled *Eco* CRISPRi libraries during interbacterial competition.

CRISPRi reveals toxin-specific and non-specific determinants of *Eco* fitness against H1-T6SS

To reveal specific *Eco* genes that shape intrinsic susceptibility to H1-T6SS-mediated antagonism, we identified KD strains which were significantly depleted or enriched at least three-fold ($L2FC \leq -1.585$ for depletion or $L2FC \geq 1.585$ for enrichment, and $-\log_{10} p\text{-adj} \leq 0.05$) after competition against Pae^{WT} , $Pae^{\Delta tae1}$, or $Pae^{inactive}$. Our goal was to prioritize KDs which had a unique effect on fitness against Pae^{WT} relative to conditions lacking Tae1. With CRISPRi induced, we found a select cohort of KDs with significant loss of fitness ($n=12$) or gain of fitness ($n=11$) against Pae^{WT} (**Fig. 2.5a**). We were surprised that some KDs caused resistance to Tae1 despite the combined challenge of essential gene depletion and H1-T6SS antagonism.

Competition against Pae^{WT} with basal CRISPRi diminished the pool of significant candidate KDs (**Fig. 2.6a**), reinforcing our observation that KD strains' fitness changes against *Pae* are dependent on CRISPRi induction. Against $Pae^{\Delta tae1}$ (CRISPRi induced), we observed seventeen KDs with significant fitness changes (**Fig. 2.5b**) which were also CRISPRi-dependent (**Fig. 2.6b**). These KDs were mostly distinct from those that affected *Eco* fitness against Pae^{WT} (**Fig. 2.5c**). These results indicate that the presence

or absence of Tae1 had a unique effect on the T6SS competition and thus had a distinct impact on KD fitness. Finally, we found few candidate KDs that affected fitness against *Pae*^{inactive} regardless of CRISPRi induction condition (**Fig. 2.7a-b**), suggesting that most significant phenotypes were H1-T6SS-dependent, if not Tae1-dependent. In fact, L2FC values in *Pae*^{inactive} and *Eco*^{ctrl} datasets had high correlation (**Supp. 2.7c-d**, median Pearson correlation $r = 0.98$), indicating that *Pae* is a neutral co-culture partner with its H1-T6SS inactivated.

With our interest in Tae1-specific determinants, we focused our attention on the 20 KDs which had a unique effect on *Eco* fitness against Tae1 (*Pae*^{WT} +CRISPRi induced; **Table 2.1**). Most KDs in this group targeted genes related to the cell envelope (COG category M: cell wall/membrane/envelope biogenesis, $n=13/20$). Composed of concentric layers of inner membrane (IM), cell wall PG, outer membrane (OM), and lipopolysaccharide (LPS)⁵⁴(**Fig. 2.8a**), the cell envelope is a critical structure for protecting *Eco* against environmental stress. Tae1-sensitized strains were dominated by gene targets related to the synthesis of PG (*murA*, *ftsI*, *murC*, *murl*, *mrcB*, *murJ*). Given that Tae1 targets the cell wall, these results support our initial hypothesis that PG structural integrity or composition are direct determinants of Tae1 susceptibility. In addition, we were surprised to find most KDs that rendered *Eco* resistant to *Pae*^{WT} were related to LPS and lipid membrane synthesis. Tae1 is not known to directly interact with membranes as part of its molecular mechanism. However, metabolic crosstalk does occur between the PG, LPS, and lipid biosynthesis pathways^{44,55}. Thus, our data raised the possibility that regulation of other cell envelope structures could also be implicated in mediating cell wall attack.

msbA-KD disrupts LPS biosynthesis and affords resistance to Tae1

To investigate the hypothesis that non-PG components of the cell envelope may also shape Tae1 toxicity, we focused downstream studies on Tae1-resistant KDs related to the synthesis of LPS, an essential lipidated surface sugar that offers protection and structure to the OM⁵⁶. Candidate KDs targeted highly-conserved, essential genes in Kdo₂-Lipid A synthesis (*lpxA*, *lpxK*, *kdsB*, *waaA*, *msbA*) (**Fig. 2.8a**). Kdo₂-Lipid A synthesis is the most-upstream arm of LPS biosynthesis with rate-limiting control over the entire pathway^{57,58}. In our screen, the strongest resistance phenotypes we observed were in KDs targeting *lpxK* (*lpxK_-1as* and *lpxK_32as*) (**Table 2.1**). LpxK is a kinase that phosphorylates the Lipid-A intermediate tetraacyldisaccharide 1-phosphate to form Lipid IV_A^{59,60}. In *Eco*, *lpxK* is in an operon with *msbA* (**Fig. 2.8b**), which encodes the IM Kdo₂-Lipid A flippase MsbA^{61,62}. A KD of *msbA* (*msbA_40as*) also conferred resistance to *Pae*^{WT} in our screen (**Table 2.1**).

We first experimentally validated pooled screen results by individually testing *lpxK-KD* and *msbA-KD* fitness in binary competitions against *Pae*. We regenerated and validated KD strains for *lpxK* (*lpxK_-1as*; “*lpxK-KD*”) and *msbA* (“*msbA-KD*”) for use in these experiments (**Fig. 2.9**). Consistent with our screen, *msbA-KD* gained Tae1-specific resistance in H1-T6SS-mediated competitions (**Fig. 2.8d**), exhibiting loss of sensitivity to *Pae*^{WT} relative to *Pae*^{Δ*tae1*}. In contrast, we could not validate Tae1 resistance for *lpxK-KD* (**Fig. 2.8e**). Like *rfp-KD* (**Fig. 2.8c**), *lpxK-KD* maintains sensitivity to *Pae*^{WT} relative to *Pae*^{Δ*tae1*}. The gene expression of *msbA* and *lpxK* are co-dependent, so we were surprised that *msbA-KD* and *lpxK-KD* did not equally reproduce Tae1 resistance.

However, CRISPRi-dependent phenotypes could be controlled by factors such as transcriptional polar effects or off-target CRISPRi effects. To address their phenotypic disparities, we quantified transcriptional KD efficacy and specificity for *lpxK-KD* and *msbA-KD* with qRT-PCR. For *msbA-KD* with CRISPRi induced, we found repression of *msbA* (29-fold), *lpxK* (15-fold), and *ycaQ* (3.6-fold) expression (**Fig. 2.9a**). Thus, owing to downstream polar effects, our *msbA-KD* strain is a KD of both LPS candidate genes, *msbA* and *lpxK*. Conversely, *lpxK-KD* only repressed *lpxK* (71-fold) and *ycaQ* (11-fold) (**Fig. 2.9b**), but not *msbA*. Therefore, *msbA-KD* and *lpxK-KD* yield distinct transcriptional consequences despite targeting the same operon using CRISPRi.

Next, we investigated phenotypic consequences of inducing CRISPRi in *msbA-KD* and *lpxK-KD* by comparing their cellular morphologies with cryo-electron tomography. Disruption of *msbA* and *lpxK* typically leads to structural deformation in the *Eco* cell envelope from aberrant accumulation of Kdo₂-Lipid A intermediates in the IM^{60,62,63}. Unlike *rfp-KD* negative control cells (**Fig. 2.8f**), *msbA-KD* cells developed irregular buckling in the IM and OM (**Fig. 2.8g**, red arrows). We also observed vesicular or tubular membrane structures within the cytoplasm (**Fig. 2.8g**, blue arrows). Such structural abnormalities are consistent with physical crowding of Kdo₂-Lipid A intermediates in the IM that are relieved by vesicular internalization. On the other hand, while *lpxK-KD* had a distended IM and vesicles (**Fig. 2.8h**, red and blue arrows), the OM appeared smooth and regular. This phenotypic divergence points to two distinct KD effects: defects in the IM (both *msbA-KD* and *lpxK-KD*) and defects in the OM (*msbA-KD* only). Together with our transcriptional analyses, these results demonstrate that

msbA-KD and *lpxK-KD* have unique consequences for LPS integrity and Tae1 susceptibility despite targeting the same operon. We focused the remainder of our study on the validated *msbA-KD* strain which damages the IM and OM.

Tae1 resistance is independent of LPS biosynthesis master-regulator LpxC

LPS synthesis is constitutively active and rate-limited by the activity of the deacetylase LpxC, which itself is negatively regulated by the protease FtsH^{64,65}. We were surprised to see that knockdowns in neither *lpxC* nor *ftsH* had a strong fitness phenotype in our screen, despite their master-regulatory roles. Indeed, when we tested target gene KD efficiency for *lpxC-KD* and *ftsH-KD*, we found that both were unable to repress the transcription of their respective target gene (**Fig. 2.10a-b**). We suspected that the critical roles of these enzymes for *Eco* would render their CRISPRi strains susceptible to suppressor mutations or reversions that override the CRISPRi module. By Western blot analysis of dCas9 expression after inducing CRISPRi, we saw that neither *lpxC_62as* nor *ftsH_14as* express appreciable levels of dCas9 relative to *rfp_124as* (**Fig. 2.10c**), suggesting that a compensatory mutation of dCas9 affecting its expression may be responsible for knockdown deficiency. Therefore, we were unable to study *lpxC* or *ftsH* using CRISPRi.

Using an orthogonal approach, we tested if resilience against lysis by Tae1 could be achieved by chemical inhibition of LpxC alongside exogenous Tae1 overexpression. Growing *Eco* in media containing a sub-MIC concentration of an LpxC chemical inhibitor, PF 05081090, induces a growth defect consistent with the interruption of LPS

biosynthesis (**Fig. 2.10f**)^{66,67}. Exogenous, periplasmic Tae1^{WT} overexpression causes population-level lysis (**Fig. 2.10d**) which can be rescued by overexpression of a catalytic mutant, Tae1^{C30A} (**Fig. 2.10e**). We observe that PF05081090 pre-treatment has an additive effect on Tae1-mediated lysis, indicating that LpxC inhibition sensitizes *Eco* to Tae1^{WT}. These data demonstrate that chemical inhibition of LPS biosynthesis is not sufficient to orthogonally validate the Tae1 resilience we observed in *msbA-KD*. The relationship between LPS biosynthesis and Tae1 sensitivity may therefore only concern portions of the LPS biosynthesis pathway downstream of the master regulator *lpxC* (including *msbA*, *lpxK*, *kdsB*, and *waaA*).

Wildtype *Eco* downregulate Lipid-A biosynthesis genes during Tae1 attack

Given their strong connection to Tae1 susceptibility, we were motivated to understand how native *msbA* and *lpxK* regulation translated to Tae1 susceptibility in wildtype *Eco*. We performed qRT-PCR analysis of *ycaI-msbA-lpxK-ycaQ* transcription during Tae1 overexpression in *Eco* parent strain BW25113. We found that each gene in this operon was downregulated during Tae1^{WT} overexpression, with *msbA* and *lpxK* being the most strongly downregulated (**Fig. 2.11a**). This recapitulated the transcriptional knockdown we observed in *msbA-KD*. In comparison, Tae1^{C30A} did not trigger this operon-level knockdown, but it did perturb *lpxK* and *ycaQ*. This observation suggests that transcriptional regulation in this operon is sensitive to relative Tae1 activity. Similarly, transcription of the LPS master regulator *lpxC* was specifically repressed with Tae1^{WT} overexpression, but not with Tae1^{C30A} expression (**Fig. 2.11b**). Thus, wildtype *Eco* intrinsically downregulates the expression of LPS genes in response to Tae1^{WT}

hydrolysis. This behavior is similar to the transcriptional profile in *msbA-KD*, indicating that downregulation of *msbA* and *lpxK* may be part of a natural stress response to Tae1 exposure. However, *msbA-KD* may be effective at resisting Tae1-dependent lysis because CRISPRi knockdown triggers LPS repression and its associated phenotypes in advance of Tae1 exposure.

Finally, we tested if intrinsic transcriptional regulation of Lipid A genes in response to Tae1 also translated to the natural T6SS competition setting. We assayed the transcriptional regulation of *msbA*, *lpxK*, and *lpxC* in wildtype *Eco* during competition with *Pae* (*Pae*^{WT}, *Pae*^{Δ*tae1*}, *Pae*^{inactive}). We did not observe specific changes in *msbA* and *lpxK* transcription under any competition condition (**Fig 2.11c-d**). However, *lpxC* transcription is downregulated in competition with *Pae*^{WT} (**Fig 2.11e**), suggesting that LPS regulation may indeed be directly implicated in the survival of *Eco* that are targeted by Tae1 during T6SS competition.

DISCUSSION

To effectively discover *Eco* genes that contribute to its sensitivity to H1-T6SS and Tae1, our genetic screen required a design that leveraged the unique sensitivity *Eco* has to Tae1-dependent lysis. A major advantage of using CRISPRi in this context was that it allowed for stable, tunable disruption of gene expression which was amenable to H1-T6SS-mediated competition assays. Critically, this system allowed us the unique ability to manipulate and test essential gene functions, which we hypothesized would meaningfully interact with T6SS toxins. An exciting outcome from our study was the

finding that essential KDs related to LPS biosynthesis offer *Eco* a novel resistance to Tae1. As such, the wildtype expression and function of these LPS genes may naturally prime Tae1 sensitivity in interbacterial competition. Our observation that *msbA*, *lpxK*, and *lpxC* transcription is naturally repressed upon exogenous Tae1^{WT} expression also indicates a direct relationship between PG hydrolysis and LPS regulation. The consequences of Tae1-dependent transcriptional regulation of LPS genes remains an open question, as LPS biosynthesis activity is classically regulated post-transcriptionally by proteolysis of LpxC. Nonetheless, the sensitivity of LPS biosynthetic gene expression to Tae1 activity demonstrates that individual cell envelope layers are responsive to each other's integrity during T6SS attack.

One major open question in the T6SS field concerns the mechanisms underscoring the correct localization of T6SS effectors in determining their toxicity. For Tae1, compartmentalization to the periplasm is required to increase the local probability of Tae1:PG interactions³⁰. Blocking the flow of LPS to the OM, as in *msbA-KD*, causes structural damage to the IM and OM which could impede proper Tae1 localization to the periplasmic space. Cytoplasmic vesicles formed by the crowded IM could trap Tae1, thus sequestering it away from its target. Furthermore, impairing LPS disrupts the OM permeability barrier^{68,69}, perhaps allowing Tae1 molecules to leak into the environment and away from PG. Given the highly-expressed endogenous Tae1 overexpression system we used, a toxin-sequestration hypothesis may not be a major contributor to the *msbA-KD* resistance phenotype. However, in native H1-T6SS competition, it is possible that fewer than a hundred effectors of each type may be delivered in a single injection

due to the limited cargo capacity of the T6SS itself^{70,71}. Therefore, incorrect compartmentalization of Tae1 at low copy-numbers via damaged membranes may have a significant effect on its toxicity *in situ*. Future work may concern the role of membrane integrity as it relates to periplasmic T6SS effector compartmentalization and efficiency.

Given that Tae1 is a PG-degrading enzyme, the emergence of PG-related essential genes with KDs that sensitize *Eco* to Tae1 was a reassuring control. These results indicate that perturbation of the cell wall amplifies the toxicity of Tae1, perhaps by generating a weakened PG substrate which is more sensitive to lysis. We identified multiple *mur* genes (*murA*, *murI*, *murJ*), whose KDs sensitized *Eco* to Tae1 in competition. Mur enzymes are essential, constitutive IM proteins that assemble the fundamental muropeptide monomer unit of PG and transport it to the periplasm.

Fosfomycin, an epoxide antibiotic targeting *murA*, sensitizes *Eco* to lysis by blocking the first step in PG synthesis and thus interrupting constitutive cell wall maintenance^{72,73}.

KDs which interrupt the *mur* pathway could also sensitize *Eco* to lysis by blocking the flow of muropeptide intermediates to sites of nascent PG incorporation. Tae1 hydrolysis could thus trigger lysis more readily by damaging a PG substrate which, as a result of the *mur* KDs, cannot be replaced or repaired.

We also identified *mrcB* (PBP1B) and *ftsI* (PBP3) as PG genes whose KDs sensitize *Eco* to Tae1. These IM- localized enzymes are involved in the synthesis and maturation of PG in the assembled sacculus. PBP1B is a bifunctional PG synthase that constitutively assembles nascent glycan strands (transglycosylase) and forms structural

crosslinks (transpeptidase), while PBP3 is a transpeptidase that remodels septal PG during cell division⁷⁴. PBP1B and PBP3 have been shown to form an IM-bound complex at the septum during cell division, thus demonstrating how PG synthesis can be spatially regulated for coordinated synthesis and remodeling⁷⁵. Antibiotic disruption to PBP1B renders *Eco* sensitive to lysis, while disruption of PBP3 blocks cell division and triggers filamentation⁷⁶. As both *ftsI-KD* and *mrcB-KD* sensitize *Eco* to competitors including Tae1, our screen indicates that disrupting cell wall synthesis and cell division can enable lysis by further Tae1-mediated damage. As such, PG integrity and its relationship to growth and division are key elements to understanding the intrinsic sensitivity of *Eco* to Tae1.

In conclusion, our screen demonstrates that the essential LPS and PG biosynthesis pathways contribute to the intrinsic sensitivity of *Eco* to Tae1 as delivered by H1-T6SS. By exclusively studying Tae1 in the native context of live *Eco*, we developed a nuanced understanding that toxin: substrate biochemistry operates alongside homeostatic cell biology features to determine survival against T6SS. LPS and PG diverge from other T6SS susceptibility determinants in that they are highly-conserved across Gram-negative bacteria and thus could be pan-species determinants of toxin sensitivity. An exciting prospect for future studies may involve understanding if Tae1 sensitivity can be tuned in other T6SS recipient species by modulation of their LPS or PG activity. Furthermore, there may also be value in assessing the relationship between recipient cell envelope pathways and other T6SS toxins, particularly those that also target the cell envelope (e.g. PG muramidases and membrane lipases). With an emerging interest in

integrative approaches to understanding the T6SS interaction, our interbacterial competition screening approach may be amenable to studies of effector activities *in vivo* including multi-effector synergy and specialization of T6SS target species ranges.

METHODS

Bacterial growth and selection

Escherichia coli strains were cultured in LB or LB-no salt (LBNS) at 37°C with orbital shaking. *Pseudomonas aeruginosa* strains were cultured in LB+ 0.01% Triton at 37°C with orbital shaking. Interbacterial competitions between *Eco* and *Pae*, and all *Eco* assays requiring solid growth, were conducted on LB+agar or LBNS+agar plates at 30°C. Where necessary, bacterial strains and plasmids were selected for growth using the following antibiotics: carbenicillin (Carb; 50 µg/ml) (Grainger), chloramphenicol (Chl; 25 µg/ml) (MP Biomedicals), gentamicin (Gent; 50 µg/ml)(Alfa Aesar), irgasan (Irg; 25 µg/ml) (Sigma-Aldrich), trimethoprim (Trm;15 µg/ml) (Sigma-Aldrich), or kanamycin (Kan; 50 µg/ml.) (VWR).

Eco CRISPRi library construction and use

The *Eco* CRISPRi collection was received in pooled format as a gift from the laboratory of Carol Gross (UCSF). CRISPRi strains were derived from K12 strain BW25113⁷⁷ and are each engineered with a chromosomal insertion of *dcas9* (constitutive expression) and a custom sgRNA sequence for inducible dCas9-mediated knockdown of a single gene-of-interest⁵⁰. Transcriptional knockdown is induced with addition of 100µM IPTG (“induced”) into growth media, though growth without inductant also results in a mild knockdown phenotype (“basal”)⁵⁰. Except where indicated, CRISPRi knockdown is induced in this study. CRISPRi strains *msbA-KD* and *lpxK-KD* were reconstructed from the parent strain for individual use in this study. Reconstructed strains were validated by Sanger sequencing (of the sgRNA and dCas9 chromosomal inserts), qRT-PCR (for

knockdown efficiency), and Western blot (for dCas9 expression). See **Table 2.2** for strain descriptions and **Table 2.3** for primer sequences used for construction and validation.

***Pae* strain construction**

Pae ^{Δ tae1} (Δ retS Δ pppA Δ tae1; *clpV*-GFP) and *Pae*^{inactive} (Δ retS Δ pppA Δ icmF; *clpV*-GFP) strains were constructed from biparental mating of parent strain *Pae*^{WT} (B515: PAO1 Δ retS Δ pppA; *clpV*-GFP)¹⁴ with *Eco* SM10 λ pir⁷⁸ bearing suicide vector pEXG2 cloned with homology to the gene(s) of interest and a spacer sequence for replacement. pEXG2 plasmids were cloned using splice-overlap extension³⁰. After mating, transformants were isolated by negative selection on LB-agar + 5% sucrose and confirmed as scarless knockout mutants by colony PCR of the locus of interest. See **Table 2.2** for strain descriptions and **Table 2.3** for primer sequences used for construction and validation.

Pooled interbacterial competition screen

Competition assays were performed with overnight *Pae* cultures (*Pae*^{WT}, *Pae* ^{Δ tae1}, *Pae*^{inactive}) and pooled *Eco* CRISPRi libraries. Flash-frozen glycerol stocks of *Eco* pools were resuspended in LB, back-diluted to OD₆₀₀=0.25, and recovered for 90 minutes at 37°C with shaking. All cultures were washed twice with fresh LB, then OD₆₀₀-adjusted to 2.0 (for *Pae*) or 1.0 (for *Eco*) in either LB (basal CRISPRi) or LB+100 μ M IPTG (induced CRISPRi). An aliquot of each CRISPRi pool was reserved by pelleting and flash-freezing for sequencing-based analysis of strain abundances in the starting population.

Media-matched *Pae* and *Eco* were mixed at a 1:1 volumetric ratio, except for *Eco*^{ctrl} populations (for which *Eco* pools were not mixed with *Pae*). Six, 10µl aliquots of coculture were applied to nitrocellulose membranes (0.2µm, GVS) atop LB-agar (basal CRISPRi) or LB-agar +100µM IPTG (induced CRISPRi) plates to match liquid media conditions. Covering the agar surface with nitrocellulose allows for nutrient transfer from the media to the bacteria, while aiding in bacterial recovery from the surface after competition. Cocultures were dried down to the membrane under flame-sterilization, then incubated at 30°C for 6h. Cocultures were removed from the plate by scalpel-excision of surrounding nitrocellulose and resuspended into 1ml fresh PBS by bead-beating for 45s on a tabletop vortex. The six aliquots per experiment were pooled, centrifuged (2min at 9000xG, RT), and PBS was decanted. Pellets were flash frozen in liquid nitrogen and stored at -80°C.

Sequencing library preparation

Genomic DNA was extracted from frozen bacterial pellets by phenol: chloroform extraction and RNase treatment⁷⁹, followed by quantification on a Nanodrop 2000 spectrophotometer (Thermo Scientific). PCR amplification was used to isolate *Eco* sgRNA sequences from mixed genomic DNA and to attach Illumina Truseq index adapters for high-throughput sequencing. Sequencing libraries were purified by gel electrophoresis on 8% TBE gels (Invitrogen Novex), stained with SYBR Gold (Invitrogen) to visualize library bands, and scalpel-excised (200-300bp region) under blue light imaging (Azure Biosystems c600). Excised libraries were gel-extracted and precipitated⁸⁰, then resuspended in nuclease-free distilled water (Invitrogen UltraPure).

Library concentration was quantified on a Qubit 2.0 fluorimeter (Invitrogen) using the dsDNA high-sensitivity assay, and assayed for purity on a 2100 Bioanalyzer (Agilent) using the high-sensitivity DNA assay. Single-end sequencing was performed on an Illumina NextSeq 500 using a custom sequencing primer and a read length of 75bp. Multiplexed samples were spiked with 5% PhiX Control v3 DNA (Illumina) to account for low diversity among sgRNA sequences. See **Table 2.3** for custom primers used for library preparation and sequencing.

Sequencing data analysis

Raw FASTQ files were aligned to the library oligos and counted using ScreenProcessing (<https://github.com/mhorlbeck/ScreenProcessing>). Counts were normalized to a total of 20,000,000 reads, pseudocounts of 1 were added, and \log_2 fold change (L2FC) from t0 was calculated for each strain with at least 100 counts at t0. L2FC was further corrected by subtracting the median L2FC of the non-targeting control sgRNAs from that sample⁸¹. The L2FC of each sgRNA were averaged across four biological replicates to calculate the L2FC for that condition. Finally, to account for differences in the number of generations experienced (growth) in each of the experimental conditions, L2FC values for the *Pae*^{WT}, *Pae* ^{Δ tae1}, *Pae*^{inactive} experiments were corrected by the coefficient of a robust (MM-type) intercept free linear regression between the experimental L2FC values and the CRISPRi induction-matched (induced/basal) *Eco*^{ctrl} experiment. See **Table 2.4** for correction coefficients and corrected L2FC values. Differences between conditions were then calculated for each sgRNA as:

$$\text{Diff} = (\text{L2FC } [condition]) - (\text{L2FC } Eco^{ctrl})$$

Final Diff values are listed in **Table 2.5** and were used for all further analyses.

COG analysis

Gene ontology information was compiled from the NIH Database of Clusters of Orthologous Genes (COGs) (<https://www.ncbi.nlm.nih.gov/research/cog>) and reported previously⁵⁰.

Data availability and software

Illumina sequencing data from this study is accessible at the NCBI Sequence Read Archive under accession PRJNA917770. Principal component analysis was performed using R⁸² and visualized using ggplot2⁸³. All other data visualizations were prepared using GraphPad Prism 9.4.1 (GraphPad Software, San Diego, California USA, www.graphpad.com).

Pairwise Interbacterial T6SS competition assay

Competition assays were performed with overnight liquid cultures of *Pae* and *Eco* CRISPRi strains. *Eco* cultures were back-diluted 1:4 in LB-no salt (LBNS; cite) + 100 μ M IPTG and grown for 1h at 37°C with shaking to pre-induce CRISPRi before competition. Strains were washed and mixed in a 1:1 volumetric ratio of *Pae* (OD₆₀₀=2) and *Eco* (OD₆₀₀=1) in LBNS+100 μ M IPTG. Three, 10 μ l aliquots of each liquid co-culture applied to nitrocellulose membranes (0.2 μ m, GVS) atop LB-agar+100 μ M IPTG and dried down by flame-sterilization to encourage interbacterial competition. Cocultures were

incubated at 30°C for 6h. For initial *Eco* colony-forming unit measurements ($CFU_{t=0h}$), 20µl of each liquid co-culture input was serially diluted (10-fold dilutions x 8) in a 96-well plate (Corning) and plated onto LB-agar + Gent (*Eco*-selective). After the competition, coculture spots were harvested from the plate by scalpel-excision of the surrounding nitrocellulose, and pooled by resuspension into 1ml fresh PBS by bead-beating for 45s on a tabletop vortex. Resuspensions were serially diluted (10x8) and plated onto LB+Gent. All serial dilution plates were incubated overnight at 37°C. Dilution plates with approximately 20-200 colonies-per-plate were counted for *Eco* CFU abundance ($CFU_{t=0h}$, $CFU_{t=6h}$). Fold-change in *Eco* CFUs was determined by back-calculating CFUs per ml from dilution plates, and then calculating $CFU_{t=6h}/CFU_{t=0h}$. Experiment was performed for three biological replicates. Statistical test: two-tailed unpaired *t*-test.

qRT-PCR

Overnight cultures of *Eco* were washed and OD_{600} -corrected to 1.0 in LB or LBNS +/- 100µl IPTG. Three, 10µl aliquots of each culture were applied to nitrocellulose membranes (0.2µm, GVS) atop LB-agar+100µM IPTG or LBNS-agar+100µM IPTG and dried down by flame-sterilization. After growing 6 hours at 30°C, the spots were scalpel-excised, pooled, and resuspended into PBS by bead beating, then pelleted for RNA extraction. RNA was extracted using TRIzol Reagent (Invitrogen) with Max Bacterial Enhancement Reagent (Invitrogen), followed by treatment with Turbo DNA-free kit (Invitrogen) to remove contaminating DNA. After quantification by Nanodrop (Thermo Scientific), total RNA was reverse transcribed into cDNA using qScript cDNA Supermix (QuantaBio). A 1:5 dilution of cDNA and custom primers were input into qPCR reactions

with PowerUP SYBR Green Master Mix (Applied Biosystems). qRT-PCR was performed using a QuantStudio 3 Real Time PCR system (ThermoFisher Scientific) using cycling parameters as defined by the master mix instructions. Fold-change in transcript levels was calculated using $\Delta\Delta C_t$ analysis, using *rpoD* as a control gene. Three biological and three technical replicates were used per experiment. Statistical test: two-tailed unpaired *t*-test. Custom primers for qPCR of *Eco* genes can be found in Table 3.

For qRT-PCR analysis of *Eco* gene expression during interbacterial competition, *Pae:Eco* cocultures were prepared as in “Pairwise interbacterial T6SS competition assay” with wildtype *Eco* (BW25113) on LBNS-agar media. After four hours of competition at 30°C, coculture spots were harvested, resuspended into PBS, then pelleted by centrifugation. RNA was extracted from fresh cell pellets, prepared for qRT-PCR, and analyzed for transcriptional fold-change as above. Transcriptional fold-changes were normalized to transcript levels for *Eco* grown on LBNS for 4h without *Pae*.

Cryo-ET imaging

Overnight cultures of *Eco* strains were diluted in LB 1:100 and grown at 37°C. At $OD_{600}=0.2$, 150 μ M IPTG was added to the liquid culture to induce CRISPRi knockdown. Bacteria were grown for another 90 min and then flash-frozen in liquid nitrogen. Cell cultures were mixed with 10 nm protein A gold at 20:1 ratio (Utrecht), then aliquots of 3 μ L mixtures were applied to glow-discharged R2/2, 200 mesh copper Quantifoil grids (Quantifoil Micro Tools). The sample was blotted for 3 s at 20°C and at

80% humidity. The grids were plunge-frozen in liquid ethane using Leica EM GP system (Leica Microsystems) and stored in liquid nitrogen. Cryo-ET was performed on a Talos electron microscope equipped with a Ceta CCD camera (ThermoFisher). Images were taken at magnification 22,000x corresponding to a pixel size of 6.7 Å. Tilt series were collected using SerialEM⁸⁴ with a continuous tilt scheme (−48° to 48°, every 3° increment). The defocus was set to -6 to -8 μm and the cumulative exposure per tilt series was 150 e⁻/Å². Tomograms were reconstructed with the IMOD software package⁸⁵.

Western blotting

dCas9 detection: Total protein was extracted from the organic layer of bacterial pellets treated with TRIzol Reagent (prepared as described in **qRT-PCR**), according to manufacturer's protocol. Protein samples were diluted to 1mg/ml in PBS + 1x Laemmli denaturing buffer, boiled for 10 minutes then centrifuged at 20,000xg at RT for 2 minutes. Fifteen μl of supernatant was loaded onto an anyKD MiniPROTEAN gel (BioRad), alongside ProteinPlus Ladder (BioRad). Gels were run according to manufacturer's protocol in 1x SDS-PAGE running buffer to separate proteins. Protein was transferred to nitrocellulose (0.2μm; GVS) via semi-dry transfer with a TransBlot Turbo transfer system (BioRad) and matching transfer buffer (BioRad) under the following conditions: 45 min @ 15V, 2.5 Amp. Transfer was validated by Ponceau stain. Blots were blocked for one hour at RT with shaking in 3% milk+TBST. Primary antibody was applied: 1:1000 mouse anti-Cas9 (Abcam ab191468) in TBST, overnight, at 4C with shaking. Blots were washed four times in TBST. Secondary antibody was applied:

1:5000 anti-mouse HRP (Advansta R-05071-500) in TBST, for one hour at RT, with shaking. Blots were washed four times in TBST. Blots were treated with Clarity ECL Western blotting substrate (BioRad) for chemiluminescent detection on an Azure c400 imager. Visible light images were also taken to visualize protein ladder. Densitometry analysis was performed in Fiji^{86,87}. Statistical test: two-tailed unpaired *t*-test. Three biological replicates.

Tae1 detection: Chemically competent *Eco* cells were transformed with *Tae1* overexpression constructs (*pBAD24::tae1^{WT}*, *pBAD24::tae1^{C30A}*, *pBAD24*) by standard 42°C heat-shock and a 45-minute recovery in LB at 37°C with shaking. A transformant population was selected overnight in liquid LB+Carb. Cultures were back-diluted to OD₆₀₀=0.1 in LBNS + Carb +100µM IPTG, then incubated in a Synergy H1 plate reader (BioTek) at 37°C with shaking (2 technical x 3 biological replicates). OD₆₀₀ reads were taken every five minutes to track population growth. At OD₆₀₀=0.25, *Tae1* expression was induced with the addition of 0.125% arabinose to each well. Bacteria were grown for 60 minutes with *Tae1* induction, before technical replicates were harvested and pooled. Samples were pelleted by centrifugation and media was decanted before cells were resuspended in PBS + 1x Laemmli denaturing buffer. Western blotting protocol then proceeded as above, excepting the use of a custom rabbit anti-*Tae1* primary antibody (1:2500 in TBST) (ThermoFisher) and anti-rabbit HRP secondary antibody (1:5000 in TBST) (Advansta R-05072-500).

Tae1 overexpression plasmid construction and use

Plasmids for periplasmic Tae1 overexpression in *Eco* were constructed using splice-overlap extension cloning of *tae1*^{WT} and *tae1*^{C30A} coding sequences derived from *Pae* (PAO1) into *pBAD24*^{22,88}. A *pelB* leader sequence was fused to *tae1* for localization to the periplasm. Expression from *pBAD24* plasmids transformed into *Eco* was induced by addition of 0.125% arabinose (w/v) (Spectrum Chemical) into liquid LBNS media at early log phase (OD₆₀₀ ~0.25).

PF 05081090 +Tae1 overexpression lysis assay

Chemically competent *Eco* were transformed with Tae1 overexpression constructs (*pBAD24::tae1*^{WT}, *pBAD24::tae1*^{C30A}, *pBAD24*) by standard 42°C heat-shock and a 45-minute recovery in LB at 37°C with shaking. A transformant population was selected overnight in liquid LB+Carb, then back-diluted to OD₆₀₀=0.1 in LBNS+Carb +/- 100µM IPTG in a 96-well format. LpxC inhibitor PF 05081090 (final conc. 0.1 ng/µl) or PBS (negative) was added to cultures to test the impact of blocking LPS synthesis on Tae1-mediated lysis. Cultures were incubated on a Synergy H1 plate reader (BioTek) at 37°C with shaking (2 technical x 3 biological replicates). OD₆₀₀ reads were taken every five minutes to generate a growth curve. At OD₆₀₀=0.25 (early log-phase), Tae1 expression was induced from *pBAD24* with the addition of 0.125% arabinose to each well, and grown for 500 minutes at 37°C with shaking. Bacterial growth curves were normalized to blank growth curves (LBNS+Carb, no bacteria), and average growth curves from all biological and technical replicates were plotted in Prism (GraphPad).

Chapter 3. Disruption of lipopolysaccharide biosynthesis provides novel immunity to PG hydrolysis by Tae1

INTRODUCTION

Lipopolysaccharide (LPS) is an essential outward-facing glycolipid in the *Eco* OM, composed of a lipidated disaccharide (Lipid A) bound to a sugar core and an O-antigen⁵⁶. LPS is a major antigen for microbial surface recognition and forms a charged protective layer to occlude the cell from external stressors. In *Eco* K-12, mutations in the *rfb* gene cluster interrupt the production of O-antigen, and thus LPS in *Eco* BW25113 (the parent strain for all *Eco* used in this study) consists of only the essential Lipid A-sugar core moieties (called “rough” LPS)⁸⁹. Damage or depletion of LPS precursors leads to a leaky OM as well as lethal accumulation of LPS intermediate molecules^{60,63,68,69}. Due to its essential structural and molecular roles in protecting the cell surface, LPS and its regulation remain challenging to study *in vivo*.

Identifying *msbA* and *lpxK* as potential Tae1 resistance determinants provided us a novel opportunity to study mechanisms by which LPS integrity impacts susceptibility to cell wall damage. Previous work indicates that LPS and PG are co-regulated *in vivo* in *Eco*. Both molecules are synthesized from a common starting metabolite, UDP-GlcNAc, on the cytoplasmic side of the inner membrane⁹⁰. The flux of UDP-GlcNAc from LPS to PG synthesis can relieve a toxic overproduction of LPS molecules⁹¹, indicating that resource-sharing between LPS and PG pathways can be leveraged for homeostatic regulation of cell envelope activities. OM damage can also stimulate compensatory PG remodeling to fortify the cell envelope⁴⁴. Considering their reactive relationship to each other’s integrity, we hypothesized that LPS KDs might protect *Eco* from Tae1 across several scales: direct

Tae1-PG interactions, cellular responses to Tae1 hydrolysis, broad physiological conditions that affect mechanical lysis, or some combination of these.

RESULTS

Resistance to Tae1 in *msbA-KD* is independent of cell wall hydrolysis

To study the direct relationship between Tae1 and LPS, we adapted an orthogonal *in vivo* assay to isolate the effect of Tae1 activity on *msbA-KD* cells in the absence of *Pae* and other co-delivered H1-T6SS toxins. We measured lysis for *rfp-KD* and *msbA-KD* upon induction of exogenous wild-type Tae1 (Tae1^{WT}) expression in the cell wall-containing periplasm^{21,22} and found that *msbA-KD* had increased survival against Tae1^{WT} relative to *rfp-KD* (**Fig. 3.1a**). *Eco* resistance was dependent on Tae1 activity, as evidenced by loss of the *msbA-KD* resistance phenotype with catalytically-attenuated Tae1^{C30A} (**Fig. 3.1c**) and no-enzyme (empty) (**Fig. 3.1c**) controls. There were no major differences in Tae1 expression levels across conditions (**Fig. 3.2a-b**), which ruled out the possibility that fitness was tied to toxin dose. Complementation of *msbA* by overexpression partially rescued Tae1^{WT} susceptibility in *msbA-KD* (**Fig. 3.3a-c, g**), while *lpxK* overexpression did not (**Fig. 3.3d-f, h**). Given the multigenic knockdown in *msbA-lpxK-ycaQ* in *msbA-KD*, these data suggest that *msbA* is a partial determinant of Tae1 susceptibility in the strain.

Next, we tested whether *msbA-KD* directly impacts Tae1–PG physical interactions by triggering changes to the chemical composition of *Eco* PG, which can occur downstream of OM stress⁴⁴. PG remodeling could alter intrinsic Tae1 susceptibility by

changing the relative abundance of targetable peptides in the cell wall. We isolated and characterized the composition of PG purified from *rfp-KD* and *msbA-KD* by HPLC muropeptide analysis. Both strains had highly similar and stereotypical *Eco* muropeptide profiles (**Fig. 3.1d**). PG peptides containing the scissile bond and structural context for Tae1 recognition (4,3-crosslinked dimers; D44)²¹ were found at an approximate 1:1 ratio with another dominant species of muropeptide (tetrapeptide monomers; M4)⁹². Our results suggest that the PG composition of *msbA-KD* is not modified downstream of LPS damage, indicating that Tae1 resistance cannot be explained by biochemical changes to the Tae1:PG interaction.

We tested an alternative hypothesis that resistance may derive from decreased efficiency in Tae1 hydrolysis. We reasoned that structural deformations in the *msbA-KD* cell envelope (**Fig. 2.8g**) could occlude or delay the accessibility of PG to Tae1, thus slowing the kinetics of cell wall degradation and cell lysis. To test this, we monitored the relative degradation of D44 peptides after Tae1 induction in *rfp-KD* and *msbA-KD* populations. Empty-vector and Tae1^{C30A} conditions were included as negative controls (**Fig. 3.1e; Fig. 3.4a**). At 60 minutes of induction (just prior to lysis in *rfp-KD* populations), we found that D44 peptides were similarly hydrolyzed between strains, with a 32.58% loss in *rfp-KD* and 27.73% of in *msbA-KD* (**Fig. 3.1e-f**). Thus, Tae1 hydrolyzes *msbA-KD* PG as efficiently as *rfp-KD* PG. Collectively, these data show that both cell wall recognition and hydrolysis by Tae1 are unchanged in *msbA-KD*, ruling out the possibility that direct changes to PG are responsible for differential cellular lysis outcomes.

PG synthesis is suppressed in *msbA-KD* but sensitive to Tae1 activity

Given that we did not find any effects on direct Tae1–cell wall interactions in *msbA-KD*, we next explored indirect resistance mechanisms. The PG sacculus is dynamically synthesized, edited, and recycled *in vivo* to maintain mechanical support to the cell during growth and stress^{40,93}. We hypothesized that Tae1 hydrolysis could also impact PG synthesis activity in *Eco* by generating a need to replace damaged PG with new substrate. The ability to repair PG could thus be a valuable determinant of Tae1 susceptibility. To determine if PG synthesis is sensitive to Tae1 exposure, we measured the incorporation of the fluorescent D-amino acid HADA into *rfp-KD* cell walls both with and without exogenous Tae1 expression. When normalized against control cells (*empty*), PG synthesis in *rfp-KD* cells increased by 22% in response to Tae1^{WT} and decreased by 6.5% in response to Tae1^{C30A} (**Fig. 3.5a; Table 3.1**). These data show that PG synthesis is stimulated by Tae1 exposure, and this response is dependent on toxin activity.

PG synthesis is also coordinated to other essential processes in *Eco*, and sensitive to their genetic or chemical perturbations^{44,94}. We investigated if *msbA-KD* impacts the dynamic PG synthesis response to Tae1. Tae1^{WT} exposure yielded a 26.5% increase in PG activity in *msbA-KD*, and no significant change in activity with Tae1^{C30A} (**Fig. 3.5b; Table 3.1**). These results indicate that PG synthesis is still actively regulated in *msbA-KD* in accordance with relative Tae1 activity. However, when normalized against baseline *rfp-KD* activity, all PG synthesis measurements for *msbA-KD* were significantly diminished (**Fig. 3.6a; Table 3.1**). This observation indicates that PG

synthesis activity is globally suppressed as a consequence of CRISPRi in *msbA*. Thus, we conclude that PG dynamism in *Eco* is sensitive to Tae1 hydrolysis of PG, and that *msbA-KD* alters the global capacity for PG synthesis activity without altering its sensitivity to Tae1. Furthermore, these data demonstrate a reactive crosstalk between LPS and PG synthesis activities *in vivo*.

Blocks to growth and protein synthesis accompany Tae1 resistance in *msbA-KD*

Based on its responsiveness to Tae1 exposure, we might hypothesize that *Eco* stimulates PG synthesis to attempt protection against lysis by Tae1. However, suppressed PG synthesis activity alongside tolerance to wildtype-levels of PG damage in *msbA-KD* suggested that *msbA-KD* may survive lysis by Tae1 using an additional strategy to support or even supersede PG integrity. *Eco* can resist lysis upon acute PG stress by entering a transient dormant state called persistence in which homeostatic growth processes like DNA replication, protein synthesis, and cell division are arrested to prioritize stress responses to critical damage⁹⁵⁻⁹⁷. Additionally, a recent study showed that a CRISPRi KD in *lpxA*, the first enzyme in Lipid A biosynthesis, triggered hallmark signs of a dormancy stress response called the stringent response⁹⁸. We hypothesized that decreased PG synthesis activity in *msbA-KD* may be symptomatic of persistence, which could protect against Tae1 activity by passive tolerance.

To observe the effects of Tae1 and CRISPRi on cellular growth and lysis behaviors over time, we performed timelapse microscopy of *rfp-KD* and *msbA-KD* cells in competition with *Pae*. Across all *Pae* competitions, *msbA-KD* cells grew slowly without dividing or

lysing (**Fig. 3.7a; Fig. 3.8a-b**). By contrast, *rfp-KD* cells grew and divided rapidly, but lysed when in competition against *Pae* strains with active H1-T6SSs (*Pae*^{WT}, *Pae*^{Δ*tae1*}) (**Fig. 3.7a; Fig. 3.8a-b**). These data demonstrate that stunted cell growth and division are additional consequences of CRISPRi in *msbA-KD*. Another hallmark of persistence is slowed protein production in the cell. To assess whether global protein synthesis is affected in *msbA-KD*, we used pulse-chase fluorescent labelling of nascent protein synthesis in *msbA-KD* and *rfp-KD*. Overall protein synthesis levels were significantly lower in *msbA-KD* relative to *rfp-KD* under all conditions tested (**Fig. 3.7b**). From these data we conclude that *msbA-KD* cells show signs of persistence, suggesting that broad changes in cellular physiology may underscore the ability of *msbA-KD* cells to resist the toxic activity of Tae1.

DISCUSSION

The species composition of mixed-microbial communities can be driven by competitive strategies that bacteria use to antagonize their neighbors. However, our understanding of microbial weapons is primarily derived from *in vitro* studies of their molecular mechanisms. In this study, we wanted to understand how Tae1, a PG-degrading H1-T6SS effector toxin, specifically aided *Pae* in antagonizing *Eco* *in vivo*. By combining T6SS-mediated competition with CRISPRi against essential *Eco* genes, our high-throughput genetic screen was poised to uncover new molecular details about the interaction between Tae1 and essential functions in recipient cells. We found that dynamic regulation of both direct (PG) and indirect (LPS, growth) aspects of cell wall hydrolysis had critical roles in defining the intrinsic sensitivity to Tae1-mediated lysis.

Thus, Tae1 toxicity *in vivo* is driven not only by its ability to destroy PG but also by broader physiological and regulatory context.

Through the lens of LPS perturbation (*msbA-KD*), we discovered that cellular persistence is associated with resistance to Tae1-dependent lysis. The protective nature of dormancy has been demonstrated for survival against other cell wall-degrading enzymes, lytic bacteriophages, and antibiotics⁹⁹⁻¹⁰³. However, previous work has shown that fast growth protects recipient cells from T6SS by establishing stable microcolonies more quickly than T6SS can kill the recipient cell type^{104,105}. Our work provides an additional layer of complexity to the community context by demonstrating that arrested cell growth may also control T6SS efficacy. Similarly to how dead, unlysed cells can act as “corpse barriers” to block T6SS-wielding competitors from progressing in space¹⁰⁶, transiently dormant cells may also prevent the physical takeover of aggressive competitors by absorbing T6SS attacks to protect their kin. However, dormancy is a reversible phenotype that may be less-costly than altruistic death as a strategy to survive T6SS within communities. We propose that fast-growing recipient species may be more effectively controlled by T6SS effectors like Tae1 in some settings because their high cell activity primes sensitivity to lysis. Future work may serve to determine if dormancy phenotypes can be triggered by T6SS attack in recipient cells, or if cells that are already slow-growing in mixed populations could be passively robust against T6SS and Tae1.

Another key insight from our study is that PG synthesis is stimulated in response to Tae1, indicative of an active *Eco* counterresponse. However, wild-type levels of PG synthesis were coincident with, not counter to, lytic death. Diminished PG synthesis activity in *msbA-KD* could therefore enable resistance by suppressing a toxic dysregulation of homeostatic activities. We propose that Tae1 activity leads to *Eco* cell death, in part, by triggering a futile cycle of Tae1 hydrolysis and PG synthesis that does not resolve in cell wall homeostasis. An exciting prospect for future studies could involve determining the molecular mechanisms that control PG synthesis stimulation after Tae1 hydrolysis, including whether Tae1 may synergize or hijack endogenous cell wall enzymes to amplify its damage to PG¹⁰⁷.

The simultaneous block to LPS synthesis alongside PG synthesis in *msbA-KD* also constitutes a novel example of the co-regulation between PG and LPS. Critically, we did not observe PG remodeling in *msbA-KD*. As MsbA is located upstream of LPS transport to the OM, our finding suggests that the IM (Kdo₂-Lipid A synthesis pathway) and OM (Lpt pathway) portions of LPS biosynthesis may have different regulatory relationships to PG.

In conclusion, we propose a model in which Tae1 susceptibility *in vivo* is determined at multiple levels of specificity in *Eco*: not only at the level of local PG damage but also by crosstalk between essential cell envelope pathways and the general growth state of the cell. As mediated through damage to LPS in *msbA-KD*, we posit that such crosstalk between essential cell functions can be helpful for slowing reactivity and thus increasing

tolerance to acute PG stress. By the same token, the enmeshment of essential pathways may render fast-growing *Eco* vulnerable to Tae1 by creating a sudden chain-reaction of imbalances in critical functions which the cell must also resolve alongside the initial PG damage.

Our work highlights how recipient susceptibility in interbacterial competition may be more complex than direct toxin-substrate interactions alone. Toxins with essential targets not only impact specific molecules but also a dynamic network of interconnected pathways. T6SSs often encode multiple toxins that antagonize different essential features¹⁷, including components of the cell envelope and other metabolic pathways. We posit that T6SSs deploy a cocktail of toxins that can act in coordination to disrupt the network beyond repair, or even weaponize protective homeostatic mechanisms themselves. This study points to the importance of studying the role of essential genes in the context of T6S-mediated bacterial antagonism.

METHODS

Overexpression plasmid construction and use

Plasmids for periplasmic Tae1 overexpression in *Eco* were constructed using splice-overlap extension cloning of *tae1^{WT}* and *tae1^{C30A}* coding sequences derived from *Pae* (PAO1) into *pBAD24^{22,88}*. A *pelB* leader sequence was fused to *tae1* for localization to the periplasm. Expression from *pBAD24* plasmids transformed into *Eco* was induced by addition of 0.125% arabinose (w/v) (Spectrum Chemical) into liquid LBNS media at early log phase ($OD_{600} \sim 0.25$). Overexpression constructs for *msbA* and *lpxK* were constructed by cloning each full-length gene from *Eco* into the NdeI/HindIII restriction sites of *pSCrhaB2¹⁰⁸*. Overexpression from *pSCrhaB2* plasmids transformed into *Eco* was induced by addition of 0.1% rhamnose (w/v) (Thermo Scientific) into liquid media. See **Table S2** for primer sequences used for cloning and PCR validation.

Tae1 overexpression lysis assay

Chemically competent *Eco* were transformed with Tae1 overexpression constructs (*pBAD24::tae1^{WT}*, *pBAD24::tae1^{C30A}*, *pBAD24*) by standard 42°C heat-shock and a 45-minute recovery in LB at 37°C with shaking. A transformant population was selected overnight in liquid LB+Carb; the more-traditional method of selecting on solid media was skipped to discourage the formation of Tae1-resistant compensatory mutations. Overnight transformant cultures were back-diluted to $OD_{600}=0.1$ in LBNS+Carb +/- 100µM IPTG, then incubated in a Synergy H1 plate reader (BioTek) at 37°C with shaking (2 technical x 3 biological replicates). OD_{600} reads were taken every five minutes to generate a growth curve. At $OD_{600}=0.25$ (early log-phase), Tae1 expression

was induced from *pBAD24* with the addition of 0.125% arabinose to each well, and grown for 500 minutes at 37°C with shaking. Bacterial growth curves were normalized to blank growth curves (LBNS+Carb, no bacteria), and average growth curves from all biological and technical replicates were plotted in Prism (GraphPad).

For *msbA* and *lpxK* complementation assays, *pSCrhaB2* plasmids were transformed alongside *pBAD24* plasmids, and overnight selection was performed in liquid LB+Carb+Trm. The next day, cultures were washed and back-diluted at $OD_{600}=0.1$ into LBNS+Carb+Trm+0.1% rhamnose. The experiment then proceeded in the plate reader as described above.

Western blotting

Tae1 detection: Chemically competent *Eco* cells were transformed with *Tae1* overexpression constructs (*pBAD24::tae1^{WT}*, *pBAD24::tae1^{C30A}*, *pBAD24*) by standard 42°C heat-shock and a 45-minute recovery in LB at 37°C with shaking. A transformant population was selected overnight in liquid LB+Carb. Cultures were back-diluted to $OD_{600}=0.1$ in LBNS + Carb +100µM IPTG, then incubated in a Synergy H1 plate reader (BioTek) at 37°C with shaking (2 technical x 3 biological replicates). OD_{600} reads were taken every five minutes to track population growth. At $OD_{600}=0.25$, *Tae1* expression was induced with the addition of 0.125% arabinose to each well. Bacteria were grown for 60 minutes with *Tae1* induction, before technical replicates were harvested and pooled. Samples were pelleted by centrifugation and media was decanted before cells were resuspended in PBS + 1x Laemmli denaturing buffer. Western blotting protocol

then proceeded as in *dCas9 detection* (Ch. 2 Methods, “Western Blotting”), excepting the use of a custom rabbit anti-Tae1 primary antibody (1:2500 in TBST) (ThermoFisher) and anti-rabbit HRP secondary antibody (1:5000 in TBST) (Advansta R-05072-500).

Muropeptide analysis

Chemically competent *Eco* cells were transformed with Tae1 overexpression constructs (*pBAD24::tae1^{WT}*, *pBAD24::tae1^{C30A}*, *pBAD24*) by standard 42°C heat-shock and a 45-minute recovery in LB at 37°C with shaking. A transformant population was selected overnight in liquid LB+Carb. Cultures were back-diluted to OD₆₀₀=0.1 in LBNS+Carb +100µM IPTG, and grown with shaking. At early log phase (OD₆₀₀=0.25), 0.125% arabinose was added to induce *pBAD24* expression. Cells were grown for 60 minutes, then harvested by centrifugation. For PG purification, cells were boiled in 3% SDS to extract crude PG, then treated with Pronase E (100µg/ml in Tris-HCl (pH 7.2) + 0.06% NaCl) (VWR Chemicals) for 2 hours at 60C to remove proteins covalently bound to PG. Mutanolysin digestion (40µg/ml in Tris-HCl (pH 7.2) + 0.06% NaCl) was performed overnight at 37C to solubilize PG into muropeptides for HPLC analysis. Samples were reduced with sodium borohydride (Fisher Chemical) then pH-corrected to 3-4 using o-phosphoric acid(Fisher Chemical)¹⁰⁹. Muropeptides were separated on a 1220 Infinity II HPLC (Agilent) with UV-visible detection (λ =206nm). Muropeptide separation was achieved over 54 minutes at 0.5 ml/min using a Hypersil ODS C18 column (Thermo Scientific) and a gradient elution from 50mM sodium phosphate + 0.04% NaN₃ (Buffer A) to 75mM sodium phosphate +15% methanol (Buffer B). Chromatograms were integrated in ChemStation software (Agilent) to determine peak area, height, and elution

time. Experimental chromatograms were normalized against a chromatogram from a blank run (ddH₂O). Chromatograms were also internally normalized against the most abundant M4 (monomer muuropeptide) peak; this allowed for direct relative comparisons of peak heights between samples. To calculate the percent change in D44 (4,3-crosslinked dimer) peptides after Tae1 overexpression, the normalized area under the curve (AUC) for D44 was divided by the total chromatogram area to calculate the relative D44 peak area for each condition (AUC_{WT}, AUC_{C30A}, AUC_{EV}). Then, within a given strain, (AUC_{WT}/AUC_{EV})*100 and (AUC_{C30A}/AUC_{EV})*100 were calculated to determine the percent of D44 peak area lost to Tae1^{WT} or Tae1^{C30A} treatment, relative to EV treatment. Three biological replicates were performed per condition. Statistical test: two-tailed unpaired *t*-test.

HADA incorporation imaging

Chemically competent cells were transformed with *pBAD24* constructs:

(*pBAD24::tae1^{WT}*, *pBAD24::tae1^{C30A}*, or *pBAD24*) and selected with Carb overnight in liquid LB. Transformant cultures were back-diluted to OD₆₀₀=0.1 in 1ml LBNS+Carb +100μM IPTG, and grown with shaking. At early log phase (OD₆₀₀=0.25), 0.125% arabinose added to induce *pBAD24* expression. Cells were grown for 30 minutes, then 250μM HADA added to culture. Cells were grown an additional 30 minutes, then collected by centrifugation and washed 3x with cold PBS + sodium citrate (pH 3.0) to block hydrolysis of labelled septal PG¹¹⁰. Cells were fixed by treatment with 3% PFA for 15 minutes on ice. Fixed cells were washed 3x in cold PBS, then resuspended in PBS +20% DMSO. Fluorescence imaging was performed on a Nikon Eclipse Ti2-E inverted

microscope equipped with a 100x/1.40 oil-immersion phase objective and an EMCCD camera (Prime 95B). Fluorescence (DAPI channel) and phase-contrast images were captured using NIS-Elements AR Viewer 5.20. Images were analyzed for single-cell fluorescence intensity using MicrobeJ for Fiji^{87,111}. 200 cells/sample measured, 3 biological replicates. Statistical test: unpaired *t*-test.

Nascent protein synthesis imaging

Chemically competent cells were transformed with *pBAD24* constructs: (*pBAD24::tae1^{WT}*, *pBAD24::tae1^{C30A}*, or *pBAD24*) and selected with Carb overnight in liquid LB. Cultures were diluted by 1:100 and grown in LBNS+ Carb+ 100μM IPTG at 37 °C with shaking. At early log phase (~80 minutes) 0.125% arabinose was added to induce *Tae1* expression. After 35 minutes, 13μM O-propargyl-puromycin (OPP) was added to cultures to label new peptide synthesis before harvesting (Click-iT™ Plus OPP Alexa Fluor™ 488 Protein Synthesis Assay Kit, Invitrogen)¹¹². After labelling, cells were pelleted and fixed in 3.7% formaldehyde in PBS. Cells were permeabilized with 0.3% Triton X-100 in PBS for 15 min, then labelled for imaging with Click-iT reaction cocktail for 20 min in the dark, washed then resuspended in PBS. Fluorescence imaging was performed on a Nikon Eclipse Ti2-E inverted microscope equipped with a 100x/1.40 oil-immersion objective and an EMCCD camera (Prime 95B). The 488-nm laser illumination fluorescence and phase-contrast images were captured using NIS-Elements AR Viewer 5.20 and analyzed using MicrobeJ software for Fiji^{87,111}.

Time-lapse imaging of T6SS competitions

Competition microscopy experiments were performed with overnight liquid cultures of *Pae* (LB) and *Eco* CRISPRi strains (LB+Gent+Cam). Cultures were diluted 1:50 in fresh medium and grown for 2h. *Pae* cells were diluted again 1:50 in fresh medium (LB) and grown at 37°C to OD 1.2 – 1.5 (~1 hour). Similarly, *E. coli* strains were diluted 1:100 in fresh medium (LB+150µM IPTG) supplemented with antibiotics (Gent / Cam) and grown at 37°C to OD 1.2 – 1.5 (~1 hour). Then, cultures were washed with LB, resuspended in LB + 150µM IPTG and mixed 2:1 (*Pae:Eco*). 1 µl of the mixed cells was spotted on an agarose pad containing propidium iodide and imaged for 2h at 37°C. A Nikon Ti-E inverted motorized microscope with Perfect Focus System and Plan Apo 1003 Oil Ph3 DM (NA 1.4) objective lens was used to acquire images. If not indicated otherwise, time-lapse series of competitions were acquired at 10 s acquisition frame rate during 120 min. SPECTRA X light engine (Lumencore), ET-GFP (Chroma #49002) and ET-mCherry (Chroma #49008) filter sets were used to excite and filter fluorescence. VisiView software (Visitron Systems, Germany) was used to record images with a sCMOS camera pco.edge 4.2 (PCO, Germany) (pixel size 65 nm). The power output of the SPECTRA X light engine was set to 20% for all excitation wavelengths. GFP, phase-contrast and RFP / propidium iodide (PI) images were acquired with 50-100 ms exposure time. Temperature and humidity were set to 37°C, 95% respectively, using an Okolab T-unit objective heating collar as well as a climate chamber (Okolab). Fiji was used for imaging processing⁸⁷. Acquired time-lapse series were drift-corrected using a custom StackReg based software^{9,113}.

FIGURES

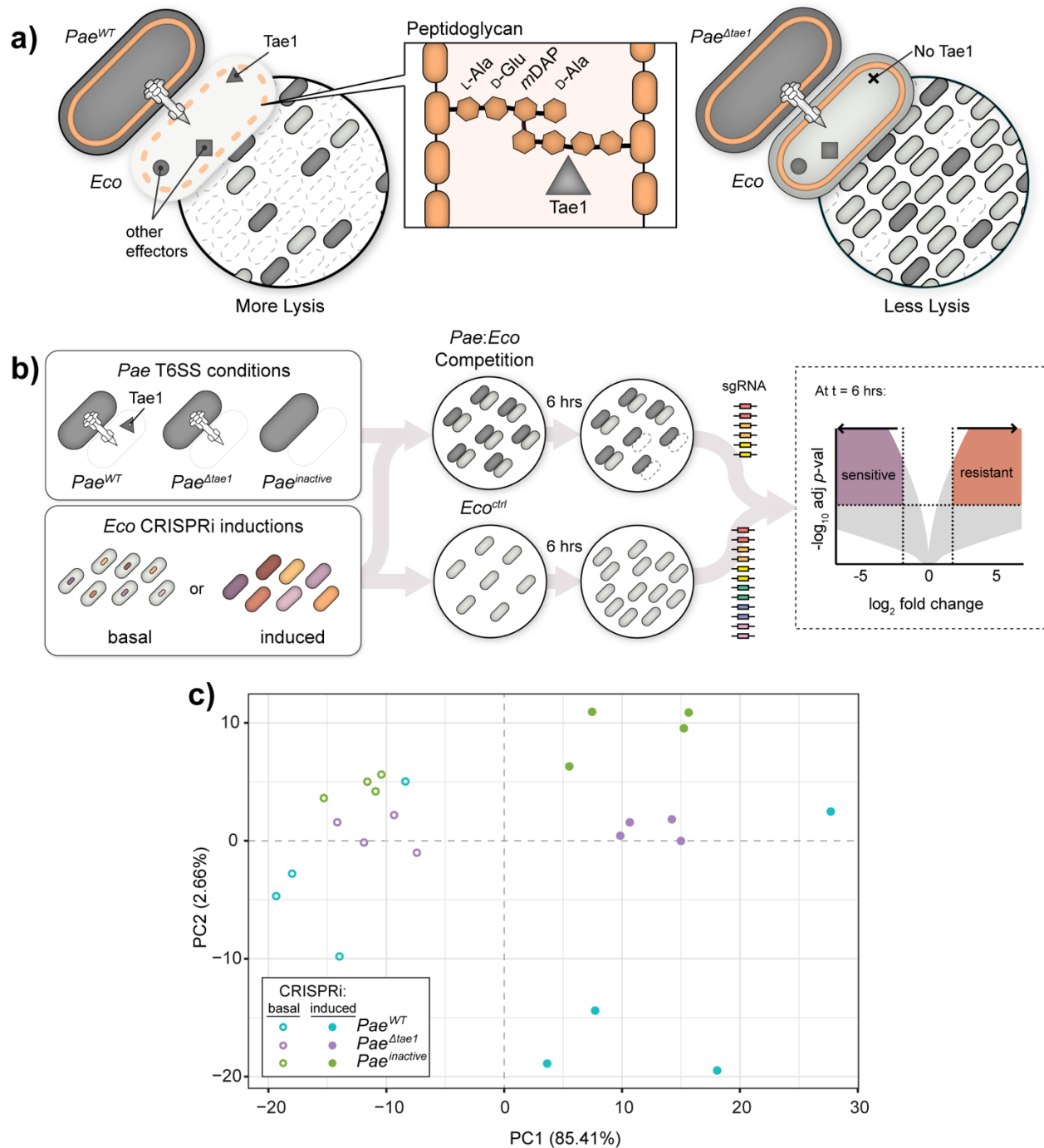


Figure 2.1: Adaptation of native T6SS competitions to study *Eco* susceptibility to *Tae1* a) *Tae1* from *Pseudomonas aeruginosa* (*Pae*) degrades the *Escherichia coli* (*Eco*) cell wall to promote H1-T6SS-mediated lysis. Left: *Pae*^{WT} (dark grey) outcompetes *Eco* (light grey) using H1-T6SS to deliver a cocktail of toxic effectors, including *Tae1* (triangle) which degrades peptidoglycan (orange). Center: *Tae1* hydrolyzes D-Glu-*mDAP* peptide bonds in the donor stem peptides of 4,3-crosslinked peptidoglycan. Right: *Pae*^{Δ*tae1*} is less effective at outcompeting *Eco* using H1-T6SS. b) Method for a

genetic screen to test *Eco* gene function toward fitness against Tae1 from *Pae*. Left: *Pae* strains (dark grey) were engineered with modified H1-T6SS activities including: constitutively active *Pae*^{WT} ($\Delta retS\Delta pppA$), Tae1-deficient *Pae* ^{$\Delta tae1$} ($\Delta retS\Delta pppA\Delta tae1$), and T6SS-inactive *Pae*^{inactive} ($\Delta retS\Delta pppA\Delta icmF$). Each *Pae* strain was mixed with a pool of *Eco* KD (knockdown) strains engineered to conditionally disrupt a single gene (CRISPRi induced vs. basal). Center: each *Pae* strain was cocultured with an *Eco* CRISPRi strain pool for 6 hours. The *Eco* CRISPRi strain pool was also grown for 6 hours without *Pae* (*Eco*^{ctrl}) as a negative control. Genomic sgRNA sequences harvested from competitions were amplified into Illumina sequencing libraries. Right: sgRNA barcode abundances after 6 hours were used to calculate a normalized log₂ fold-change (L2FC) for each *Eco* KD strain under each condition. Above a -log₁₀ *p*-value cutoff, a positive L2FC value indicates a KD strain which is resistant to a given condition relative to WT *Eco*; a negative L2FC value indicates a KD strain which is sensitive to a given condition relative to WT *Eco*. c) Interbacterial competition and CRISPRi induction have distinct effects on the composition of the *Eco* CRISPRi strain library. Principal component analysis of *Eco* library composition after competition against *Pae*^{WT} (blue), *Pae* ^{$\Delta tae1$} (purple), or *Pae*^{inactive} (green), with induced (solid circles) or basal (hollow circles) CRISPRi induction. Four biological replicates per condition.

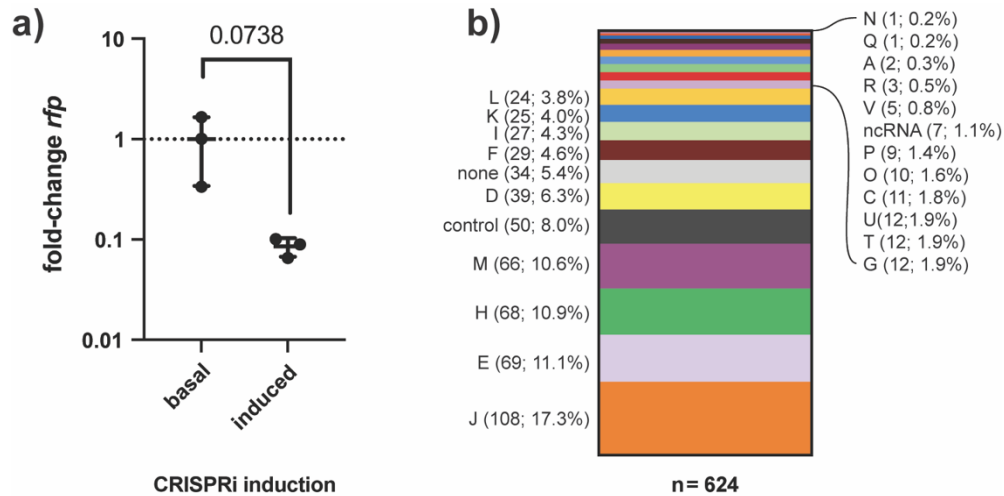


Figure 2.2 : CRISPRi conditionally knocks down transcription across hundreds of *Eco* gene targets. a) CRISPRi induction produces mild transcriptional knockdown of endogenous *rfp* (11.7-fold decrease) in *Eco*. qRT-PCR measurement of relative *rfp* RNA expression in *Eco* strain SC363 after 6 hours of growth on solid LB media with basal or induced CRISPRi. Data shown: 3 biological replicates with mean \pm s.d. Statistical test: unpaired two-tailed *t*-test. b) CRISPRi targets *Eco* genes that collectively represent 21 clusters of orthogonal genes (COGs). CRISPRi target genes ($n=596$) were binned by their NCBI COG functional assignment. The relative representation of each COG in the strain collection is displayed as a percent of all COGs. Some genes are represented by multiple COGs, resulting in a greater number of COGs ($n=624$) than target genes. Non-targeting negative controls (“control”, $n=50$) genes without COG assignments (“none”, $n=34$), and genes coding for non-coding RNAs (“ncRNA”, $n=7$) were also binned.

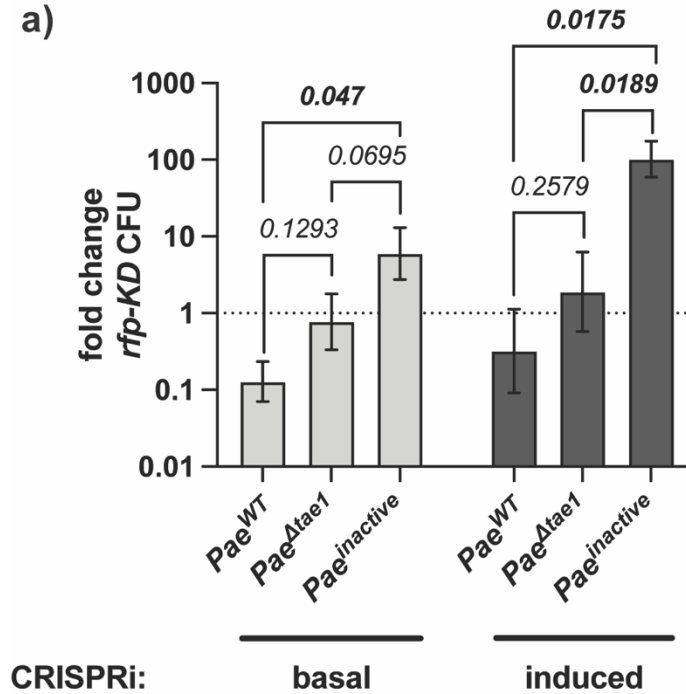


Figure 2.3: Non-targeting CRISPRi induction has little effect on *Eco* fitness in T6SS competition. a) CRISPRi induction does not disrupt T6SS- and Tae1-dependent targeting of *Eco* by *Pae*. Interbacterial competition between *Pae* (*Pae*^{WT}, *Pae* ^{Δ tae1}, *Pae*^{inactive}) and an *Eco* negative-control KD strain (*rfp-KD*), with induced or basal CRISPRi. Data shown: mean fold-change (\pm geometric s.d.) of *rfp-KD* colony forming units (CFUs) after six hours of competition against *Pae*. Statistical test: unpaired two-tailed *t*-test; *p*-value ≤ 0.05 displayed in bold font.

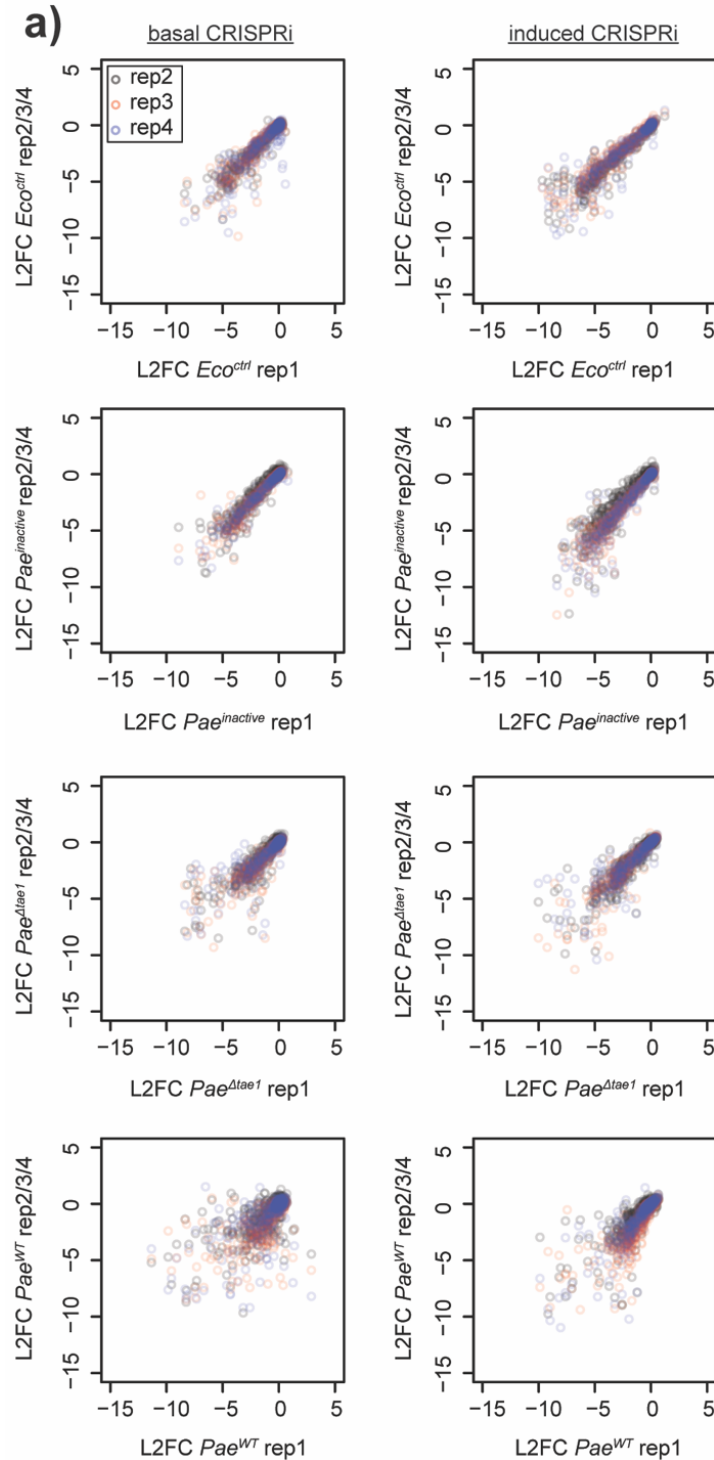


Figure 2.4: CRISPRi library fitness in T6SS screen is reproducible across biological replicates. a) CRISPRi library fitness in T6SS screen is reproducible across biological replicates. Replica plots showing the uncorrected L2FC values for each *Eco* CRISPRi strain after competition against *Pae*^{WT}, *Pae*^{Δtae1}, *Pae*^{inactive}, for four biological replicates. For each plot, replicate 1 is compared to replicate 2 (grey), replicate 3 (red), or replicate 4 (blue). Median Pearson's *r* between all replicates = 0.91.

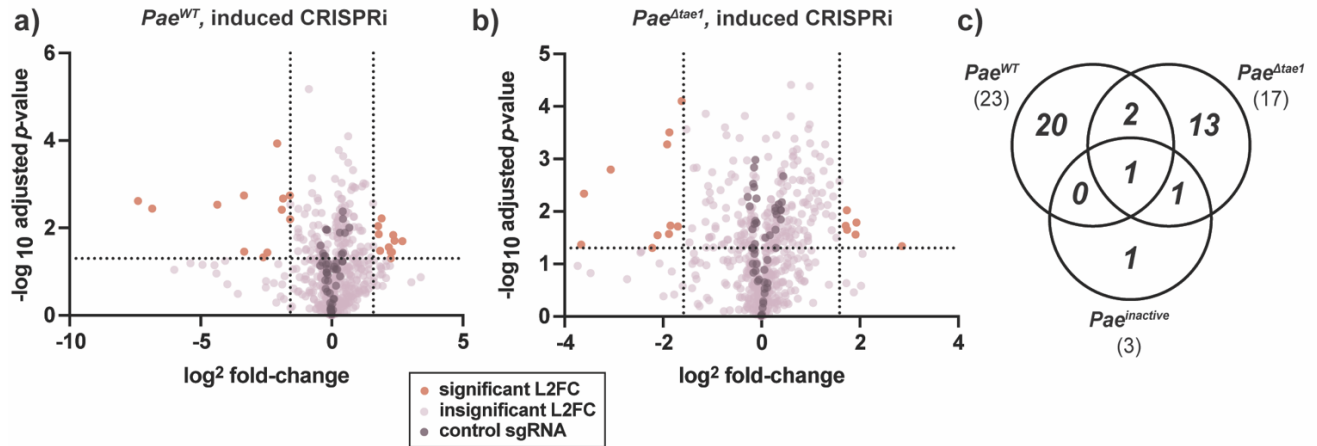


Figure 2.5: CRISPRi reveals toxin-specific and non-specific determinants of *Eco* fitness against H1-T6SS. a-b) CRISPRi knockdowns promote *Eco* survival against *Pae*^{WT} (a) and *Pae*^{Δtae1} (b). Volcano plots showing log₂-fold change (L2FC) values for each KD strain after interbacterial competition (induced CRISPRi). Data shown: mean from four biological replicates. Statistical test: Wald test. Vertical dotted lines indicate arbitrary cutoffs for L2FC at $x = -1.58$ and $x = 1.58$ (absolute FC $x = -3$ or $x = 3$). Horizontal dotted line indicates statistical significance cutoff for log₁₀ adjusted p -value (≤ 0.05). Orange points represent KDs with L2FC ≥ 1.58 or ≤ -1.58 and log₁₀-adj. p -value ≤ 0.05 . Dark purple points represent non-targeting negative control KDs ($n = 50$). Lavender points represent KDs that do not meet cutoffs for L2FC or statistical test. c) T6SS competitions identify CRISPRi strains with distinct fitness changes against T6SS and Tae1. Venn diagram of total KDs significantly enriched OR depleted after competition against *Pae*^{WT} ($n = 23$), *Pae*^{Δtae1} ($n = 17$), and *Pae*^{inactive} ($n = 5$).

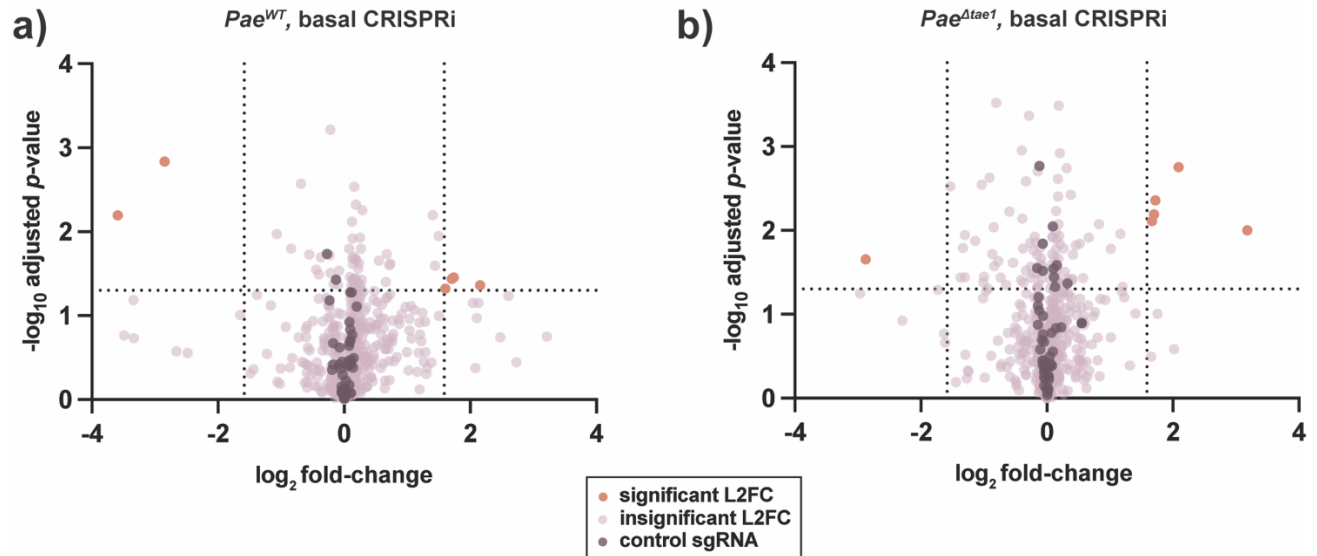


Figure 2.6: Pooled T6SS competitions with basal CRISPRi attenuate significant fitness phenotypes. a-b) Basal CRISPRi attenuates *Eco* fitness phenotypes against *Pae^{WT}* (a) and *Pae^{Δtae1}* (b). Volcano plots showing \log_2 -fold change (L2FC) values for each KD strain after interbacterial competition (basal CRISPRi). Data shown: mean from four biological replicates. Statistical test: Wald test. Vertical dotted lines indicate arbitrary cutoffs for L2FC at $x = -1.58$ and $x = 1.58$ (absolute FC $x = -3$ or $x = 3$). Horizontal dotted line indicates statistical significance cutoff for \log_{10} adjusted p -value (≤ 0.05). Orange points represent KDs with L2FC ≥ 1.58 or ≤ -1.58 and \log_{10} -adj. p -value ≤ 0.05 . Dark purple points represent non-targeting negative control KDs ($n=50$). Lavender points represent KDs that do not meet cutoffs for L2FC or statistical test.

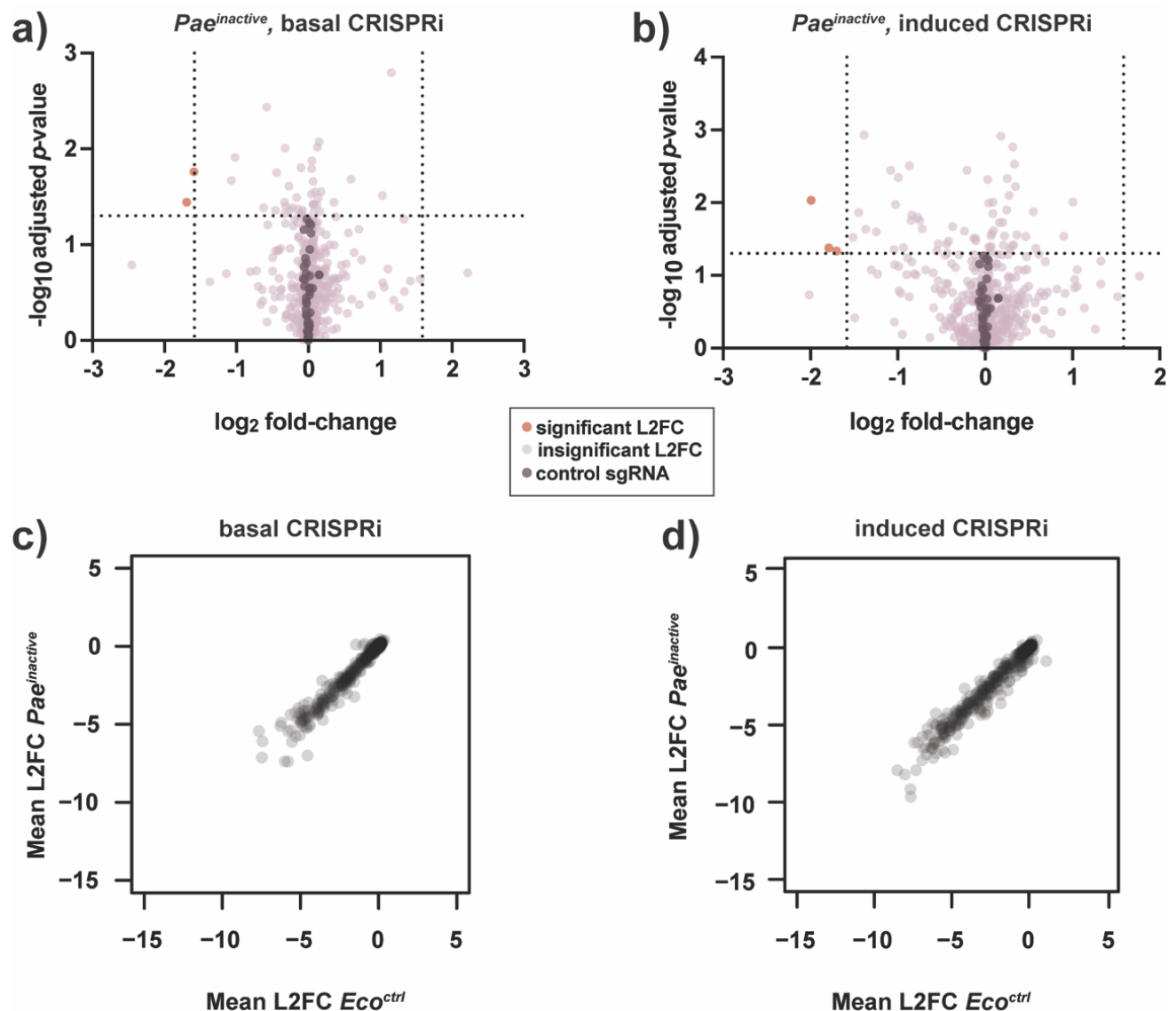


Figure 2.7: *Pae^{inactive}* is a neutral co-culture partner for *Eco*. a-b) Competition against *Pae^{inactive}* reveals few *Eco* fitness determinants. Volcano plots showing \log_2 -fold change (L2FC) values for each KD strain after interbacterial competition with induced (a) or basal (b) CRISPRi. Data shown: mean from four biological replicates. Statistical test: Wald test. Vertical dotted lines indicate arbitrary cutoffs for L2FC at $x = -1.58$ and $x = 1.58$ (absolute FC $x = -3$ or $x = 3$). Horizontal dotted line indicates statistical significance cutoff for \log_{10} adjusted *p*-value (≤ 0.05). Orange points represent KDs with L2FC ≥ 1.58 or ≤ -1.58 and \log_{10} -adj. *p*-value ≤ 0.05 . Dark purple points represent non-targeting negative control KDs ($n = 50$). Lavender points represent KDs that do not meet cutoffs for L2FC or statistical test. c-d) KD strain abundance is highly similar after competition with *Pae^{inactive}* and after growth without competition (*Eco^{ctrl}*). Scatter plots comparing mean L2FC for each *Eco* KD strain after competition with *Pae^{inactive}* or *Eco^{ctrl}* treatment, with basal (c) or induced (d) CRISPRi. Median Pearson correlation $r = 0.98$.

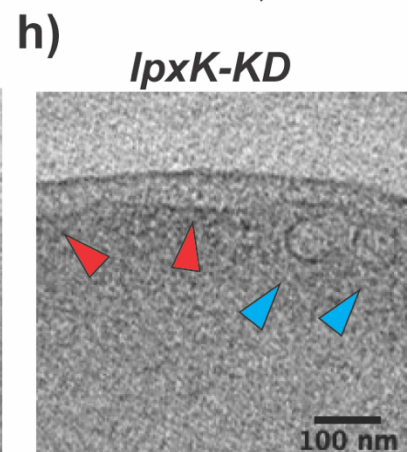
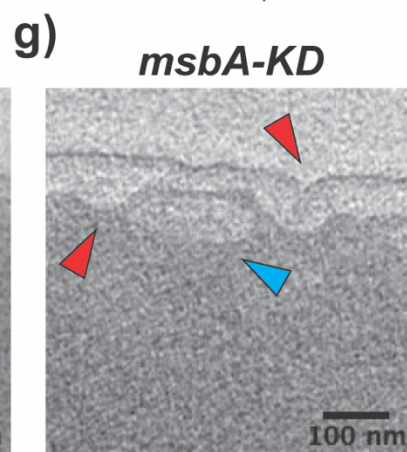
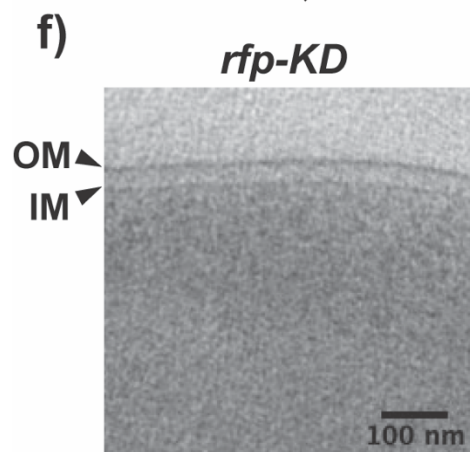
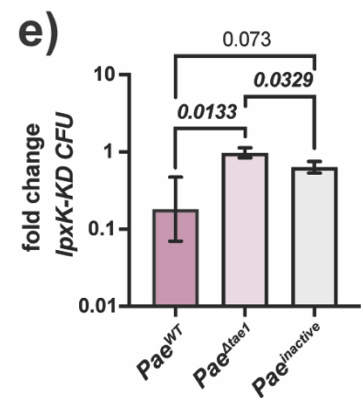
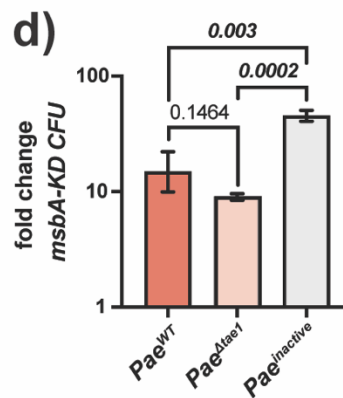
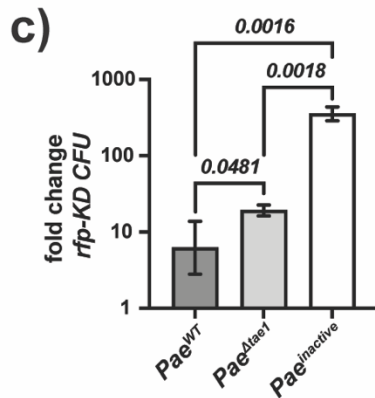
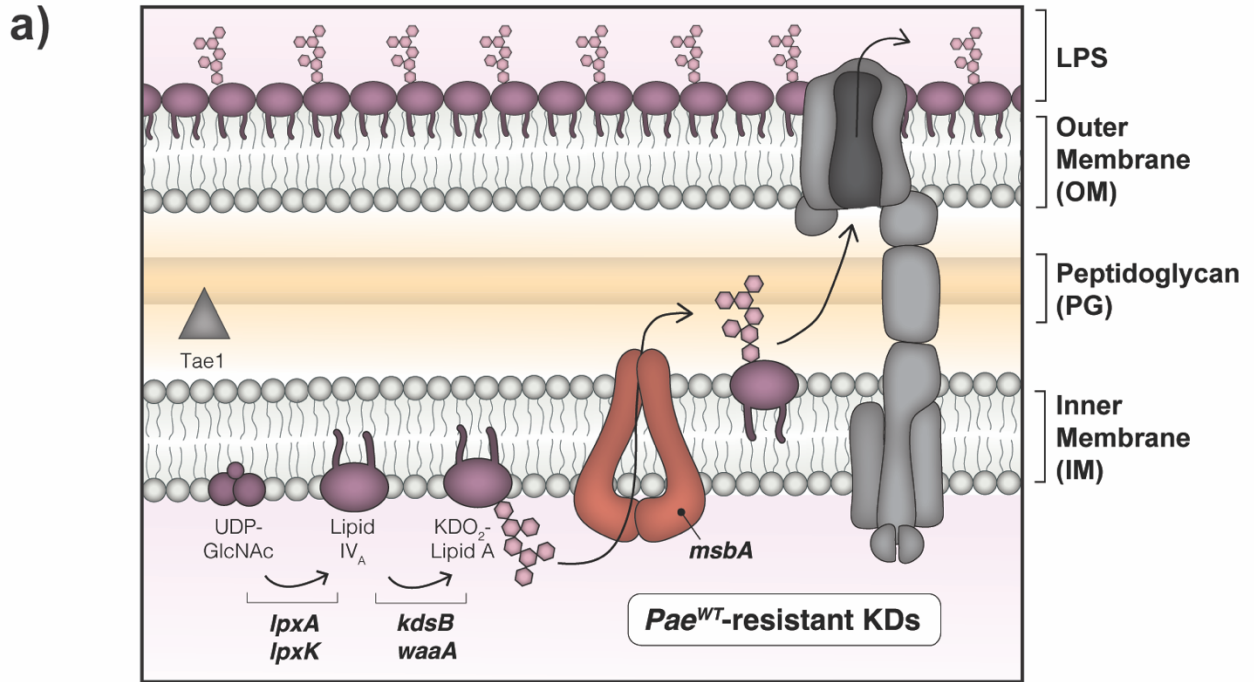


Figure 2.8: *msbA*-KD disrupts LPS biosynthesis and imparts *Tae1* resistance. a) *Tae1* resistance emerges in KDs that target the lipopolysaccharide (LPS) biosynthesis pathway. Schematic representation of the LPS biosynthesis pathway and its distribution across the *Eco* cell envelope. Genes with KDs that render *Eco* resistant to *Pae*^{WT} are involved in the biosynthesis of Kdo₂-Lipid A (*lpxA*, *lpxK*, *kdsB*, *waaA*, *msbA*). Note that *Tae1* (grey triangle) targets peptidoglycan (PG), which is physically separate from Kdo₂-Lipid A synthesis in the IM. b) The Kdo₂-Lipid A biogenesis genes *msbA* and *lpxK* are integral members of the *ycal-msbA-lpxK-ycq* operon in *Eco*. *msbA* (orange) and *lpxK* (purple) are co-expressed at the transcriptional level. c-e) *msbA*-KD loses sensitivity to *Tae1* in interbacterial competition against *Pae* but *lpxK*-KD does not. Interbacterial competitions between *Pae* (*Pae*^{WT}, *Pae*^{Δ*tae1*}, *Pae*^{inactive}) and *rfp*-KD (c; grey), *msbA*-KD (d; orange), or *lpxK*-KD (e; purple). Data shown are average fold-change in *Eco* colony forming units (CFUs) after 6 hours of competition (geometric mean 3 biological replicates ± s.d). Statistical test: unpaired two-tailed *t*-test; *p*-value ≤0.05 displayed in bold font. f-h) Kdo₂-Lipid A mutants develop structural damage to membranes. Cryo-EM tomographs of *rfp*-KD (f), *msbA*-KD (g), and *lpxK*-KD (h) with CRISPRi induced, highlighting cross-sections of the cell envelope (including IM and OM; black arrows). Deformed membranes (red arrows) and novel intracellular vesicles (blue arrows) are demarcated in (g) and (h). Scale bar: 100nm.

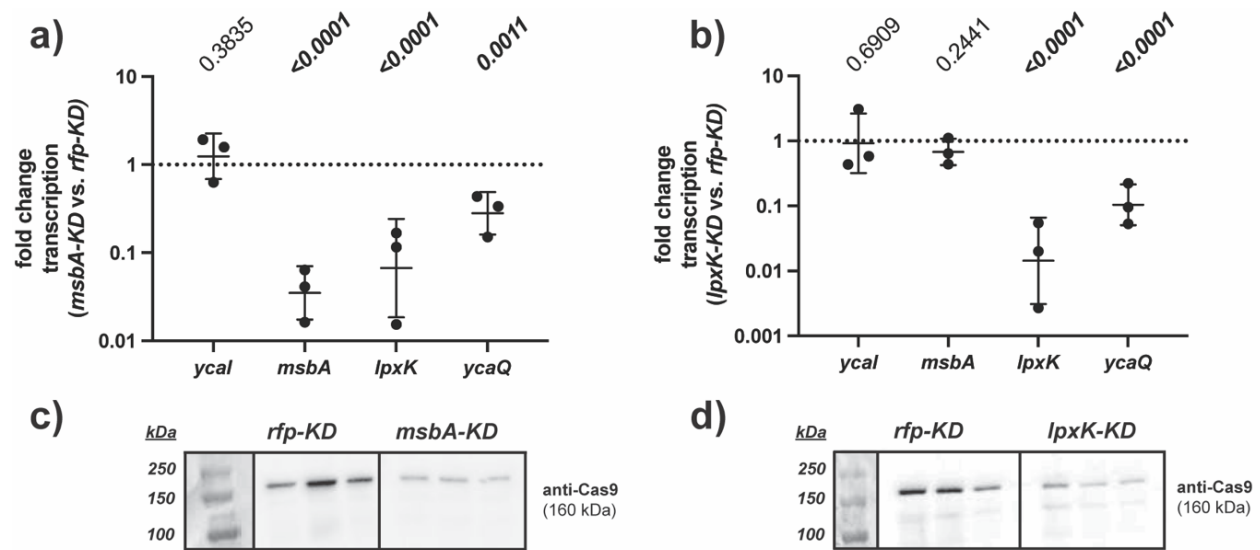


Figure 2.9: *lpxK-KD* and *msbA-KD* modulate target gene expression and show polar effects. a-b) Transcriptional knockdowns in *msbA* and *lpxK* have off-target polar effects on transcription in their operon. qRT-PCR analysis of transcriptional fold-change in *ycal-msbA-lpxK-ycaQ* in *msbA-KD* (a) and in *lpxK-KD* (b) after growth for 6 hours with induced CRISPRi, normalized to expression in *rfp-KD*. Data shown are geometric average of 3 biological replicates \pm s.d. Statistical test: unpaired two-tailed *t*-test; *p*-value ≤ 0.05 displayed in bold font. c-d) *msbA-KD* and *lpxK-KD* express a catalytically dead Cas9 (dCas9) enzyme for CRISPRi-mediated transcriptional knockdown. Western blot analysis of dCas9 protein expression (160 kDa) from *rfp-KD*, *msbA-KD* (c), and *lpxK-KD* (d). Three independent biological replicates shown.

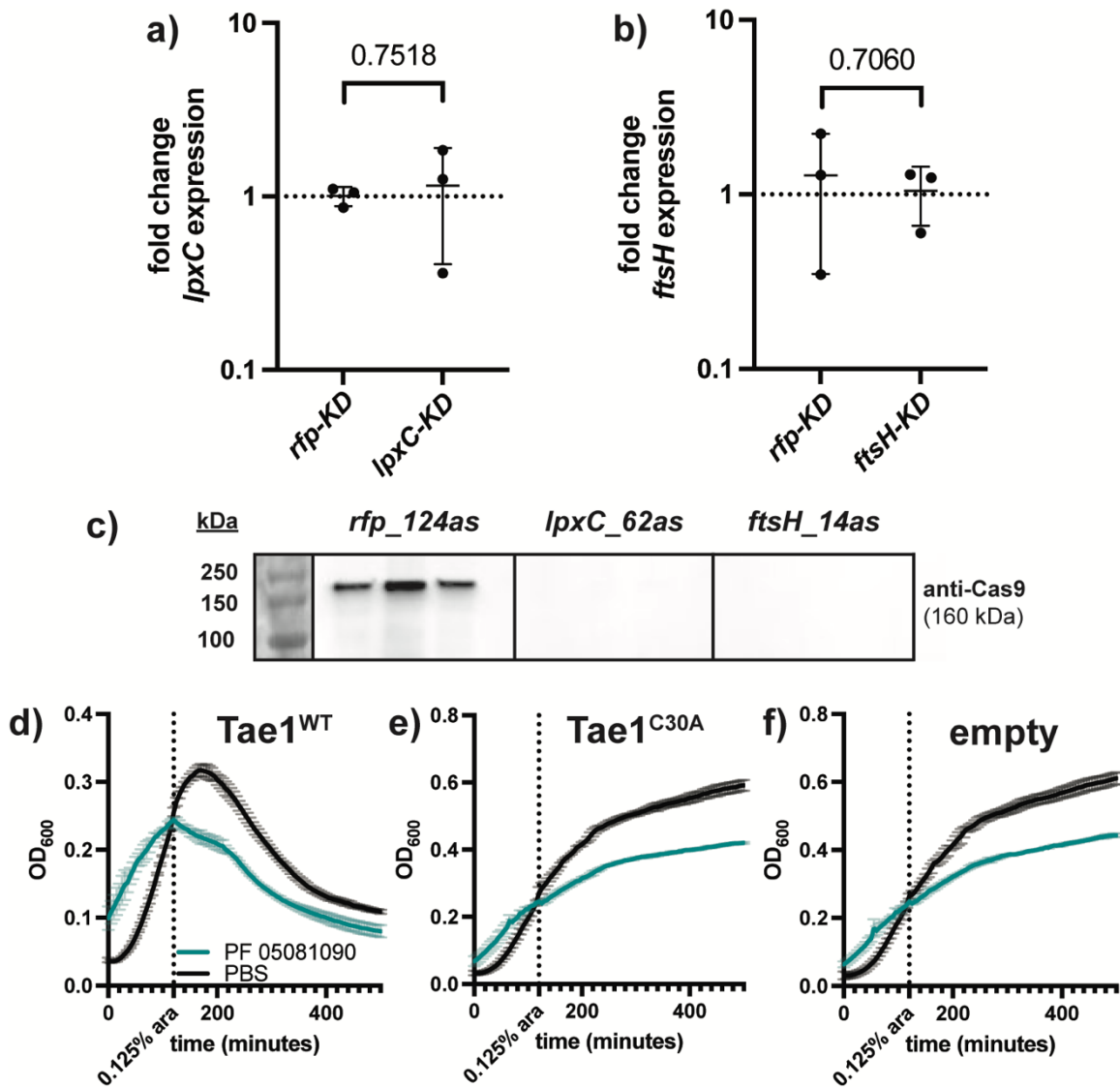


Figure 2.10: Tae1 resistance is independent of LPS biosynthesis master-regulator LpxC a-b) CRISPRi strains *lpxC-KD* and *ftsH-KD* do not disrupt transcription of their target genes. Fold-change in transcription of *lpxC* (a) or *ftsH* (b) expression in *lpxC-KD* (a) or *ftsH-KD* (b) after growth for 6 hours with induced CRISPRi, normalized to expression in *rfp-KD*. Data shown are geometric average of 3 biological replicates \pm s.d. Statistical test: unpaired two-tailed *t*-test; *p*-value ≤ 0.05 displayed in bold font. c) *lpxC-KD* and *ftsH-KD* do not express dCas9. Western blot analysis of dCas9 protein expression (160 kDa) from *rfp-KD*, *lpxC-KD* (c), and *ftsH-KD*. Three independent biological replicates shown. d-f) Chemical inhibition of LpxC does not provide Tae1 resistance. OD₆₀₀ growth curves of wildtype *Eco* pretreated with sub-MIC PF 05081090 (green) or PBS (black), and overexpressing *pBAD24::peIB-tae1^{WT}* (Tae1^{WT}), *pBAD24::peIB-tae1^{C30A}* (Tae1^{C30A}), or *pBAD24* (empty). Data shown: average of 3 biological replicates \pm s.d. Dotted vertical line indicates plasmid induction timepoint (at OD₆₀₀=0.25)

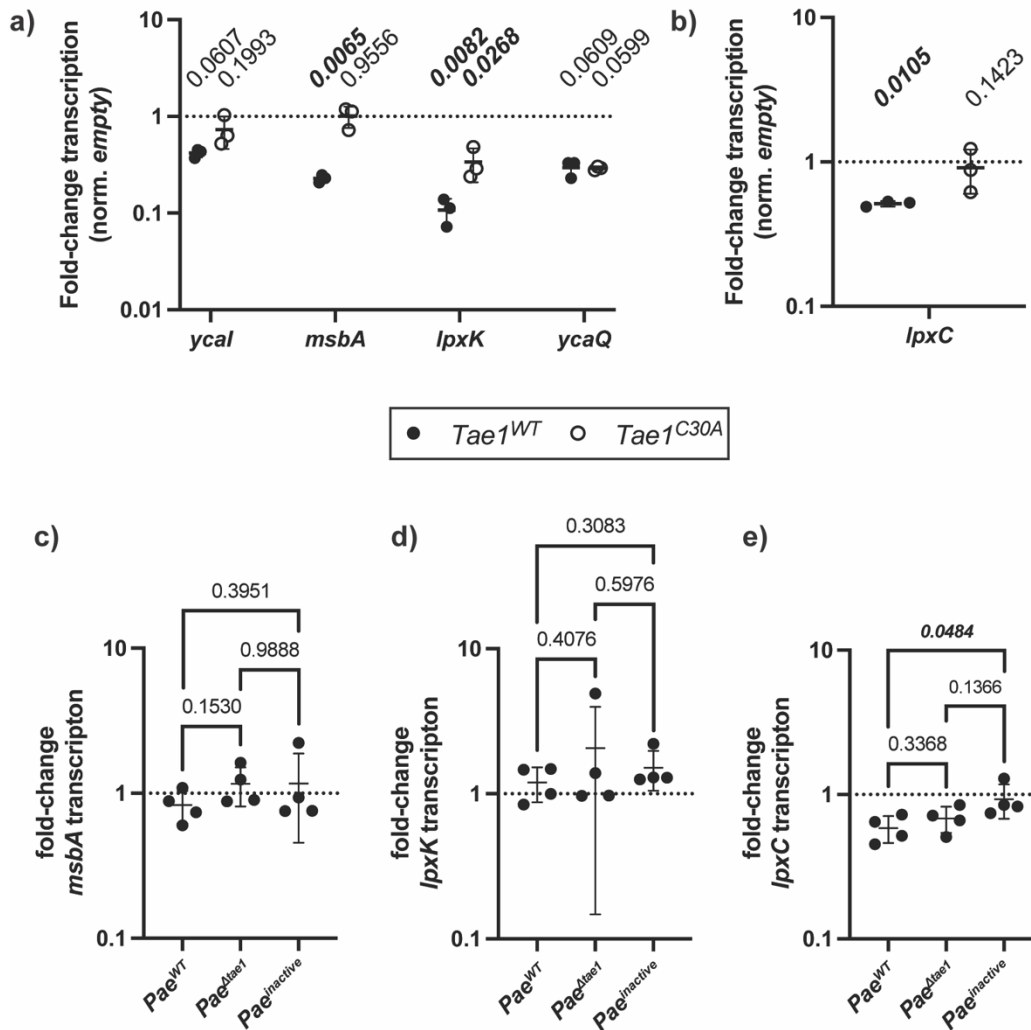


Figure 2.11: Wildtype *Eco* downregulate Lipid-A biosynthesis genes during *Tae1* attack a-b) *msbA*, *lpxK*, and *lpxC* are transcriptionally downregulated after *Tae1* overexpression. Fold-change in transcription for *ycal-msbA-lpxK-ycaQ* (a) and *lpxC* (b) in wildtype *Eco* after 60 minutes of *pBAD24::pelB-tae1^{WT}* (*Tae1^{WT}*; black points) or *pBAD24::pelB-tae1^{C30A}* (*Tae1^{C30A}*; white points) overexpression, normalized to transcription with *pBAD24* (empty) overexpression. Data shown are geometric average of 3 biological replicates \pm s.d. Statistical test: unpaired two-tailed *t*-test; *p*-value ≤ 0.05 displayed in bold font. c-e) Native *Tae1* delivery by T6SS has a mild downregulatory effect on *lpxC*, but not *msbA* or *lpxK*. Fold-change in transcription for *msbA* (c), *lpxK* (d), and *lpxC* in wildtype *Eco* after four hours of interbacterial competition against *Pae^{WT}*, *Pae^{Δtae1}*, or *Pae^{inactive}*. Data shown are geometric average of 3 biological replicates \pm s.d. Statistical test: unpaired two-tailed *t*-test; *p*-value ≤ 0.05 displayed in bold font.

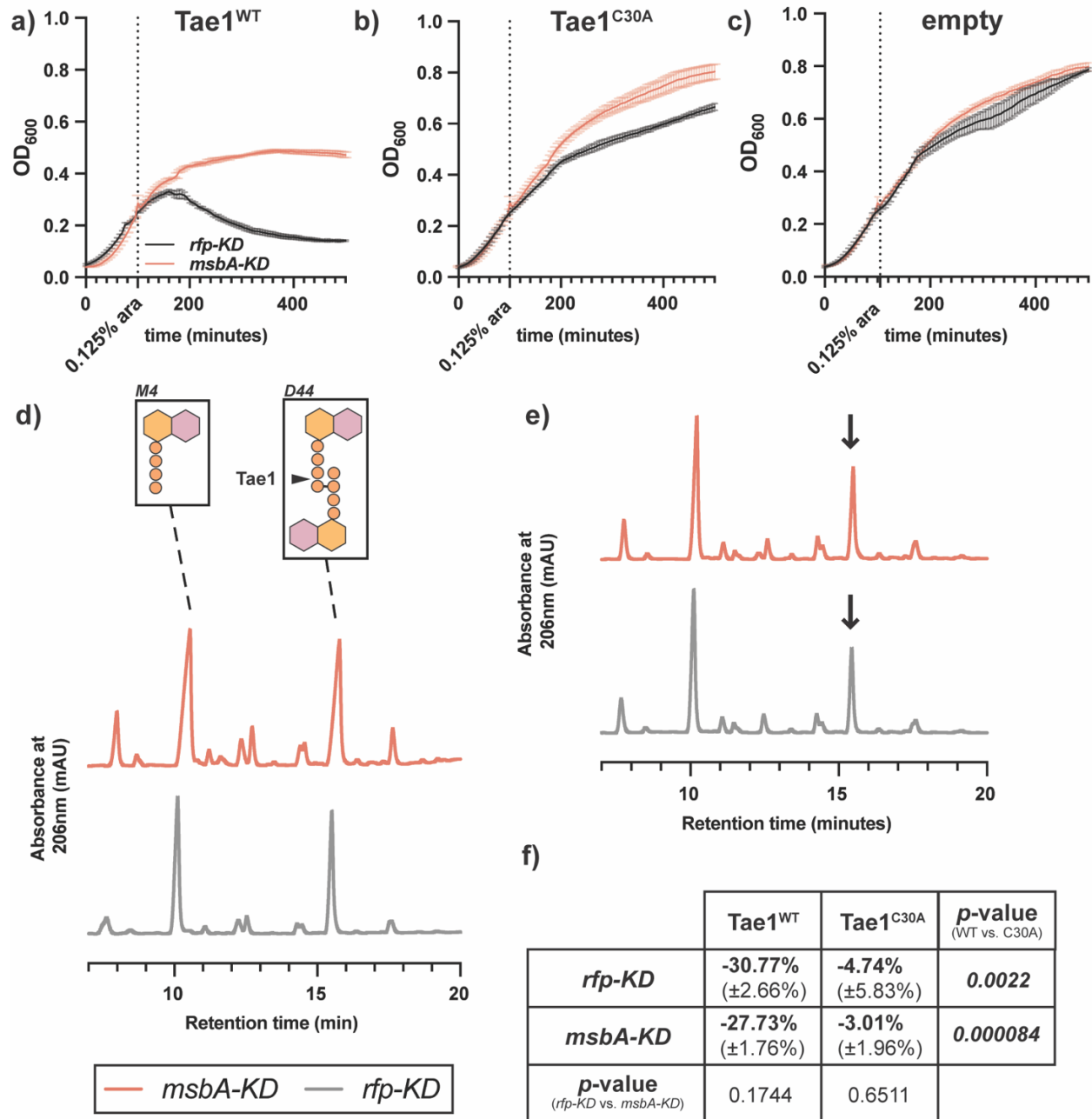


Figure 3.1: Resistance to $Tae1$ in *msbA-KD* is independent of cell wall hydrolysis.

a-c) *msbA-KD* populations have a $Tae1$ -dependent growth advantage. OD₆₀₀ growth curves of *msbA-KD* (orange) and *rfp-KD* (black) with CRISPRi induced, overexpressing (a) $pBAD24::peIB-tae1^{WT}$ ($Tae1^{WT}$), (b) $pBAD24::peIB-tae1^{C30A}$ ($Tae1^{C30A}$), or (c) $pBAD24$ (empty). Data shown: average of 3 biological replicates ± s.d. Dotted vertical line indicates plasmid induction timepoint (at OD₆₀₀=0.25). d) The mucopeptide composition of *msbA-KD* PG is identical to control *rfp-KD*. HPLC chromatograms of mucopeptides purified from *msbA-KD* (orange) and *rfp-KD* (grey) expressing $pBAD24$ (empty). Inset: major mucopeptide species in *Eco* include tetrapeptide monomers (M4; r.t. ~10 minutes) and 4,3-crosslinked tetra-tetra dimers (D44; r.t. ~15.5 minutes). $Tae1$

digests D44 peptides (black arrow). Data shown: representative from 3 biological replicates. e) $Tae1^{WT}$ digests PG from both *msbA-KD* and *rfp-KD* PG *in vivo*. HPLC chromatograms of muropeptides purified from *msbA-KD* (orange) and *rfp-KD* (grey) expressing *pBAD24::pelB-tae1^{WT}* ($Tae1^{WT}$). Black arrow indicates D44 peptide partially digested by $Tae1$. Data shown: representative from 3 biological replicates. f) $Tae1$ is equally efficient at digesting PG in *msbA-KD* and *rfp-KD*. Percent loss of D44 peptide after 60 minutes of periplasmic $Tae1^{WT}$ or $Tae1^{C30A}$ expression. Data shown: average of 3 biological replicates (\pm s.d.). Statistical test: two-tailed unpaired *t*-test; *p*-value ≤ 0.05 displayed in bold font.

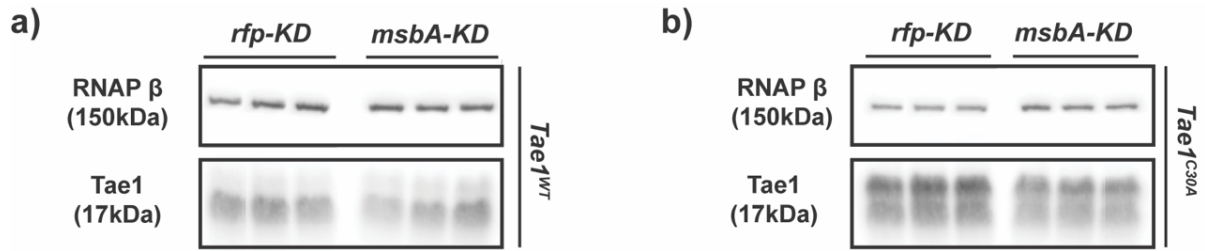


Figure 3.2: Tae1 protein expression is unaffected in *msbA-KD*. a-b) Bulk Tae1 protein expression is similar between *msbA-KD* and *rfp-KD*. Western blot analysis of periplasmic Tae1 protein (17kDa) from (a) *pBAD24::pelB-tae1^{WT}* (Tae1^{WT}) or (b) *pBAD24::pelB-tae1^{C30A}* (Tae1^{C30A}) in *rfp-KD* and *msbA-KD* (with induced CRISPRi). Protein expression of RNA polymerase (β subunit) (150kDa) is used as an internal loading control.

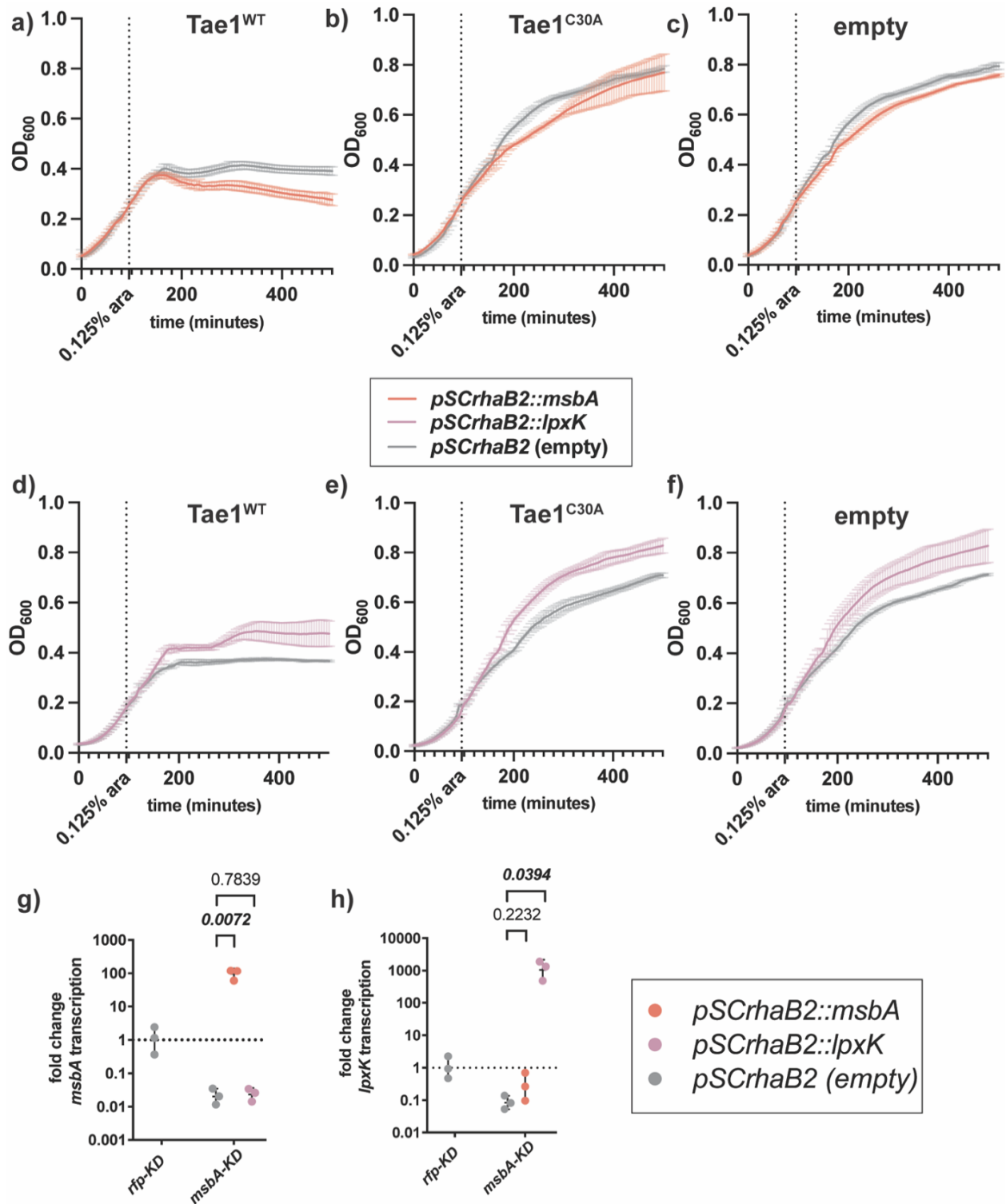


Figure 3.3: Plasmid-borne overexpression of *msbA* partially rescues *Tae1* sensitivity in *msbA-KD*. a-c) Plasmid-borne *msbA* overexpression partially rescues *msbA-KD* resistance to lysis by *Tae1*. OD₆₀₀ growth curves of *msbA-KD* with induced CRISPRi, overexpressing *pSCrhaB2::msbA* (orange) or *pSCrhaB2* (empty) (grey)

alongside (a) *pBAD24::pelB-tae1^{WT}* (Tae1^{WT}), (b) *pBAD24::pelB-tae1^{C30A}* (Tae1^{C30A}), or (c) *pBAD24* (empty). Data shown: average of 3 biological replicates \pm s.d. Dotted vertical line indicates *pBAD24* induction timepoint (at OD₆₀₀=0.25) (0.125% arabinose w/v). d-f) Plasmid-borne *lpxK* overexpression enhances *msbA-KD* resistance to lysis by Tae1. OD₆₀₀ growth curves of *msbA-KD* with CRISPRi induced, overexpressing *pSCrhaB2::lpxK* (purple) or *pSCrhaB2* (empty) (grey) alongside (d) *pBAD24::pelB-tae1^{WT}* (Tae1^{WT}), (e) *pBAD24::pelB-tae1^{C30A}* (Tae1^{C30A}), or (f) *pBAD24* (empty). Data shown: average of 3 biological replicates \pm s.d. Dotted vertical line indicates *pBAD24* induction timepoint (at OD₆₀₀=0.25) (0.125% arabinose w/v). g-h) *pSCrhaB2* vectors selectively rescue transcription of their target gene by overexpression. qRT-PCR analysis of transcriptional fold-change in (g) *msbA* or (h) *lpxK* expression with constitutive rhamnose induction of *pSCrhaB2::msbA* (orange), *pSCrhaB2::lpxK* (purple), or (c) *pSCrhaB2* (empty; grey) in *msbA-KD* with induced CRISPRi. Expression normalized against basal *msbA* expression in *rfp-KD* + *pSCrhaB2* (empty). Data shown: geometric average of 3 biological replicates \pm s.d. Statistical test: unpaired two-tailed *t*-test; *p*-value ≤ 0.05 displayed in bold font.

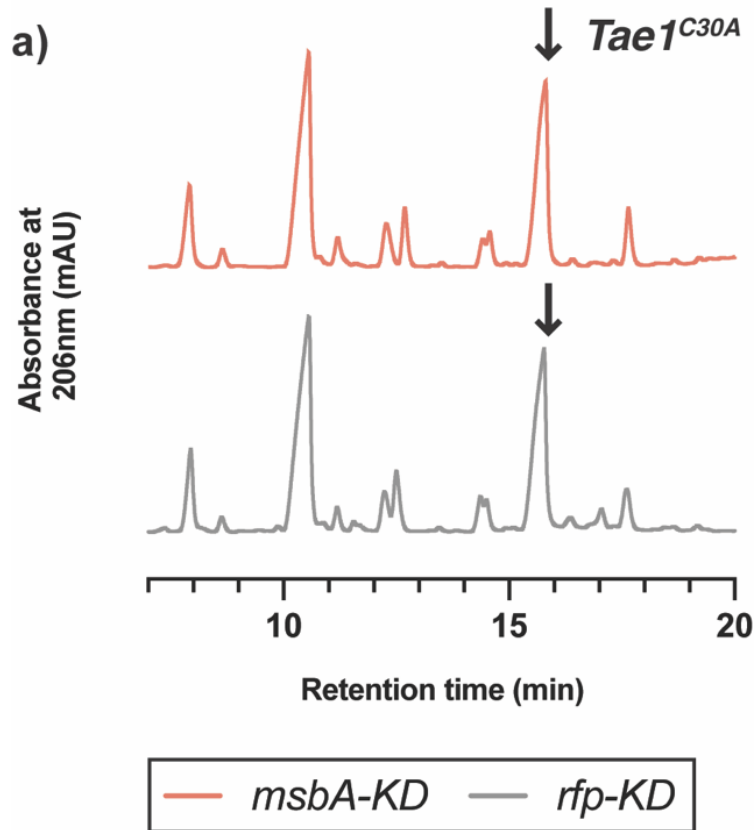


Figure 3.4: *Tae1^{C30A}* hydrolyzes D44 muropeptides in *rfp-KD* and *msbA-KD*
 a) *Tae1^{C30A}* overexpression yields minor digestion of D44 muropeptides. HPLC chromatograms of muropeptides purified from *msbA-KD* (orange) and *rfp-KD* (grey) expressing *pBAD24::pelB-tae1^{C30A}* (*Tae1^{C30A}*). Black arrow indicates D44 peptide partially digested by *Tae1^{C30A}*. Data shown: representative from 3 biological replicates.

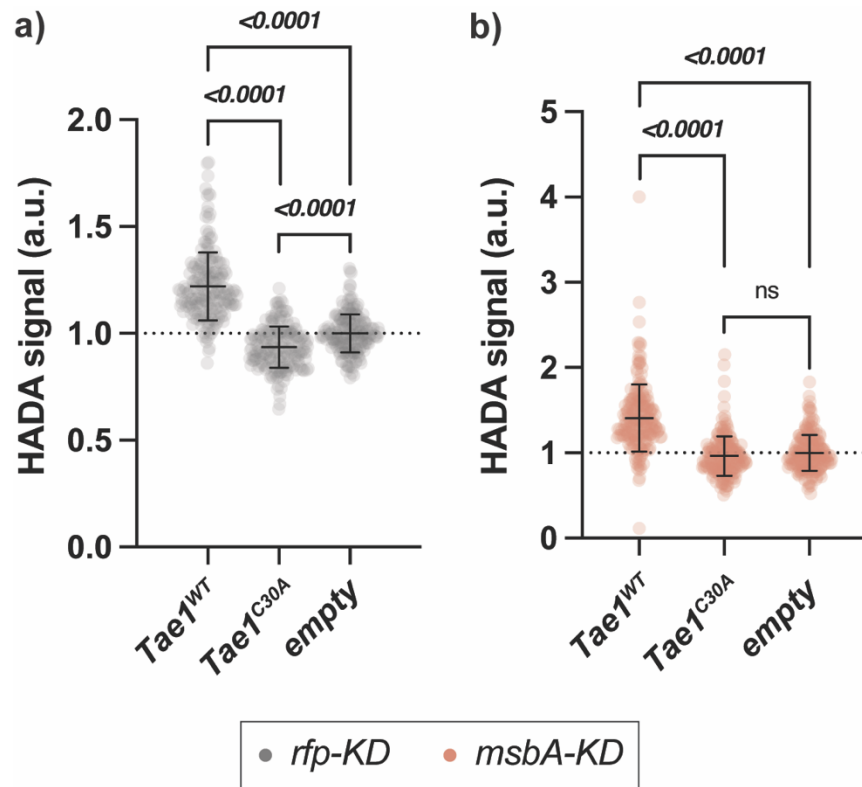


Figure 3.5: PG synthesis is suppressed in *msbA-KD* but sensitive to Tae1 activity
 a-b) PG synthesis activity is sensitive to Tae1 overexpression. Single-cell fluorescence intensity measurements for *rfp-KD* (a; grey) or *msbA-KD* (b; orange) after incorporating the fluorescent D-amino acid HADA into PG after 60 minutes of overexpressing *pBAD24::pelB-tae1^{WT}* (*Tae1^{WT}*), *pBAD24::pelB-tae1^{C30A}* (*Tae1^{C30A}*), or *pBAD24* (*empty*), with CRISPRi induced. Data shown: 600 cells (200 cells x 3 biological replicates), with average \pm s.d. Statistical test: unpaired two-tailed *t*-test; *p*-value ≤ 0.05 displayed in bold font.

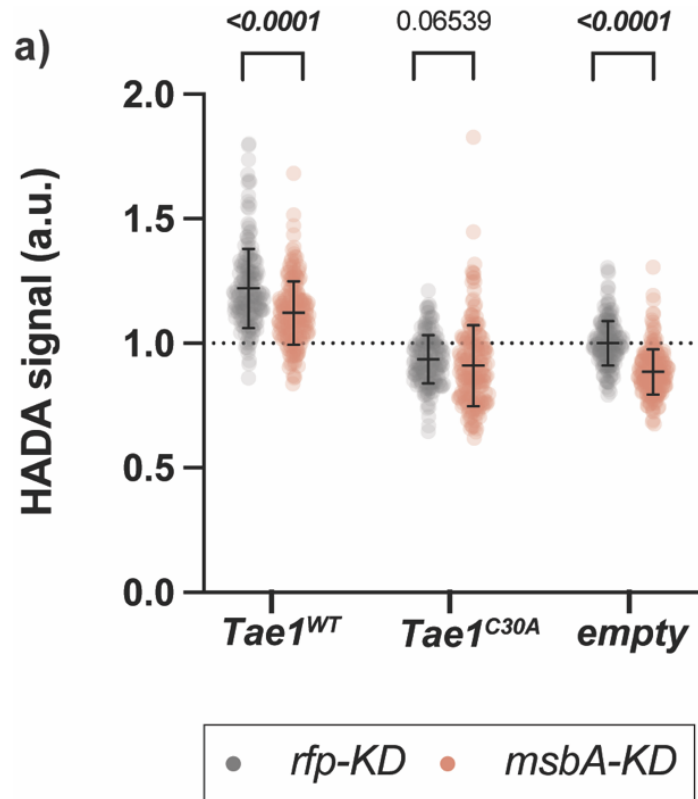


Figure 3.6: PG synthesis activity in *msbA-KD* is suppressed across all conditions
 a) PG synthesis activity in *msbA-KD* is attenuated under all tested conditions. Single-cell fluorescence intensity measurements for *rfp-KD* (grey) or *msbA-KD* (orange) incorporating the fluorescent D-amino acid HADA into PG after 60 minutes of overexpressing *pBAD24::pelB-tae1*^{WT} (*Tae1*^{WT}), *pBAD24::pelB-tae1*^{C30A} (*Tae1*^{C30A}), or *pBAD24* (empty), with CRISPRi induced. All data normalized to average HADA signal in *rfp-KD* + empty. Data shown: 600 cells (200 cells x 3 biological replicates), with average \pm s.d. Statistical test: unpaired two-tailed *t*-test; *p*-value ≤ 0.05 displayed in bold font.

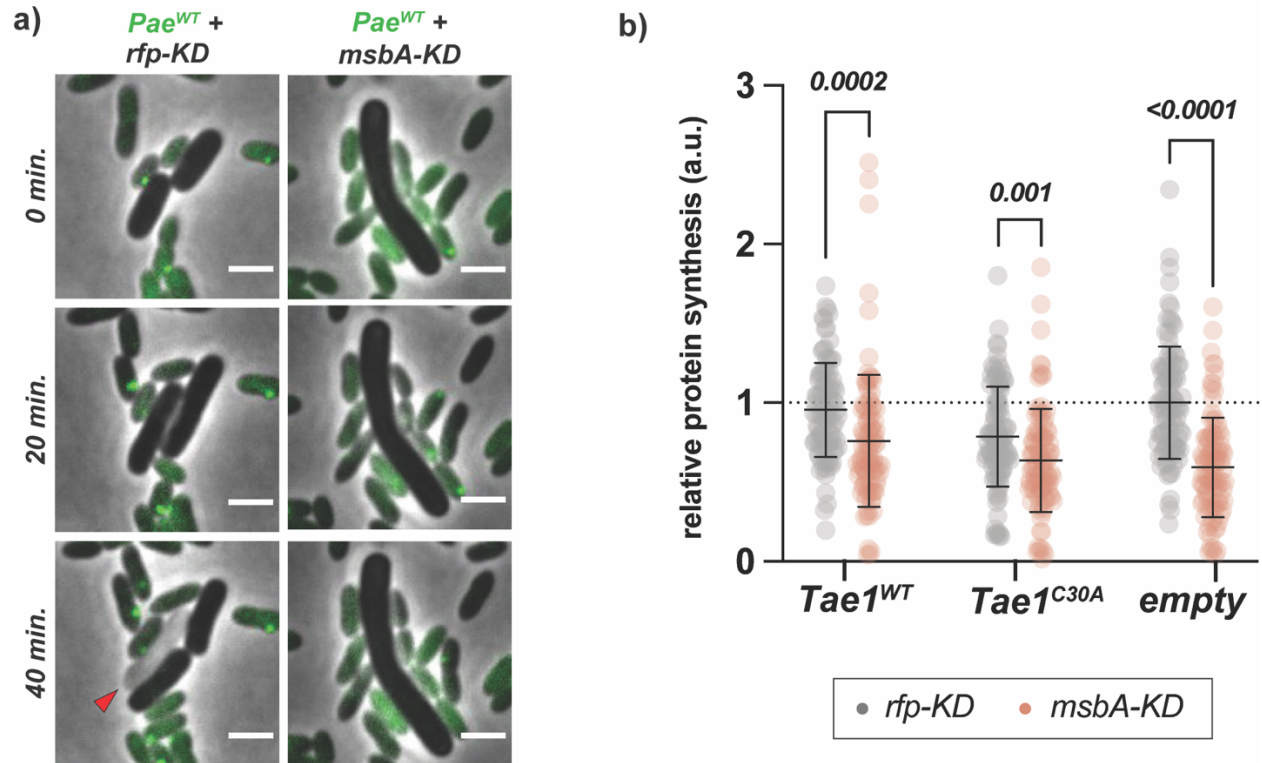


Figure 3.7: Blocks to growth and protein synthesis accompany *Tae1* resistance in *msbA-KD*. a) *msbA-KD* cells resist lysis from *Pae*^{WT} while growing slowly without dividing. Representative frames from time-course imaging of *rfp-KD* (left column; grey) and *msbA-KD* (right column; grey) co-cultured with *Pae*^{WT} (green), with CRISPRi induced. Green foci in *Pae*^{WT} indicate aggregates of GFP-labelled ClpV, which signal a H1-T6SS firing event. Red arrow indicates lysed cell. Data shown are merged phase and fluorescent channels. Scale bar: 2µm. b) Protein synthesis activity is attenuated in *msbA-KD*. Single-cell fluorescence intensity measurements for *rfp-KD* (grey) or *msbA-KD* (orange) cells after incorporating fluorescently-labelled O-propargyl-puromycin (OPP) into nascent peptides during overexpression of *pBAD24::pelB-tae1*^{WT} (*Tae1*^{WT}), *pBAD24::pelB-tae1*^{C30A} (*Tae1*^{C30A}), or *pBAD24* (empty), with CRISPRi induced. All data normalized to average OPP signal in *rfp-KD* + empty. Data shown: 100 cells/condition, with average ± s.d. Statistical test: unpaired two-tailed *t*-test; *p*-value ≤0.05 displayed in bold font.

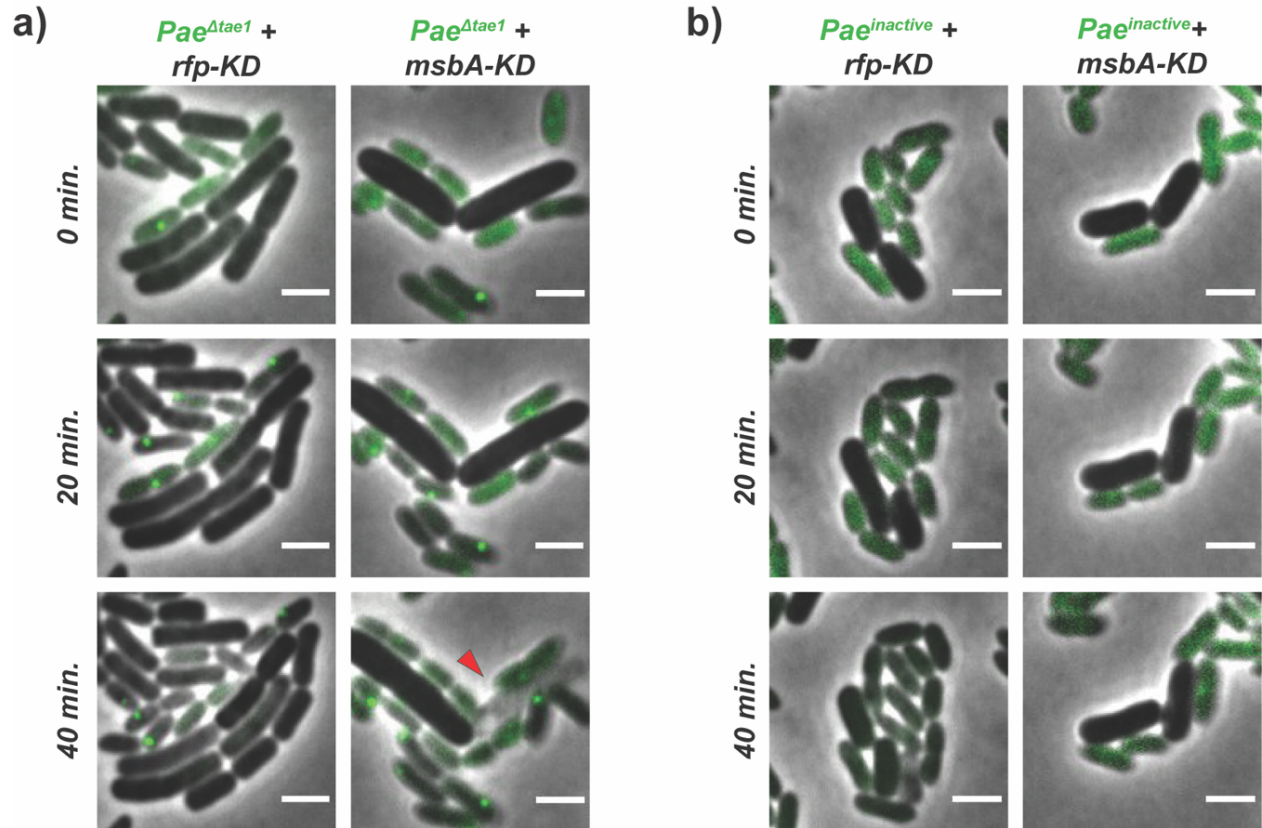


Figure 3.8: *msbA-KD* growth defects are independent of *Pae* T6SS activity

a-b) msbA-KD cells maintain growth defects regardless of *Pae* competitor.

Representative frames from time-course imaging of *rfp-KD* (left column; grey cells) and *msbA-KD* (right column; grey cells) co-cultured with *Pae*^{Δtae1} (a) or *Pae*^{inactive} (b) (green cells), and with induced CRISPRi. Green foci in *Pae*^{WT} indicate aggregates of GFP-labelled ClpV, which signal H1-T6SS firing events. Red arrow indicates lysed cell. Data shown are merged phase and fluorescent channels. Scale bar: 2μm.

TABLES

Table 2.1: Cell envelope gene KDs develop strong fitness changes against Tae1 in competition. KDs that target PG synthesis can increase *Pae*^{WT} sensitivity, while targeting other cell envelope processes can result in sensitivity or resistance. Data shown: normalized L2FC values for all 20 KD strains with unique and significant fitness changes against *Pae*^{WT} (which secretes Tae1); average of four biological replicates.

KD target	pathway/process	Avg. L2FC (<i>Pae</i> ^{WT})	fitness against <i>Pae</i> ^{WT}
<i>murA</i>	PG synthesis	-7.40	sensitive
<i>ftsI</i>	Cell division	-6.85	sensitive
<i>accD</i>	Lipid metabolism	-4.37	sensitive
<i>lptC</i>	LPS synthesis	-3.35	sensitive
<i>murC</i>	PG synthesis	-2.61	sensitive
<i>bamA</i>	OM protein assembly	-2.46	sensitive
<i>murI</i>	PG synthesis	-1.86	sensitive
<i>mrcB</i>	PG synthesis	-1.60	sensitive
<i>murJ</i>	PG synthesis	-1.59	sensitive
<i>pssA</i>	Lipid metabolism	1.77	resistant
<i>hemE</i>	Heme metabolism	1.79	resistant
<i>msbA</i>	LPS synthesis	1.84	resistant
<i>waaA</i>	LPS synthesis	1.91	resistant
<i>lpxA</i>	LPS synthesis	2.18	resistant
<i>ffs</i>	Membrane trafficking/ secretion	2.25	resistant
<i>acpP</i>	Lipid metabolism	2.25	resistant
<i>ffh</i>	Membrane trafficking/ secretion	2.30	resistant
<i>kdsB</i>	LPS synthesis	2.35	resistant
<i>lpxK</i> (<i>lpxK</i> _{-1as})	LPS synthesis	2.39	resistant
<i>lpxK</i> (<i>lpxK</i> _{32as})	LPS synthesis	2.69	resistant

Table 2.2: Bacterial strains and plasmids used in this study. Supplemental file.

Table 2.3: Primer sequences. Supplemental file.

Table 2.4: Corrected L2FC values from screen. Supplemental file.

Table 2.5: Final Diff values from screen. Supplemental file.

Table 3.1: PG synthesis activity is sensitive to CRISPRi and Tae1 overexpression. Descriptive statistics for normalized percent change in HADA fluorescence in *rfp-KD* and *msbA-KD* as related to **Fig.5** and **Supp. Fig. 10**. Data shown: average of 600 single-cell measurements \pm s.d.

		% change (intra- strain)	% change (<i>rfp-KD</i> norm.)
<i>rfp-KD</i>	Tae1 ^{WT}	22% (\pm 3.6%)	
	Tae1 ^{C30A}	-6.5% (\pm 2.6%)	
	empty	0% (\pm 1.6%)	
<i>msbA-KD</i>	Tae1 ^{WT}	26.5% (\pm 2.5%)	12% (\pm 2.5%)
	Tae1 ^{C30A}	2.82% (\pm 3.2%)	-9% (\pm 3.2%)
	empty	0% (\pm 2.0%)	-11.5% (\pm 2.0%)

REFERENCES

- (1) Ghoul, M.; Mitri, S. The Ecology and Evolution of Microbial Competition. *Trends Microbiol* **2016**, *24* (10), 833–845. <https://doi.org/10.1016/j.tim.2016.06.011>.
- (2) Stubbendieck, R. M.; Straight, P. D. Multifaceted Interfaces of Bacterial Competition. *Journal of Bacteriology* **2016**, *198* (16), 2145–2155. <https://doi.org/10.1128/JB.00275-16>.
- (3) Costa, T. R. D.; Felisberto-Rodrigues, C.; Meir, A.; Prevost, M. S.; Redzej, A.; Trokter, M.; Waksman, G. Secretion Systems in Gram-Negative Bacteria: Structural and Mechanistic Insights. *Nature Reviews Microbiology* **2015**, *13* (6), 343–359. <https://doi.org/10.1038/nrmicro3456>.
- (4) Green, E. R.; Meccas, J. Bacterial Secretion Systems – An Overview. *Microbiol Spectr* **2016**, *4* (1), 10.1128/microbiolspec.VMBF-0012–2015. <https://doi.org/10.1128/microbiolspec.VMBF-0012-2015>.
- (5) Trivedi, A.; Gosai, J.; Nakane, D.; Shrivastava, A. Design Principles of the Rotary Type 9 Secretion System. *Frontiers in Microbiology* **2022**, *13*.
- (6) Boyer, F.; Fichant, G.; Berthod, J.; Vandenbrouck, Y.; Attree, I. Dissecting the Bacterial Type VI Secretion System by a Genome Wide in Silico Analysis: What Can Be Learned from Available Microbial Genomic Resources? *BMC Genomics* **2009**, *10*, 104. <https://doi.org/10.1186/1471-2164-10-104>.
- (7) Alcoforado Diniz, J.; Liu, Y.; Coulthurst, S. J. Molecular Weaponry: Diverse Effectors Delivered by the Type VI Secretion System. *Cell Microbiol* **2015**, *17* (12), 1742–1751. <https://doi.org/10.1111/cmi.12532>.

- (8) Bingle, L. E.; Bailey, C. M.; Pallen, M. J. Type VI Secretion: A Beginner's Guide. *Current Opinion in Microbiology* **2008**, *11* (1), 3–8.
<https://doi.org/10.1016/j.mib.2008.01.006>.
- (9) Ringel, P. D.; Hu, D.; Basler, M. The Role of Type VI Secretion System Effectors in Target Cell Lysis and Subsequent Horizontal Gene Transfer. *Cell Rep* **2017**, *21* (13), 3927–3940. <https://doi.org/10.1016/j.celrep.2017.12.020>.
- (10) Cherrak, Y.; Flaugnatti, N.; Durand, E.; Journet, L.; Cascales, E. Structure and Activity of the Type VI Secretion System. **2019**, *12*.
- (11) Wang, J.; Brodmann, M.; Basler, M. Assembly and Subcellular Localization of Bacterial Type VI Secretion Systems. *Annual Review of Microbiology* **2019**, *73* (1).
<https://doi.org/10.1146/annurev-micro-020518-115420>.
- (12) Basler, M.; Pilhofer, M.; Henderson, G. P.; Jensen, G. J.; Mekalanos, J. J. Type VI Secretion Requires a Dynamic Contractile Phage Tail-like Structure. *Nature* **2012**, *483* (7388), 182–186. <https://doi.org/10.1038/nature10846>.
- (13) Basler, M. Type VI Secretion System: Secretion by a Contractile Nanomachine. *Philos Trans R Soc Lond B Biol Sci* **2015**, *370* (1679), 20150021.
<https://doi.org/10.1098/rstb.2015.0021>.
- (14) Vettiger, A.; Basler, M. Type VI Secretion System Substrates Are Transferred and Reused among Sister Cells. *Cell* **2016**, *167* (1), 99-110.e12.
<https://doi.org/10.1016/j.cell.2016.08.023>.
- (15) Unterweger, D.; Kitaoka, M.; Miyata, S. T.; Bachmann, V.; Brooks, T. M.; Moloney, J.; Sosa, O.; Silva, D.; Duran-Gonzalez, J.; Provenzano, D.; Pukatzki, S.
Constitutive Type VI Secretion System Expression Gives *Vibrio Cholerae* Intra- and

- Interspecific Competitive Advantages. *PLoS One* **2012**, 7 (10), e48320.
<https://doi.org/10.1371/journal.pone.0048320>.
- (16) Chen, L.; Zou, Y.; She, P.; Wu, Y. Composition, Function, and Regulation of T6SS in *Pseudomonas Aeruginosa*. *Microbiological Research* **2015**, 172, 19–25.
<https://doi.org/10.1016/j.micres.2015.01.004>.
- (17) Jurėnas, D.; Journet, L. Activity, Delivery, and Diversity of Type VI Secretion Effectors. *Molecular Microbiology* **2021**, 115 (3), 383–394.
<https://doi.org/10.1111/mmi.14648>.
- (18) LaCourse, K. D.; Peterson, S. B.; Kulasekara, H. D.; Radey, M. C.; Kim, J.; Mougous, J. D. Conditional Toxicity and Synergy Drive Diversity among Antibacterial Effectors. *Nat Microbiol* **2018**, 3 (4), 440–446.
<https://doi.org/10.1038/s41564-018-0113-y>.
- (19) Mougous, J. D.; Cuff, M. E.; Raunser, S.; Shen, A.; Zhou, M.; Gifford, C. A.; Goodman, A. L.; Joachimiak, G.; Ordoñez, C. L.; Lory, S.; Walz, T.; Joachimiak, A.; Mekalanos, J. J. A Virulence Locus of *Pseudomonas Aeruginosa* Encodes a Protein Secretion Apparatus. *Science* **2006**, 312 (5779), 1526–1530.
<https://doi.org/10.1126/science.1128393>.
- (20) Ho, B. T.; Basler, M.; Mekalanos, J. J. Type 6 Secretion System-Mediated Immunity to Type 4 Secretion System-Mediated Horizontal Gene Transfer. *Science* **2013**, 342 (6155), 250–253. <https://doi.org/10.1126/science.1243745>.
- (21) Chou, S.; Bui, N. K.; Russell, A. B.; Lexa, K. W.; Gardiner, T. E.; LeRoux, M.; Vollmer, W.; Mougous, J. D. Structure of a Peptidoglycan Amidase Effector

- Targeted to Gram-Negative Bacteria by the Type VI Secretion System. *Cell Reports* **2012**, 1 (6), 656–664. <https://doi.org/10.1016/j.celrep.2012.05.016>.
- (22) Radkov, A.; Sapiro, A. L.; Flores, S.; Henderson, C.; Saunders, H.; Kim, R.; Massa, S.; Thompson, S.; Mateusiak, C.; Biboy, J.; Zhao, Z.; Starita, L. M.; Hatleberg, W. L.; Vollmer, W.; Russell, A. B.; Simorre, J.-P.; Anthony-Cahill, S.; Brzovic, P.; Hayes, B.; Chou, S. Antibacterial Potency of Type VI Amidase Effector Toxins Is Dependent on Substrate Topology and Cellular Context. *eLife* **2022**, 11, e79796. <https://doi.org/10.7554/eLife.79796>.
- (23) LaCourse, K. D.; Peterson, S. B.; Kulasekara, H. D.; Radey, M. C.; Kim, J.; Mougous, J. D. Conditional Toxicity and Synergy Drive Diversity among Antibacterial Effectors. *Nat Microbiol* **2018**, 3 (4), 440–446. <https://doi.org/10.1038/s41564-018-0113-y>.
- (24) Russell, A. B.; Singh, P.; Brittnacher, M.; Bui, N. K.; Hood, R. D.; Carl, M. A.; Agnello, D. M.; Schwarz, S.; Goodlett, D. R.; Vollmer, W.; Mougous, J. D. A Widespread Bacterial Type VI Secretion Effector Superfamily Identified Using a Heuristic Approach. *Cell Host & Microbe* **2012**, 11 (5), 538–549. <https://doi.org/10.1016/j.chom.2012.04.007>.
- (25) Whitney, J. C.; Chou, S.; Russell, A. B.; Biboy, J.; Gardiner, T. E.; Ferrin, M. A.; Brittnacher, M.; Vollmer, W.; Mougous, J. D. Identification, Structure, and Function of a Novel Type VI Secretion Peptidoglycan Glycoside Hydrolase Effector-Immunity Pair *. *Journal of Biological Chemistry* **2013**, 288 (37), 26616–26624. <https://doi.org/10.1074/jbc.M113.488320>.

- (26) Koch, A. L. How Bacteria Grow and Divide in Spite of Internal Hydrostatic Pressure. *Canadian Journal of Microbiology* **1985**, 31 (12), 1071–1084.
<https://doi.org/10.1139/m85-204>.
- (27) Vollmer, W.; Blanot, D.; De Pedro, M. A. Peptidoglycan Structure and Architecture. *FEMS Microbiology Reviews* **2008**, 32 (2), 149–167. <https://doi.org/10.1111/j.1574-6976.2007.00094.x>.
- (28) Vollmer, W. Bacterial Growth Does Require Peptidoglycan Hydrolases. *Molecular Microbiology* **2012**, 86 (5), 1031–1035. <https://doi.org/10.1111/mmi.12059>.
- (29) Errington, J.; Mickiewicz, K.; Kawai, Y.; Wu, L. J. L-Form Bacteria, Chronic Diseases and the Origins of Life. *Philos Trans R Soc Lond B Biol Sci* **2016**, 371 (1707). <https://doi.org/10.1098/rstb.2015.0494>.
- (30) Russell, A. B.; Hood, R. D.; Bui, N. K.; LeRoux, M.; Vollmer, W.; Mougous, J. D. Type VI Secretion Delivers Bacteriolytic Effectors to Target Cells. *Nature* **2011**, 475 (7356), 343–347. <https://doi.org/10.1038/nature10244>.
- (31) Benz, J.; Sendlmeier, C.; Barends, T. R. M.; Meinhart, A. Structural Insights into the Effector – Immunity System Tse1/Tsi1 from *Pseudomonas Aeruginosa*. *PLOS ONE* **2012**, 7 (7), e40453. <https://doi.org/10.1371/journal.pone.0040453>.
- (32) Shang, G.; Liu, X.; Lu, D.; Zhang, J.; Li, N.; Zhu, C.; Liu, S.; Yu, Q.; Zhao, Y.; Zhang, H.; Hu, J.; Cang, H.; Xu, S.; Gu, L. Structural Insight into How *Pseudomonas Aeruginosa* Peptidoglycanhydrolase Tse1 and Its Immunity Protein Tsi1 Function. *Biochemical Journal* **2012**, 448 (2), 201–211.
<https://doi.org/10.1042/BJ20120668>.

- (33) Espaillet, A.; Forsmo, O.; El Biari, K.; Björk, R.; Lemaitre, B.; Trygg, J.; Cañada, F. J.; de Pedro, M. A.; Cava, F. Chemometric Analysis of Bacterial Peptidoglycan Reveals Atypical Modifications That Empower the Cell Wall against Predatory Enzymes and Fly Innate Immunity. *J. Am. Chem. Soc.* **2016**, *138* (29), 9193–9204. <https://doi.org/10.1021/jacs.6b04430>.
- (34) Le, N.-H.; Peters, K.; Espaillet, A.; Sheldon, J. R.; Gray, J.; Di Venanzio, G.; Lopez, J.; Djahanschiri, B.; Mueller, E. A.; Hennon, S. W.; Levin, P. A.; Ebersberger, I.; Skaar, E. P.; Cava, F.; Vollmer, W.; Feldman, M. F. Peptidoglycan Editing Provides Immunity to *Acinetobacter Baumannii* during Bacterial Warfare. *Sci Adv* **2020**, *6* (30), eabb5614. <https://doi.org/10.1126/sciadv.abb5614>.
- (35) Hersch, S. J.; Watanabe, N.; Stietz, M. S.; Manera, K.; Kamal, F.; Burkinshaw, B.; Lam, L.; Pun, A.; Li, M.; Savchenko, A.; Dong, T. G. Envelope Stress Responses Defend against Type Six Secretion System Attacks Independently of Immunity Proteins. *Nat Microbiol* **2020**, *5* (5), 706–714. <https://doi.org/10.1038/s41564-020-0672-6>.
- (36) Kamal, F.; Liang, X.; Manera, K.; Pei, T.-T.; Kim, H.; Lam, L. G.; Pun, A.; Hersch, S. J.; Dong, T. G. Differential Cellular Response to Translocated Toxic Effectors and Physical Penetration by the Type VI Secretion System. *Cell Reports* **2020**, *31* (11), 107766. <https://doi.org/10.1016/j.celrep.2020.107766>.
- (37) Pérez-Lorente, A. I.; Molina-Santiago, C.; de Vicente, A.; Romero, D. *Sporulation Activated via σ^W Protects Bacillus from a Tse1 Peptidoglycan Hydrolase T6SS Effector*; preprint; Microbiology, 2022. <https://doi.org/10.1101/2022.02.23.481616>.

- (38) Dong, T. G.; Dong, S.; Catalano, C.; Moore, R.; Liang, X.; Mekalanos, J. J. Generation of Reactive Oxygen Species by Lethal Attacks from Competing Microbes. *Proc Natl Acad Sci U S A* **2015**, *112* (7), 2181–2186. <https://doi.org/10.1073/pnas.1425007112>.
- (39) Crisan, C. V.; Nichols, H. L.; Wiesenfeld, S.; Steinbach, G.; Yunker, P. J.; Hammer, B. K. Glucose Confers Protection to *Escherichia Coli* against Contact Killing by *Vibrio Cholerae*. *Sci Rep* **2021**, *11*, 2935. <https://doi.org/10.1038/s41598-021-81813-4>.
- (40) Typas, A.; Banzhaf, M.; Gross, C. A.; Vollmer, W. From the Regulation of Peptidoglycan Synthesis to Bacterial Growth and Morphology. *Nat Rev Microbiol* **2011**, *10* (2), 123–136. <https://doi.org/10.1038/nrmicro2677>.
- (41) Yang, D. C.; Tan, K.; Joachimiak, A.; Bernhardt, T. G. A Conformational Switch Controls Cell Wall-Remodelling Enzymes Required for Bacterial Cell Division. *Mol Microbiol* **2012**, *85* (4), 768–781. <https://doi.org/10.1111/j.1365-2958.2012.08138.x>.
- (42) Delhaye, A.; Collet, J.-F.; Laloux, G. Fine-Tuning of the Cpx Envelope Stress Response Is Required for Cell Wall Homeostasis in *Escherichia Coli*. *mBio* **2016**, *7* (1), e00047-16. <https://doi.org/10.1128/mBio.00047-16>.
- (43) Peters, K.; Kannan, S.; Rao, V. A.; Biboy, J.; Vollmer, D.; Erickson, S. W.; Lewis, R. J.; Young, K. D.; Vollmer, W. The Redundancy of Peptidoglycan Carboxypeptidases Ensures Robust Cell Shape Maintenance in *Escherichia Coli*. *mBio* **2016**, *7* (3), e00819-16. <https://doi.org/10.1128/mBio.00819-16>.
- (44) Morè, N.; Martorana, A. M.; Biboy, J.; Otten, C.; Winkle, M.; Serrano, C. K. G.; Montón Silva, A.; Atkinson, L.; Yau, H.; Breukink, E.; den Blaauwen, T.; Vollmer,

- W.; Polissi, A. Peptidoglycan Remodeling Enables Escherichia Coli To Survive Severe Outer Membrane Assembly Defect. *mBio* **2019**, *10* (1), e02729-18.
<https://doi.org/10.1128/mBio.02729-18>.
- (45) Mueller, E. A.; Egan, A. J.; Breukink, E.; Vollmer, W.; Levin, P. A. Plasticity of Escherichia Coli Cell Wall Metabolism Promotes Fitness and Antibiotic Resistance across Environmental Conditions. *Elife* **2019**, *8*, e40754.
<https://doi.org/10.7554/eLife.40754>.
- (46) Hersch, S. J.; Sejuty, R. T.; Manera, K.; Dong, T. G. *High Throughput Identification of Genes Conferring Resistance or Sensitivity to Toxic Effectors Delivered by the Type VI Secretion System*; preprint; Microbiology, 2021.
<https://doi.org/10.1101/2021.10.06.463450>.
- (47) Whitney, J. C.; Quentin, D.; Sawai, S.; LeRoux, M.; Harding, B. N.; Ledvina, H. E.; Tran, B. Q.; Robinson, H.; Goo, Y. A.; Goodlett, D. R.; Raunser, S.; Mougous, J. D. An Interbacterial NAD(P)⁺ Glycohydrolase Toxin Requires Elongation Factor Tu for Delivery to Target Cells. *Cell* **2015**, *163* (3), 607–619.
<https://doi.org/10.1016/j.cell.2015.09.027>.
- (48) Lin, H.-H.; Yu, M.; Sriramoju, M. K.; Hsu, S.-T. D.; Liu, C.-T.; Lai, E.-M. A High-Throughput Interbacterial Competition Screen Identifies ClpAP in Enhancing Recipient Susceptibility to Type VI Secretion System-Mediated Attack by *Agrobacterium Tumefaciens*. *Front Microbiol* **2020**, *10*, 3077.
<https://doi.org/10.3389/fmicb.2019.03077>.
- (49) Bikard, D.; Jiang, W.; Samai, P.; Hochschild, A.; Zhang, F.; Marraffini, L. A. Programmable Repression and Activation of Bacterial Gene Expression Using an

- Engineered CRISPR-Cas System. *Nucleic Acids Research* **2013**, *41* (15), 7429–7437. <https://doi.org/10.1093/nar/gkt520>.
- (50) Silvis, M. R.; Rajendram, M.; Shi, H.; Osadnik, H.; Gray, A. N.; Cesar, S.; Peters, J. M.; Hearne, C. C.; Kumar, P.; Todor, H.; Huang, K. C.; Gross, C. A. Morphological and Transcriptional Responses to CRISPRi Knockdown of Essential Genes in *Escherichia Coli*. *mBio* **2021**, *12* (5), e02561-21. <https://doi.org/10.1128/mBio.02561-21>.
- (51) Qi, L. S.; Larson, M. H.; Gilbert, L. A.; Doudna, J. A.; Weissman, J. S.; Arkin, A. P.; Lim, W. A. Repurposing CRISPR as an RNA-Guided Platform for Sequence-Specific Control of Gene Expression. *Cell* **2013**, *152* (5), 1173–1183. <https://doi.org/10.1016/j.cell.2013.02.022>.
- (52) Kampmann, M.; Bassik, M. C.; Weissman, J. S. Integrated Platform for Genome-Wide Screening and Construction of High-Density Genetic Interaction Maps in Mammalian Cells. *PNAS* **2013**, *110* (25), E2317–E2326. <https://doi.org/10.1073/pnas.1307002110>.
- (53) Horlbeck, M. A.; Gilbert, L. A.; Villalta, J. E.; Adamson, B.; Pak, R. A.; Chen, Y.; Fields, A. P.; Park, C. Y.; Corn, J. E.; Kampmann, M.; Weissman, J. S. Compact and Highly Active Next-Generation Libraries for CRISPR-Mediated Gene Repression and Activation. *Elife* **2016**, *5*. <https://doi.org/10.7554/eLife.19760>.
- (54) Silhavy, T. J.; Kahne, D.; Walker, S. The Bacterial Cell Envelope. *Cold Spring Harbor Perspect Biol* **2010**, *2* (5), a000414. <https://doi.org/10.1101/cshperspect.a000414>.

- (55) Klein, G.; Raina, S. Regulated Control of the Assembly and Diversity of LPS by Noncoding SRNAs. *Biomed Res Int* **2015**, 2015.
<https://doi.org/10.1155/2015/153561>.
- (56) Bertani, B.; Ruiz, N. Function and Biogenesis of Lipopolysaccharides. *EcoSal Plus* **2018**, 8 (1). <https://doi.org/10.1128/ecosalplus.ESP-0001-2018>.
- (57) Klein, G.; Raina, S. Regulated Assembly of LPS, Its Structural Alterations and Cellular Response to LPS Defects. *Int J Mol Sci* **2019**, 20 (2), 356.
<https://doi.org/10.3390/ijms20020356>.
- (58) Guest, R. L.; Rutherford, S. T.; Silhavy, T. J. Border Control: Regulating LPS Biogenesis. *Trends in Microbiology* **2021**, 29 (4), 334–345.
<https://doi.org/10.1016/j.tim.2020.09.008>.
- (59) Garrett, T. A.; Kadmas, J. L.; Raetz, C. R. Identification of the Gene Encoding the Escherichia Coli Lipid A 4'-Kinase. *J Biol Chem* **1997**, 272 (35), 21855–21864.
<https://doi.org/10.1074/jbc.272.35.21855>.
- (60) Garrett, T. A.; Que, N. L. S.; Raetz, C. R. H. Accumulation of a Lipid A Precursor Lacking the 4'-Phosphate Following Inactivation of the Escherichia Coli LpxK Gene*. *Journal of Biological Chemistry* **1998**, 273 (20), 12457–12465.
<https://doi.org/10.1074/jbc.273.20.12457>.
- (61) Karow, M.; Georgopoulos, C. The Essential Escherichia Coli MsbA Gene, a Multicopy Suppressor of Null Mutations in the HtrB Gene, Is Related to the Universally Conserved Family of ATP-Dependent Translocators. *Mol Microbiol* **1993**, 7 (1), 69–79. <https://doi.org/10.1111/j.1365-2958.1993.tb01098.x>.

- (62) Polissi, A.; Georgopoulos, C. Mutational Analysis and Properties of the MsbA Gene of Escherichia Coli, Coding for an Essential ABC Family Transporter. *Molecular Microbiology* **1996**, *20* (6), 1221–1233. <https://doi.org/10.1111/j.1365-2958.1996.tb02642.x>.
- (63) Alexander, M. K.; Miu, A.; Oh, A.; Reichelt, M.; Ho, H.; Chalouni, C.; Labadie, S.; Wang, L.; Liang, J.; Nickerson, N. N.; Hu, H.; Yu, L.; Du, M.; Yan, D.; Park, S.; Kim, J.; Xu, M.; Sellers, B. D.; Purkey, H. E.; Skelton, N. J.; Koehler, M. F. T.; Payandeh, J.; Verma, V.; Xu, Y.; Koth, C. M.; Nishiyama, M. Disrupting Gram-Negative Bacterial Outer Membrane Biosynthesis through Inhibition of the Lipopolysaccharide Transporter MsbA. *Antimicrob Agents Chemother* **2018**, *62* (11), e01142-18. <https://doi.org/10.1128/AAC.01142-18>.
- (64) Sorensen, P. G.; Lutkenhaus, J.; Young, K.; Eveland, S. S.; Anderson, M. S.; Raetz, C. R. H. Regulation of UDP-3-O-[R-3-Hydroxymyristoyl]-N-Acetylglucosamine Deacetylase in Escherichia Coli: THE SECOND ENZYMATIC STEP OF LIPID A BIOSYNTHESIS *. *Journal of Biological Chemistry* **1996**, *271* (42), 25898–25905. <https://doi.org/10.1074/jbc.271.42.25898>.
- (65) Ogura, T.; Inoue, K.; Tatsuta, T.; Suzaki, T.; Karata, K.; Young, K.; Su, L. H.; Fierke, C. A.; Jackman, J. E.; Raetz, C. R.; Coleman, J.; Tomoyasu, T.; Matsuzawa, H. Balanced Biosynthesis of Major Membrane Components through Regulated Degradation of the Committed Enzyme of Lipid A Biosynthesis by the AAA Protease FtsH (HflB) in Escherichia Coli. *Mol Microbiol* **1999**, *31* (3), 833–844. <https://doi.org/10.1046/j.1365-2958.1999.01221.x>.

- (66) Montgomery, J. I.; Brown, M. F.; Reilly, U.; Price, L. M.; Abramite, J. A.; Arcari, J.; Barham, R.; Che, Y.; Chen, J. M.; Chung, S. W.; Collantes, E. M.; Desbonnet, C.; Doroski, M.; Doty, J.; Engtrakul, J. J.; Harris, T. M.; Huband, M.; Knafels, J. D.; Leach, K. L.; Liu, S.; Marfat, A.; McAllister, L.; McElroy, E.; Menard, C. A.; Mitton-Fry, M.; Mullins, L.; Noe, M. C.; O'Donnell, J.; Oliver, R.; Penzien, J.; Plummer, M.; Shanmugasundaram, V.; Thoma, C.; Tomaras, A. P.; Uccello, D. P.; Vaz, A.; Wishka, D. G. Pyridone Methylsulfone Hydroxamate LpxC Inhibitors for the Treatment of Serious Gram-Negative Infections. *J. Med. Chem.* **2012**, *55* (4), 1662–1670. <https://doi.org/10.1021/jm2014875>.
- (67) Brown, M. F.; Reilly, U.; Abramite, J. A.; Arcari, J. T.; Oliver, R.; Barham, R. A.; Che, Y.; Chen, J. M.; Collantes, E. M.; Chung, S. W.; Desbonnet, C.; Doty, J.; Doroski, M.; Engtrakul, J. J.; Harris, T. M.; Huband, M.; Knafels, J. D.; Leach, K. L.; Liu, S.; Marfat, A.; Marra, A.; McElroy, E.; Melnick, M.; Menard, C. A.; Montgomery, J. I.; Mullins, L.; Noe, Mark. C.; O'Donnell, J.; Penzien, J.; Plummer, M. S.; Price, L. M.; Shanmugasundaram, V.; Thoma, C.; Uccello, D. P.; Warmus, J. S.; Wishka, D. G. Potent Inhibitors of LpxC for the Treatment of Gram-Negative Infections. *J. Med. Chem.* **2012**, *55* (2), 914–923. <https://doi.org/10.1021/jm2014748>.
- (68) Khadka, N. K.; Aryal, C. M.; Pan, J. Lipopolysaccharide-Dependent Membrane Permeation and Lipid Clustering Caused by Cyclic Lipopeptide Colistin. *ACS Omega* **2018**, *3* (12), 17828–17834. <https://doi.org/10.1021/acsomega.8b02260>.
- (69) Grundström, T.; Normark, S.; Magnusson, K. E. Overproduction of Outer Membrane Protein Suppresses EnvA-Induced Hyperpermeability. *J. Bacteriol* **1980**, *144* (3), 884–890. <https://doi.org/10.1128/jb.144.3.884-890.1980>.

- (70) Howard, S. A.; Furniss, R. C. D.; Bonini, D.; Amin, H.; Paracuellos, P.; Zlotkin, D.; Costa, T. R. D.; Levy, A.; Mavridou, D. A. I.; Filloux, A. The Breadth and Molecular Basis of Hcp-Driven Type VI Secretion System Effector Delivery. *mBio* **12** (3), e00262-21. <https://doi.org/10.1128/mBio.00262-21>.
- (71) Lin, L.; Lezan, E.; Schmidt, A.; Basler, M. Abundance of Bacterial Type VI Secretion System Components Measured by Targeted Proteomics. *Nat Commun* **2019**, *10* (1), 2584. <https://doi.org/10.1038/s41467-019-10466-9>.
- (72) Kahan, F. M.; Kahan, J. S.; Cassidy, P. J.; Kropp, H. The Mechanism of Action of Fosfomycin (Phosphonomycin). *Annals of the New York Academy of Sciences* **1974**, *235* (1), 364–386. <https://doi.org/10.1111/j.1749-6632.1974.tb43277.x>.
- (73) Barreteau, H.; Kovač, A.; Boniface, A.; Sova, M.; Gobec, S.; Blanot, D. Cytoplasmic Steps of Peptidoglycan Biosynthesis. *FEMS Microbiology Reviews* **2008**, *32* (2), 168–207. <https://doi.org/10.1111/j.1574-6976.2008.00104.x>.
- (74) Egan, A. J. F.; Biboy, J.; Veer, I. van't; Breukink, E.; Vollmer, W. Activities and Regulation of Peptidoglycan Synthases. *Phil. Trans. R. Soc. B* **2015**, *370* (1679), 20150031. <https://doi.org/10.1098/rstb.2015.0031>.
- (75) Bertsche, U.; Kast, T.; Wolf, B.; Fraipont, C.; Aarsman, M. E. G.; Kannenberg, K.; Von Rechenberg, M.; Nguyen-Distèche, M.; Den Blaauwen, T.; Höltje, J.-V.; Vollmer, W. Interaction between Two Murein (Peptidoglycan) Synthases, PBP3 and PBP1B, in *Escherichia Coli*. *Molecular Microbiology* **2006**, *61* (3), 675–690. <https://doi.org/10.1111/j.1365-2958.2006.05280.x>.

- (76) Bush, K.; Bradford, P. A. β -Lactams and β -Lactamase Inhibitors: An Overview. *Cold Spring Harb Perspect Med* **2016**, 6 (8), a025247.
<https://doi.org/10.1101/cshperspect.a025247>.
- (77) Baba, T.; Ara, T.; Hasegawa, M.; Takai, Y.; Okumura, Y.; Baba, M.; Datsenko, K. A.; Tomita, M.; Wanner, B. L.; Mori, H. Construction of Escherichia Coli K-12 in-Frame, Single-Gene Knockout Mutants: The Keio Collection. *Molecular Systems Biology* **2006**, 2 (1), 2006.0008. <https://doi.org/10.1038/msb4100050>.
- (78) Simon, R.; Prierer, U.; Pühler, A. A Broad Host Range Mobilization System for In Vivo Genetic Engineering: Transposon Mutagenesis in Gram Negative Bacteria. *Nat Biotechnol* **1983**, 1 (9), 784–791. <https://doi.org/10.1038/nbt1183-784>.
- (79) He, F. E. Coli Genomic DNA Extraction. *Bio-101* **2011**, e97.
<https://doi.org/10.21769/BioProtoc.97>.
- (80) Churchman, L. S.; Weissman, J. S. Nascent Transcript Sequencing Visualizes Transcription at Nucleotide Resolution. *Nature* **2011**, 469 (7330), 368–373.
<https://doi.org/10.1038/nature09652>.
- (81) Hawkins, J. S.; Silvis, M. R.; Koo, B.-M.; Peters, J. M.; Osadnik, H.; Jost, M.; Hearne, C. C.; Weissman, J. S.; Todor, H.; Gross, C. A. Mismatch-CRISPRi Reveals the Co-Varying Expression-Fitness Relationships of Essential Genes in Escherichia Coli and Bacillus Subtilis. *Cell Syst* **2020**, 11 (5), 523-535.e9.
<https://doi.org/10.1016/j.cels.2020.09.009>.
- (82) R: A Language and Environment for Statistical Computing. <https://www.R-project.org/>.

- (83) Wickham, H. *Ggplot2: Elegant Graphics for Data Analysis*; Springer-Verlag New York.
- (84) Mastronarde, D. N. Automated Electron Microscope Tomography Using Robust Prediction of Specimen Movements. *Journal of Structural Biology* **2005**, *152* (1), 36–51. <https://doi.org/10.1016/j.jsb.2005.07.007>.
- (85) Kremer, J. R.; Mastronarde, D. N.; McIntosh, J. R. Computer Visualization of Three-Dimensional Image Data Using IMOD. *J Struct Biol* **1996**, *116* (1), 71–76. <https://doi.org/10.1006/jsbi.1996.0013>.
- (86) Stael, S.; Miller, L. P.; Fernández-Fernández, Á. D.; Van Breusegem, F. Detection of Damage-Activated Metacaspase ActivityActivities by Western Blot in Plants. In *Plant Proteases and Plant Cell Death: Methods and Protocols*; Klemenčič, M., Stael, S., Huesgen, P. F., Eds.; Methods in Molecular Biology; Springer US: New York, NY, 2022; pp 127–137. https://doi.org/10.1007/978-1-0716-2079-3_11.
- (87) Schindelin, J.; Arganda-Carreras, I.; Frise, E.; Kaynig, V.; Longair, M.; Pietzsch, T.; Preibisch, S.; Rueden, C.; Saalfeld, S.; Schmid, B.; Tinevez, J.-Y.; White, D. J.; Hartenstein, V.; Eliceiri, K.; Tomancak, P.; Cardona, A. Fiji: An Open-Source Platform for Biological-Image Analysis. *Nat Methods* **2012**, *9* (7), 676–682. <https://doi.org/10.1038/nmeth.2019>.
- (88) Guzman, L. M.; Belin, D.; Carson, M. J.; Beckwith, J. Tight Regulation, Modulation, and High-Level Expression by Vectors Containing the Arabinose PBAD Promoter. *Journal of Bacteriology* **1995**, *177* (14), 4121–4130. <https://doi.org/10.1128/jb.177.14.4121-4130.1995>.

- (89) Liu, D.; Reeves, P. R. Escherichia Coli K12 Regains Its O Antigen. *Microbiology* **1994**, *140* (1), 49–57. <https://doi.org/10.1099/13500872-140-1-49>.
- (90) Sachla, A. J.; Helmann, J. D. Resource Sharing between Central Metabolism and Cell Envelope Synthesis. *Curr Opin Microbiol* **2021**, *60*, 34–43. <https://doi.org/10.1016/j.mib.2021.01.015>.
- (91) Klein, G.; Kobylak, N.; Lindner, B.; Stupak, A.; Raina, S. Assembly of Lipopolysaccharide in Escherichia Coli Requires the Essential LapB Heat Shock Protein *. *Journal of Biological Chemistry* **2014**, *289* (21), 14829–14853. <https://doi.org/10.1074/jbc.M113.539494>.
- (92) Desmarais, S. M.; De Pedro, M. A.; Cava, F.; Huang, K. C. Peptidoglycan at Its Peaks: How Chromatographic Analyses Can Reveal Bacterial Cell Wall Structure and Assembly. *Molecular Microbiology* **2013**, *89* (1), 1–13. <https://doi.org/10.1111/mmi.12266>.
- (93) Egan, A. J. F.; Errington, J.; Vollmer, W. Regulation of Peptidoglycan Synthesis and Remodelling. *Nat Rev Microbiol* **2020**, *18* (8), 446–460. <https://doi.org/10.1038/s41579-020-0366-3>.
- (94) Egan, A. J. F.; Cleverley, R. M.; Peters, K.; Lewis, R. J.; Vollmer, W. Regulation of Bacterial Cell Wall Growth. *FEBS J* **2017**, *284* (6), 851–867. <https://doi.org/10.1111/febs.13959>.
- (95) Scherrer, R.; Moyed, H. S. Conditional Impairment of Cell Division and Altered Lethality in HipA Mutants of Escherichia Coli K-12. *J Bacteriol* **1988**, *170* (8), 3321–3326.

- (96) Kwan, B. W.; Valenta, J. A.; Benedik, M. J.; Wood, T. K. Arrested Protein Synthesis Increases Persister-Like Cell Formation. *Antimicrob Agents Chemother* **2013**, *57* (3), 1468–1473. <https://doi.org/10.1128/AAC.02135-12>.
- (97) Liu, S.; Wu, N.; Zhang, S.; Yuan, Y.; Zhang, W.; Zhang, Y. Variable Persister Gene Interactions with (p)PpGpp for Persister Formation in Escherichia Coli. *Frontiers in Microbiology* **2017**, *8*.
- (98) Roghanian, M.; Semsey, S.; Løbner-Olesen, A.; Jalalvand, F. (P)PpGpp-Mediated Stress Response Induced by Defects in Outer Membrane Biogenesis and ATP Production Promotes Survival in Escherichia Coli. *Sci Rep* **2019**, *9* (1), 2934. <https://doi.org/10.1038/s41598-019-39371-3>.
- (99) Łoś, M.; Golec, P.; Łoś, J. M.; Węglewska-Jurkiewicz, A.; Czyż, A.; Węgrzyn, A.; Węgrzyn, G.; Neubauer, P. Effective Inhibition of Lytic Development of Bacteriophages λ , P1 and T4 by Starvation of Their Host, Escherichia Coli. *BMC Biotechnology* **2007**, *7* (1), 13. <https://doi.org/10.1186/1472-6750-7-13>.
- (100) Pearl, S.; Gabay, C.; Kishony, R.; Oppenheim, A.; Balaban, N. Q. Nongenetic Individuality in the Host–Phage Interaction. *PLoS Biol* **2008**, *6* (5), e120. <https://doi.org/10.1371/journal.pbio.0060120>.
- (101) Meeske, A. J.; Nakandakari-Higa, S.; Marraffini, L. A. Cas13-Induced Cellular Dormancy Prevents the Rise of CRISPR-Resistant Bacteriophage. *Nature* **2019**, *570* (7760), 241–245. <https://doi.org/10.1038/s41586-019-1257-5>.
- (102) Wiuff, C.; Zappala, R. M.; Regoes, R. R.; Garner, K. N.; Baquero, F.; Levin, B. R. Phenotypic Tolerance: Antibiotic Enrichment of Noninherited Resistance in

- Bacterial Populations. *Antimicrob Agents Chemother* **2005**, 49 (4), 1483–1494.
<https://doi.org/10.1128/AAC.49.4.1483-1494.2005>.
- (103) Lee, A. J.; Wang, S.; Meredith, H. R.; Zhuang, B.; Dai, Z.; You, L. Robust, Linear Correlations between Growth Rates and β -Lactam–Mediated Lysis Rates. *Proceedings of the National Academy of Sciences* **2018**, 115 (16), 4069–4074.
<https://doi.org/10.1073/pnas.1719504115>.
- (104) Wilmoth, J. L.; Doak, P. W.; Timm, A.; Halsted, M.; Anderson, J. D.; Ginovart, M.; Prats, C.; Portell, X.; Retterer, S. T.; Fuentes-Cabrera, M. A Microfluidics and Agent-Based Modeling Framework for Investigating Spatial Organization in Bacterial Colonies: The Case of *Pseudomonas Aeruginosa* and H1-Type VI Secretion Interactions. *Front Microbiol* **2018**, 9, 33.
<https://doi.org/10.3389/fmicb.2018.00033>.
- (105) Borenstein, D. B.; Ringel, P.; Basler, M.; Wingreen, N. S. Established Microbial Colonies Can Survive Type VI Secretion Assault. *PLOS Computational Biology* **2015**, 11 (10), e1004520. <https://doi.org/10.1371/journal.pcbi.1004520>.
- (106) Smith, W. P. J.; Vettiger, A.; Winter, J.; Ryser, T.; Comstock, L. E.; Basler, M.; Foster, K. R. The Evolution of the Type VI Secretion System as a Disintegration Weapon. *PLOS Biology* **2020**, 18 (5), e3000720.
<https://doi.org/10.1371/journal.pbio.3000720>.
- (107) Singh, S. K.; SaiSree, L.; Amrutha, R. N.; Reddy, M. Three Redundant Murein Endopeptidases Catalyse an Essential Cleavage Step in Peptidoglycan Synthesis of *Escherichia Coli* K12. *Molecular Microbiology* **2012**, 86 (5), 1036–1051.
<https://doi.org/10.1111/mmi.12058>.

- (108) Cardona, S. T.; Valvano, M. A. An Expression Vector Containing a Rhamnose-Inducible Promoter Provides Tightly Regulated Gene Expression in Burkholderia Cenocepacia. *Plasmid* **2005**, *54* (3), 219–228.
<https://doi.org/10.1016/j.plasmid.2005.03.004>.
- (109) Desmarais, S. M.; Cava, F.; de Pedro, M. A.; Huang, K. C. Isolation and Preparation of Bacterial Cell Walls for Compositional Analysis by Ultra Performance Liquid Chromatography. *J Vis Exp* **2014**, No. 83, 51183.
<https://doi.org/10.3791/51183>.
- (110) Peters, K.; Pazos, M.; VanNieuwenhze, M. S.; Vollmer, W. Optimized Protocol for the Incorporation of FDAA (HADA Labeling) for in Situ Labeling of Peptidoglycan. *Bio Protoc* **2019**, *9* (15), e3316.
<https://doi.org/10.21769/BioProtoc.3316>.
- (111) Ducret, A.; Quardokus, E. M.; Brun, Y. V. MicrobeJ, a Tool for High Throughput Bacterial Cell Detection and Quantitative Analysis. *Nat Microbiol* **2016**, *1* (7), 1–7.
<https://doi.org/10.1038/nmicrobiol.2016.77>.
- (112) Diez, S.; Ryu, J.; Caban, K.; Gonzalez, R. L.; Dworkin, J. The Alarmones (p)PpGpp Directly Regulate Translation Initiation during Entry into Quiescence. *Proceedings of the National Academy of Sciences* **2020**, *117* (27), 15565–15572.
<https://doi.org/10.1073/pnas.1920013117>.
- (113) Thevenaz, P.; Ruttimann, U. E.; Unser, M. A Pyramid Approach to Subpixel Registration Based on Intensity. *IEEE Transactions on Image Processing* **1998**, *7* (1), 27–41. <https://doi.org/10.1109/83.650848>.

Publishing Agreement

It is the policy of the University to encourage open access and broad distribution of all theses, dissertations, and manuscripts. The Graduate Division will facilitate the distribution of UCSF theses, dissertations, and manuscripts to the UCSF Library for open access and distribution. UCSF will make such theses, dissertations, and manuscripts accessible to the public and will take reasonable steps to preserve these works in perpetuity.

I hereby grant the non-exclusive, perpetual right to The Regents of the University of California to reproduce, publicly display, distribute, preserve, and publish copies of my thesis, dissertation, or manuscript in any form or media, now existing or later derived, including access online for teaching, research, and public service purposes.

DocuSigned by:

Kristine Trotta

1F946A1AFB214F9...

Author Signature

3/12/2023

Date